Development of Novel Micropneumatic Grippers for Biomanipulation

Ageel Farraj Ali Alogla

Submitted for the degree of Doctor of Philosophy

Heriot-Watt University

School of Engineering and Physical Sciences/ Institute of Biological Chemistry, Biophysics and Bioengineering

May 2014

ABSTRACT

Microbjects with dimensions from 1 μm to 1 mm have been developed recently for different aspects and purposes. Consequently, the development of handling and manipulation tools to fulfil this need is urgently required. Micromanipulation techniques could be generally categorized according to their actuation method such as electrostatic, thermal, shape memory alloy, piezoelectric, magnetic, and fluidic actuation. Each of which has its advantage and disadvantage. The fluidic actuation has been overlooked in MEMS despite its satisfactory output in the micro-scale.

This thesis presents different families of pneumatically driven, low cost, compatible with biological environment, scalable, and controllable microgrippers. The first family demonstrated a polymeric microgripper that was laser cut and actuated pneumatically. It was tested to manipulate micro-particles down to 200 microns. To overcome the assembly challenges that arise in this family, the second family was proposed.

The second family was a micro-cantilever based microgripper, where the device was assembled layer by layer to form a 3D structure. The micro-cantilevers were fabricated using photo-etching technique, and demonstrated the applicability to manipulate micro-particles down to 200 microns using automated pick-and-place procedure. In addition, this family was used as a tactile-detector as well. Due to the angular gripping scheme followed by the above mentioned families, gripping smaller objects becomes a challenging task. A third family following a parallel gripping scheme was proposed allowing the gripping of smaller objects to be visible. It comprises a compliant structure microgripper actuated pneumatically and fabricated using pico-second laser technology, and demonstrated the capability of gripping micro-object as small as 100 μm microbeads. An FEA modelling was employed to validate the experimental and analytical results, and excellent matching was achieved.

Acknowledgment

I am deeply appreciative for the support and guidance throughout the research and thesis writing process. First and foremost, I would like to thank my supervisor Dr. Will Shu for his years of guidance, feedback, encouragement, and patience throughout my PhD. I also highly appreciate Prof. Robert Reuben for his highly valuable suggestions and help.

I would like also to thank Dr. Farid Amalou, Dr. Richard Carter for their help and advice in the design and fabrication of many of the devices in this thesis. Also, I would like to thank Dr. Yifan Liu for his help in the LabView and optical detection system procedures.

And another acknowledgments my colleagues Paul Scanlan, Luke Mason, and Alan Faulkner for their continuous help in the simulation and fabrication procedures.

Lastly, and as always, I am extremely grateful towards my mother, my wife, and my brothers and sisters for their continued support and encouragement during my research and throughout my life.

To My Beloved Mother

And

To The Soul Of My Father

Table of Contents

Abbreviations

AFM	Atomic force microscope
DEP	Dielectrophoresis
EDM	Electro-Discharge Machining
EP	Electrophoresis
FEM	Finite element modeling
GMM	Giant magnetostrictive material
MEMS	Microelectromechanical
MSTL	Micro-stereolithography
PDMS	Polydimethylsiloxane
PMMA	Poly(methyl methacrylate)
PSD	Position sensitive device
SMA	Shape memory alloy
SPCA	Stack piezoelectric ceramic actuator
μTAS	Micro-total analysis systems

LIST OF SYMBOLS

E	Young's modulus
G	Modulus of rigidity
I	Moment of inertia
K_R	Rotational stiffness
F_e	Electrostatic force
ε	Permittivity of the medium between the plates
V	Applied voltage
n	Number comb fingers
L	Length of the cantilever
L_{PSD}	Length of PSD area
s	Distance from the cantilever tip to the PSD
ΔZ	Cantilever deflection
i_A i_B	Directional currents in a PSD
D	Flexural rigidity
R	Radius
P	Pressure
θ	Angular displacement
T	Torque
δ	Deflection

LIST OF PUBLICATIONS

Alogla, A., Scanlan, P., Shu, W., & Reuben, R. L. (2012). A Scalable Syringe-Actuated Microgripper for Biological Manipulation. *In the 26th European Conference on Solid-State Transducers, Eurosensors 2012. Krakow, Poland.*

Alogla, A., Scanlan, P., Shu, W., & Reuben, R. L. (2012). A Scalable Syringe-Actuated Microgripper for Biological Manipulation. *Procedia Engineering*, *47*, 882-885.

Alogla, A., Scanlan, P., Shu, W. M., & Reuben, R. L. (2013). A scalable syringe-actuated microgripper for biological manipulation. *Sensors and Actuators A: Physical*, *202*, 135-139.

Alogla, A., F. Amalou, W. M. Shu, and R. L. Reuben. (2013). A pneumatically driven cantilever for micromanipulation. *Proceedings of 2013 International Workshop on Nanomechanical Sensing.* Stanford University, Stanford, CA. p: 81-82

Alogla, A., F. Amalou, P. Scanlan, W. Shu and R.L. Reuben. Micro-Tweezers: Development of a Pneumatically Actuated Miro-Gripper for Micromanipulation and Microtactile Sensing. (In preparation for *Journal of Microengineering and Micromechanics*)

Alogla, A., G. Hao, R. Carter, D. Hand, W. Shu, and R.L. Reuben. The Development of A Compliant Mechanism Based Microgripper through Pneumatic Actuation. (In preparation for *Journal of Microeletomechanical Systems.*)

Alogla, A., F. Amalou, P. Scanlan, W. Shu and R.L. Reuben. Development of a Pneumatically Actuated Cantilever Based Miro-Tweezer. *The 28th European Conference on Solid-StateTransducers, Eurosensors2014.* (Submitted).

Alogla, A., G. Hao, R. Carter, D. Hand, W. Shu, and R.L. Reuben. Pneumatically Actuated Microgripper through Compliant Mechanism. *The 28th European Conference on Solid-State Transducers, Eurosensors 2014.* (Submitted)

Chapter 1: Introduction

1.1 Motivation

Continuous progress in medical and biological applications requires research at the cellular level. Performing an experiment on a single cell allows for better results than conventional experiments where a large population of cells are studied and the acquired data are averaged (Levsky and Singer, 2003, Bao and Suresh, 2003). Such an idea is behind the growth of interest within the biological and medical communities in techniques which enable the individual manipulation of biological objects (Voldman *et al*., 1999, Polla *et al*., 2000, Grayson *et al*., 2004, Yi *et al*., 2006, Jager *et al*., 2000)

The successful handling and manipulation of individual micro-objects is a major challenge in true assembled microsystem. The handling technique has to be precisely controlled, safe, with reliable pick-and-place of the micro-object being handled. The main motivation of this research is to develop a suitable, highly reliable microgripper which can be assembled to perform handling and manipulation of micro-objects in various media like air and liquid.

Achieving the aforementioned function requires different considerations to be taken into account. The main considerations that should not be overlooked while designing and fabricating a microgripper are the nature of the manipulated object, the operating environment, and the manufacturing cost.

Micro-manipulation is a challenging task that requires a precise, reliable, and suitably controllable manipulation set-up. In order to be able to manipulate biological samples, several criteria need to be met. For example, the micro-environment should not be negatively affected by high operating temperature or magnetic and electric fields resulting from the manipulation mechanism.

The rapid evolution in biological science has led to the requirements of manipulation at micro- and nano- scale. In general, manipulating single cells can be classified into contact and non-contact techniques and a detailed literature review of each is presented in the following two sections, with a view to select the most suitable way forward for the aim of this thesis.

1.2 Non-Contact Techniques

1.2.1 Optical Tweezer Manipulation

The optical manipulation techniques mainly employ optical principles (Juan *et al*., 2011, Wang *et al*., 2011, Zhang and Liu, 2008, Ashkin *et al*., 1986), where the highly focused laser beam is employed to manipulate and trap the microbiological objects. Optical tweezers, or laser tweezers, have been implemented widely in many applications since the early 1970s (Lang and Block, 2003). They are considered amongst the most common non-contact manipulation techniques due to their capability of manipulating micro-objects precisely without damaging them (Li *et al*., 2013). Figure 1.1 shows a typical optical manipulation system, where the Dichroic mirror reflects the expanded laser beam, that in turn is introduced into the inverted microscope. A demonstration of optical trapping of viruses and bacteria in an aqueous media without obvious damage was achieved by Ashkin *et al* using a visible argon single-beam gradient trap (Ashkin and Dziedzic, 1987). Another study of the same group using infrared (IR) light shows a larger manipulation force and less optical damage to living cells (Ashkin *et al*., 1987). Buican *et al* demonstrated the capability of laser traps not only to position the cells, but also to transport them over few centimetres (Buican *et al*., 1987).

Although this technique demonstrates a satisfactory performance in trapping and manipulating microbiological objects, it requires complex and expensive optical setup (Piggee, 2008) and has a long term negative effects on the manipulated micro-objects (König *et al*., 1996).

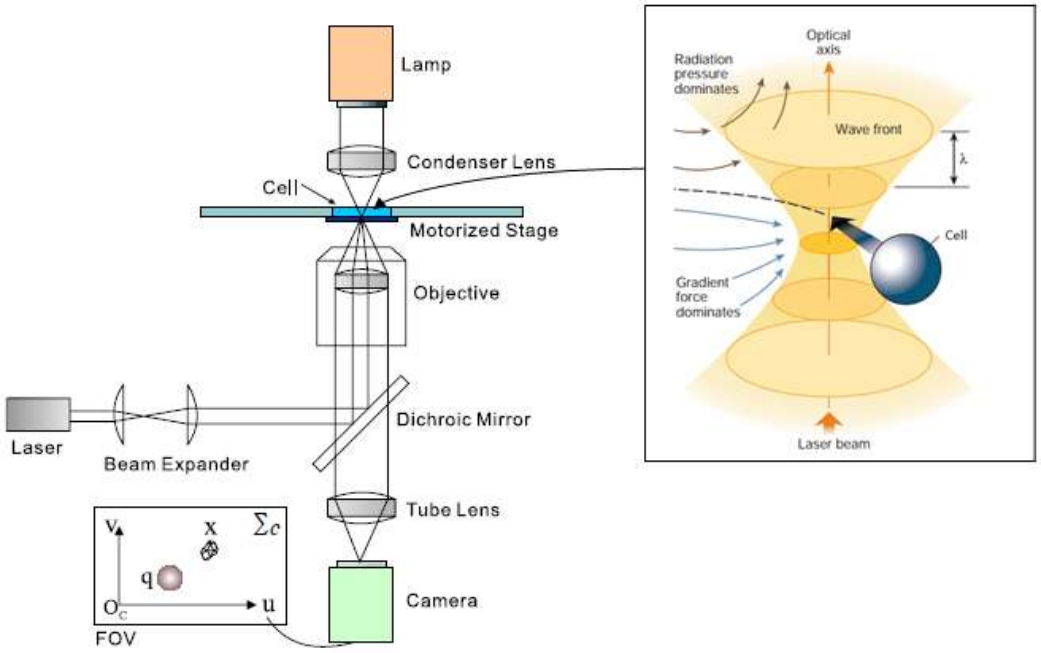

Figure 1.1: A typical optical tweezers system (Li *et al*., 2013)

1.2.2 Magnetic Field Manipulation

Magnetic forces have been employed in the application of cell manipulation where either intrinsic (e.g., the iron-containing hemoglobin in erythrocytes) or extrinsic (e.g., cells labeled with magnetic nanoparticles) magnetic properties of biological macromolecules are utilized (Yun *et al*., 2013), as shown in Figure 1.2. Implementing this technique requires adhesion or implanting magnetic beads into the cells which has not been found affecting the viability of cells and resulting in a very flexible manipulation system (Desai *et al*., 2007).

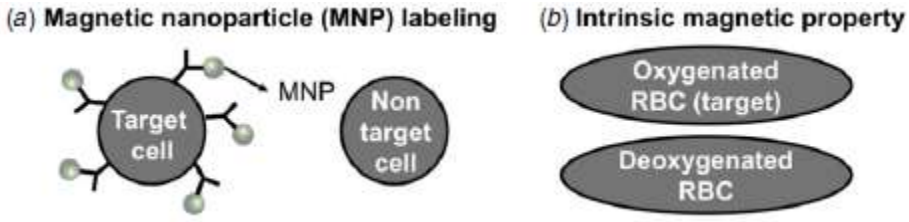

Figure 1.2: Schematic illustration of magnetic manipulation; (a) extrinsic, (b) intrinsic (Yun *et al*., 2013)

1.2.3 Electric Field Manipulation

Electric field (e.g., dielectrophoresis (DEP) and electrophoresis (EP)) is another type of non-contact techniques. DEP manipulation is determined by the polarity of the electrical charge of the manipulated particle (Yun *et al*., 2013), while EP is determined by the interaction of the manipulated particle's charge and the electric field (Voldman, 2006) as illustrated in Figure 1.3. Electric field manipulation technique has been used to manipulate different biological cells such as bacteria, yeast, and mammalian cells (Desai *et al*., 2007).

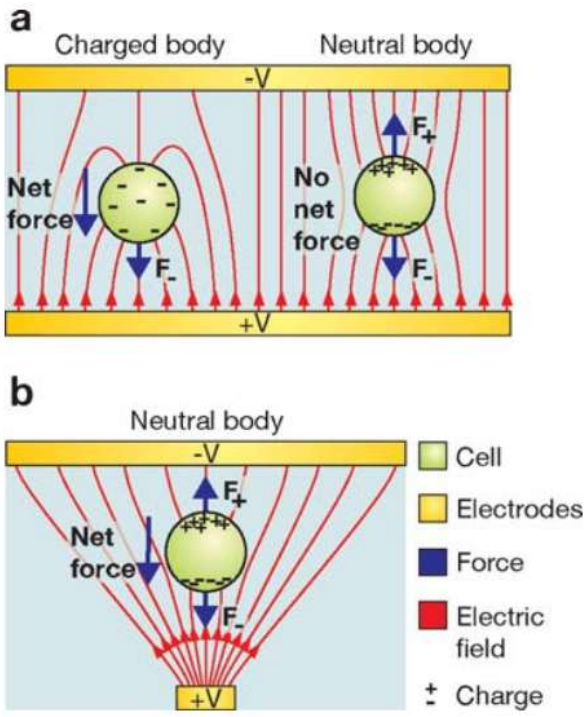

Figure 1.3: EP and DEP. (a) Charged and neutral particle in a uniform electric field. The charged particle (left) feels an EP force, whereas the dipole induced in the uncharged particle (right) will not result in a net force (F− =F+). (b) A neutral particle in a nonuniform electric field. The particle will experience a net force toward the electric-field maximum because the field magnitude is different at each end of the particle (F− >F+) (Voldman, 2006).

1.2.4 Acoustic Manipulation

Where the emitted acoustic waves are reflected by a rigid surface to obtain a standing wave. The force of this standing wave is used in the separation or manipulation of micro-particles (Jönsson *et al*., 2004, Petersson *et al*., 2005, Kozuka *et al*., 2008). The working principle of this technique is illustrated in Figure 1.4. However, precision and difficulties of precise positioning of a micro-objects using the acoustic technique is the main limitation for this technique (Fu *et al*., 2012).

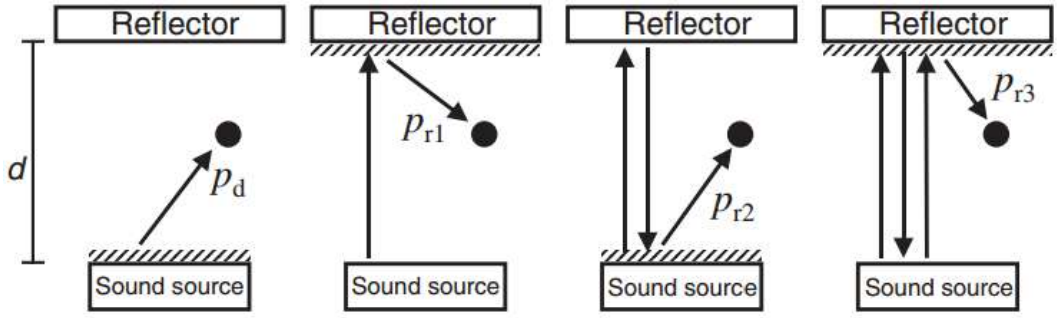

Figure 1.4: The concept of the direct and reflected wave in acoustic manipulation where p_d and p_r correspond to direct wave pressure reflected wave pressure, respectively (Kozuka *et al*., 2008).

1.3 Contact Techniques

The term "contact techniques" implies a physical interaction between the manipulated micro-object and the manipulation device. Pipettes and grippers are the most contact techniques implemented to manipulate biological micro-objects. Pipettes are employing a negative pressure that is applied through a nozzle to manipulate such micro-objects, where the suction force can be provided either by a syringe controlled pressure transducer (Sato *et al*., 1987) or piezoelectric actuator (Lee *et al*., 1994). Figure 1.5 shows a schematic drawing of the working principle of the pipettes. Also, this technique has been used extensively to study the mechanical properties of cells by employing a measured deformation of cells

attributed to a known force or stress to obtain such properties (Kim *et al*., 2009). Sato *et al.* implemented a micropipette technique to investigate the mechanical properties of cultured bovine aortic endothelial cells exposed to a fluid-imposed shear stress and then detached (Sato *et al*., 1987). However, this technique despite of its capability to hold single cells, requires highly skilled users to achieve the manipulation of biological micro-objects without damaging them. Furthermore, pipettes functionality is limited by cell size. If cells are smaller than the opening of the pipette nozzle, then several cells can be drawn into the pipette rather than isolating just one (Chan and Li, 2003).

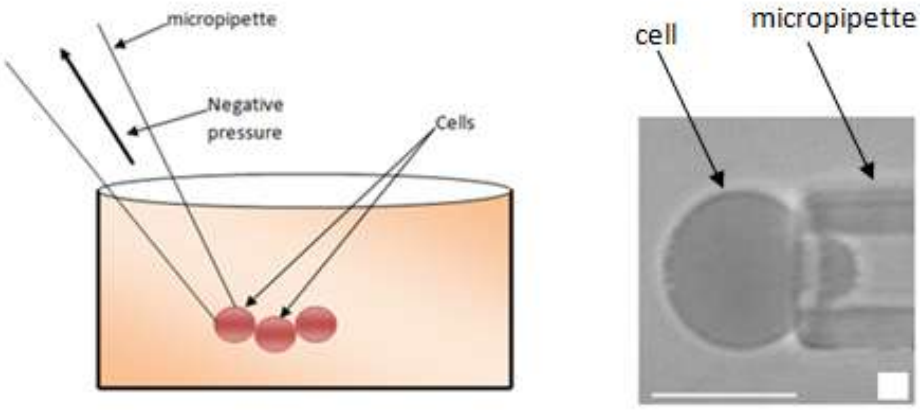

Figure 1.5: (Left) Manipulation technique of pipette, (Right) Aspiration of a 6 µm diameter swollen red cell into a pipette (Hochmuth, 2000).

The other commonly used type of contact techniques are microgrippers. Microgrippers are complex micro-electro-mechanical-systems (MEMS) (Zeman M, 2006) and a variety of microgrippers have been developed in recent years for the manipulation of micro-objects. Different actuation mechanisms have been used for microgrippers applications such as electrostatic, piezoelectric, SMA, magnetic and fluidic actuation.

However, contact techniques arise another issue, which is the releasing of the micro-object. As in macroworld, gravitational force becomes dominant and the objects could be collected and dropped easily. On the other hand, in microworld, adhesive forces dominate the procedure and the gravity is neglected. Two

different strategies could be implemented to overcome this issue. The first one is passive, where the operation conditions are employed to reduce the effects of such forces. The second one is the active strategy, which implies adding or changing the design of the device to release the micro-objects easily (Fu *et al.*, 2012).

1.3.1 Electrostatic Microgrippers

Columbic force, or electrostatic force, between two charged plates subject to a potential difference is used. These plates are considered to be the comb finger electrodes. Figure 1.6 shows the dimensions of comb finger electrodes, where "a" is the distance between the motion finger top and fixed finger root, "b" is the width of each finger, "d" is the distance between the plates, "h" is the thickness of fingers, and "y" represents the displacement of the electrostatic actuator. The generated electrostatic force is given by the formula (Chen T, 2010):

$$F_e = \varepsilon \cdot \frac{nhV^2}{d} \tag{1.1}$$

where, ε is the permittivity of the medium between the plates, n is the number comb fingers, V is the applied voltage, and d is distance between the plates.

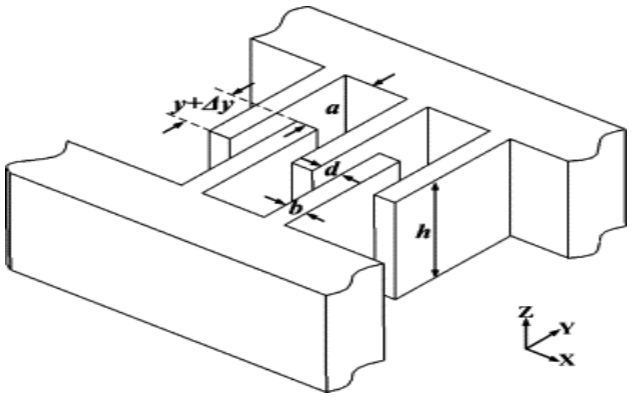

Figure 1.6: Dimensions of the comb finger electrodes (Chen T, 2010)

Microactuators driven electrostatically generate a linear motion which is converted into rotational gripping motion by a hinge system. Chen *et al.* proposed a hybrid microgripper driven electrostatically illustrated in Figure 1.7. They used a surface and bulk machining technology to fabricate this device. The microgripping of micro-objects was the result of converting the small horizontal displacement generated by the electrostatic microgripper into the big motion of the arms by an S-type flexible beam system, achieving a deflection of 25 µm at the tweezers of the gripper with an applied voltage of 80 V (Chen T, 2010). The performance of this microgripper was demonstrated experimentally by the manipulation of 100-200 µm polystyrene balls. The authors integrated a vacuum tool to get rid of adhesive forces, electrostatic forces, and surface tension forces. Vacuum tools that generate positive pressure to overcome the adhesion between microgripper and microparticles are considered to be a good way to solve releasing problems (Zesch W, 1997, Chen G, 2004, Petrovic D, 2002).

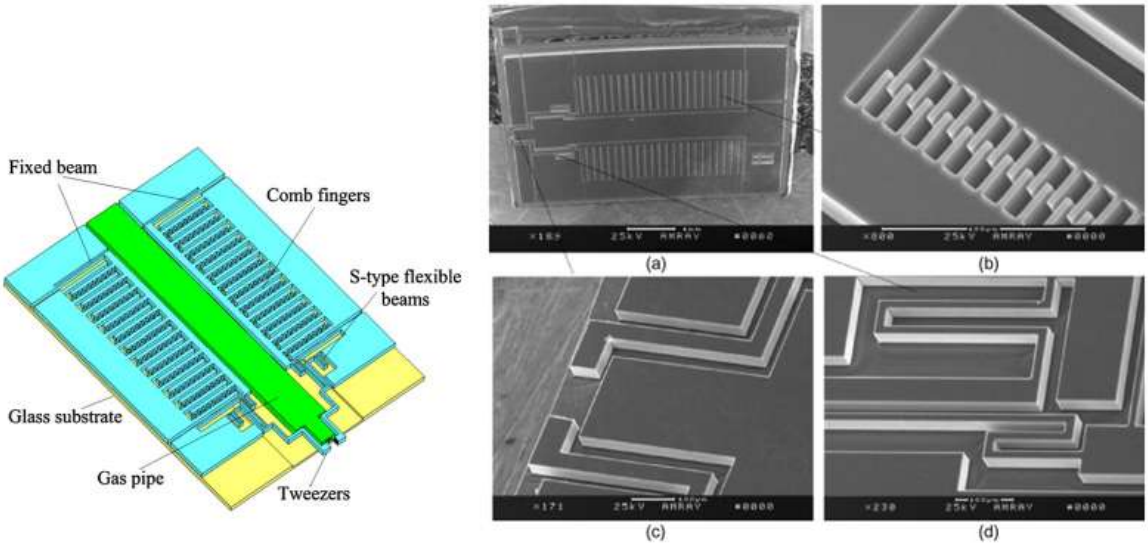

Figure 1.7: Model of microgripper (Left), SEM images of the gripper (Right) (a) The integral structure of the gripper, (b) the combs, (c) the end effector, and (d) the S-type spring beam. (Chen T, 2010).

In general, electrostatic actuation has the advantages of high energy densities, high output forces for MEMS in micro-scale, and low power consumption (Zhang *et al*., 2007, Hung and Senturia, 1999). On the other hand, microgrippers actuated electrostatically require high voltage (Zeman M, 2006). Also, electrostatic actuation becomes ineffective in ion-rich liquids (e.g. inside body fluid) due to the cancellation of surface charges (Ok *et al*., 2006).

1.3.2 Thermal Microgrippers

Microgrippers actuated thermally exploit the dissymmetry of either the thermal properties of two materials or the expansion within the same material, and could be categorized as follows (Agnus J, 2005):

- *Thermal properties of two material dissymmetry*
  In this category, a bimorph effect of two material is used to deflect the end of the two beams composing of the microgripper. Heating procedure is usually obtained by Joule effect by passing a current through the structure (Zheng *et al*., 2011)
- *Dilation dissymmetry within the same material*
  An obtained heating of a part of the material using Joule effect will obtain a lateral deflection of a compliant structure. Solano *et al.* proposed a microgripper driven by a U-shaped thermal actuator deflects at its tips due to the dissymmetry of the actuation beams, where the deflection is controlled by the difference temperature in induced between the hot and cold arm as shown in Figure 1.8 (Solano and Wood, 2007).

Microgrippers actuated thermally have the potential to generate a large output force as a result of a low input voltage (Jia and Xu, 2013), but the high temperature operation requirements may affect the surrounding environment. Furthermore, its nonlinear expansion when a high operating temperature is induced was reported (Jia and Xu, 2013).

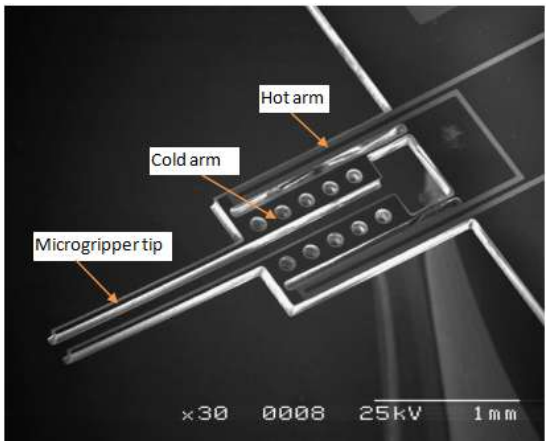

Figure 1.8: SEM of a fabricated microgripper by Solano *et al* (Solano and Wood, 2007)

1.3.3 Shape Memory Alloy (SMA) Microgrippers

SMAs are materials that can be used as actuators by deforming them at low temperature and then heating them to cause them return to the undeformed state against a load. Three types of structures can be found exploiting this principle (Agnus J, 2005) and are as follows:

- *Compliant structure grippers*

A constrained SMA actuator is used to generate mechanical work in order to deform the structure which will move significantly due to this actuation. The structure can be made of steel (Russell, 1994, Kyung *et al*., 2008), plastic (MacKenzie *et al*., 1996), or silicon (Lee *et al*., 1996, Bütefisch *et al*., 2000, Hoche *et al*., 1998), and the actuators are mostly Ni-Ti wires since they are cheap and do not require further processing as they can be cut and used (Kyung *et al*., 2008) or Ni-Ti thin films (Fu *et al*., 2008, Lee *et al*., 1996). The stroke of such micro grippers varies between 110 µm (Lee *et al*., 1996) and 2.5 mm (Russell,

1994). The microgripper shown in Figure 1.9 illustrates this type of gripper. When energizing the two SMA wires to generate heat, the wires begin to contract at the activation temperature. The linear motion of SMA wires is converted by the flexible hinge "A" into rotating motion. Since the flexible hinge B is thinner than hinge A, the stress is concentrated in hinge B and it will receive most of the gripping force. Therefore, the gripping force can be measured with the strain gauge adhered to the flexible hinge B (Kyung *et al*., 2008).

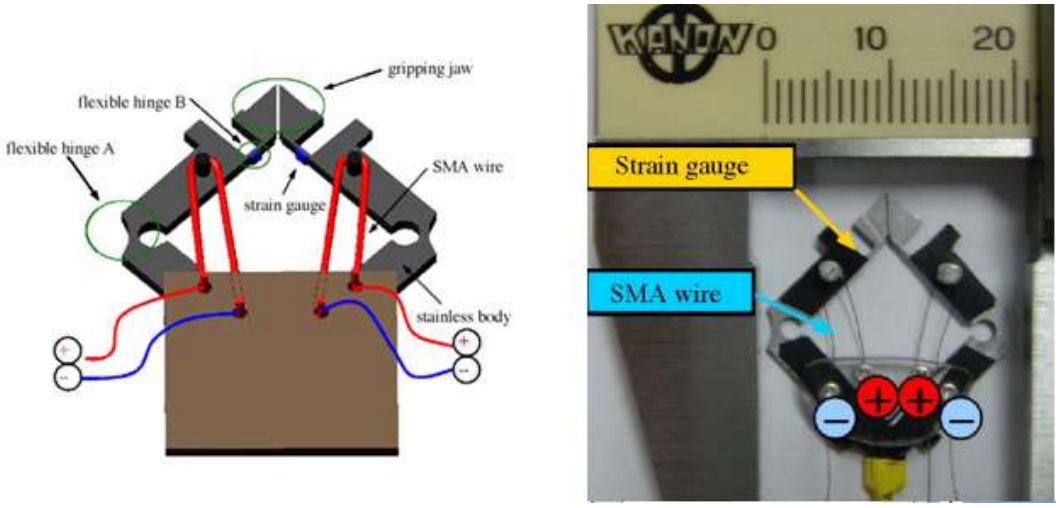

Figure 1.9: Conceptual drawing of microgripper (Left), and a fabricated microgripper (Right) (Kyung *et al*., 2008)

- *Monolithic grippers*

The mechanical structure, actuators, flexible joints and finger tips are integrated in a structure made from a single SMA material. Monolithic SMA microgrippers were supposed to overcome many defects that arise in the previous type of SMA grippers like precision in assembly, which is difficult and expensive to be achieved, is needed for these systems (Bellouard *et al*., 1998). Also, undesirable effects such as friction and interaction between parts have to draw the attention. Thus, a monolithic two way SMA microgripper was proposed by Bellouard *et al.* where a thermo-mechanical treatment (training process) to the gripper is required

(Bellouard *et al*., 1998). This device shown in Figure 1.10 achieved an opening gap by 150 µm and was demonstrated by grasping cylindrical lenses with a diameter of 250 µm and a length of 500 µm.

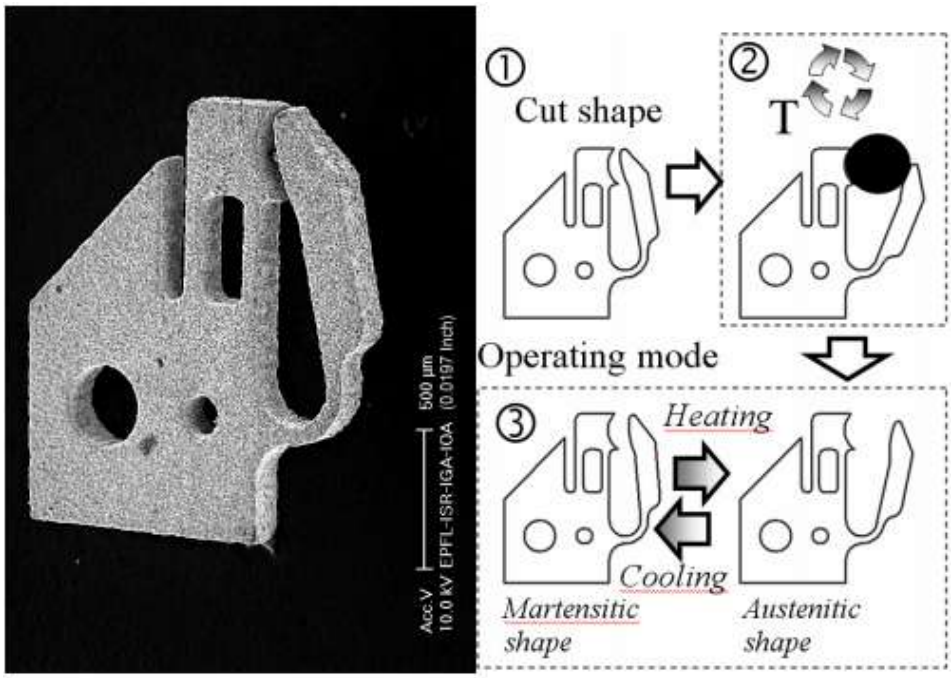

Figure 1.10: Left: Scanning Electron Microscope picture of the SMA micro-gripper for sub-millimeter lens handling. Right: the desired shape is laser cut (1) and thermo-mechanically cycled under constraint (training process) (2). The working principle is also shown (3) (Bellouard *et al*., 1998).

Another monolithic SMA microgripper was designed and fabricated by Zhang *et al.* to assemble microscopic building blocks of width of 60 µm into tissue engineering scaffolds (Zhang *et al*., 2001). All the parts were laser cut from the same Ni-Ti-Cu sheet; this device employed a localised shape memory effect obtained by heat treatment of a specific zone to actuate this zone. When an electrical current is applied to the structure to increase temperature, only the treated zone tends to return to its memorized shape generating an actuation force.

- *Antagonistic actuation*

Antagonistic structures, also called “differential” structures, are those where two actuators are used, one for opening and the other for closing the tweezers. This type of SMA microgrippers has the advantage of reducing the open - and - close time (Agnus J, 2005). Kohl *et al.* developed a microgripper of the size 2x3.9x0.1 mm^3. Two integrated actuation units working in the opposite directions to form an antagonistic pair (Kohl *et al*., 2000). The gripper comprised of two actuation units with bond pads for mechanical and electrical connection, a connection between the units, and two gripping arms. A folded-beam structure and two circular beams are the actuation units I and II, respectively. By heating unit I above the phase transformation temperature, the folded beams recover their memory shape leading to a linear movement of the link. As a consequence of that, the circular beams are deformed and the gripping arms are closed. Also, heating unit II will reset this operation leading to opening the arms. The device was manufactured by laser cutting of a cold-rolled NiTi sheet of 100 µm thickness and then mounted on a ceramic substrate by adhesive bonding. A maximum displacement of the jaws of 180 µm, gripping force of 17 mN were achieved with an open-and-close time of 32 ms during this research. Figure 1.11 shows the operational principle of the proposed device.

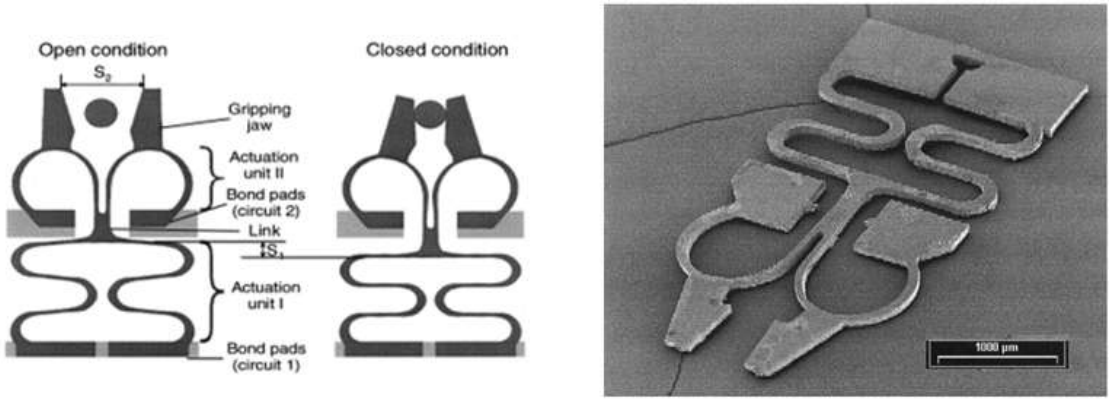

Figure 1.11: Operation principle of the SMA microgripper illustrating the two actuation units (Left), and fabricated microgripper (Right) (Kohl *et al*., 2000).

Although SMA actuators produce large force and high displacement, SMA actuators are problematic in the liquid environment due to the fact that micro devices have a very high surface-to-volume ratio and suffer from excessive heat loss. This dissipation of heat will affect the temperature in the micro-environment (Ok *et al*., 2006). Furthermore, the displacement of SMAs is hard to control because of their hard thermomechanical nonlinearities (Velazquez *et al*., 2006). Also, as SMA actuators operates as on-off actuators, it will be too complicated to precisely control the gripping force and displacement (Fu *et al*., 2012).

1.3.4 Piezoelectric Microgrippers

Piezoelectric effect was first found by Pierre and Jacques in 1880 when they observed that quartz crystals would electrically polarise when deformed by an applied force (Smith, 1976). This effect is reversible i.e. a strain will be generated on the material under an applied voltage. Thus, this displacement was used for the purpose of actuation. The main existing types of this technique were classified according to their structure of actuation into three categories:

- *Piezoelectric compliant structure grippers*

The compliant structures are structures that transfer an input force or displacement to another point through elastic body deformation (Khare *et al*., 2007). Menciassi *et al.* developed a microgripper by means of LIGA technology (German acronym for Lithography, electroplating, and molding that describes a fabrication technology used to create high-aspect-ratio microstructures), which is an expensive and long process, and introduced an amplification mechanism to overcome the drawback of the limited total displacement of such devices. A total displacement of 250 μm and a gripping force of 35 mN were obtained in this study (Menciassi *et al*., 1997). A later study achieved by Goldfarb and Celanovic aimed to design a flexure - based microgripper, Figure 1.12, actuated by a piezoelectric ceramic stack actuator (Goldfarb and Celanovic, 1999). The

displacement of the gripper was 160 µm and a gripping force of 600 mN was achieved.

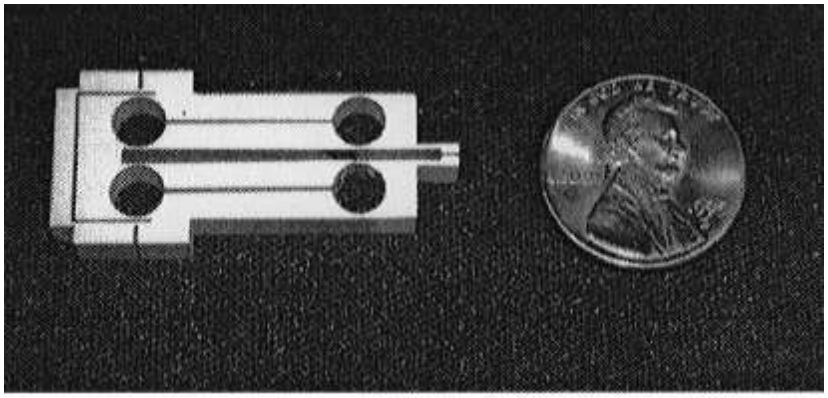

Figure 1.12: Flexure-based microgripper by (Goldfarb and Celanovic, 1999)

- *Piezoelectric bimorphs grippers*

Where the deformation of two beams that are mechanically interdependent on each other when undergoing an electric field, one will contract and the other extends (Agnus J, 2005). Seki used a piezoelectric bimorphs and adding stainless-steel finger tips. This device achieved a displacement of 400 µm under 30 V applied voltage (Seki, 2002). Chonan *et al.* developed a two-fingered parallel microgripper driven by a piezoelectric ceramic bimorph strip (Chonan *et al*., 1996). These strips were at the base of each finger while a flexible copper cantilever is located at the tip. The cantilever is driven horizontally by the bending deformation of the ceramic actuator. The output tip displacement achieved was 600 µm as a result of 50 V voltage.

A more recent study proposed piezoelectric bimorphs actuator, where the bending of the bimorphs is implemented as the microgripper fingers and each of which could be actuated separately (El-Sayed *et al*., 2013). Both fingers were fixed as cantilevers, see Figure 1.13, and driven independently by a high voltage amplifier and the deflection of the bimorphs is measured by the means of a non contact proximity sensor applied at the tip of one finger. The system achieved a tip

deflection of 500 µm as a result of an input voltage of 70 V and manipulating micro-objects down to 50 µm in size.

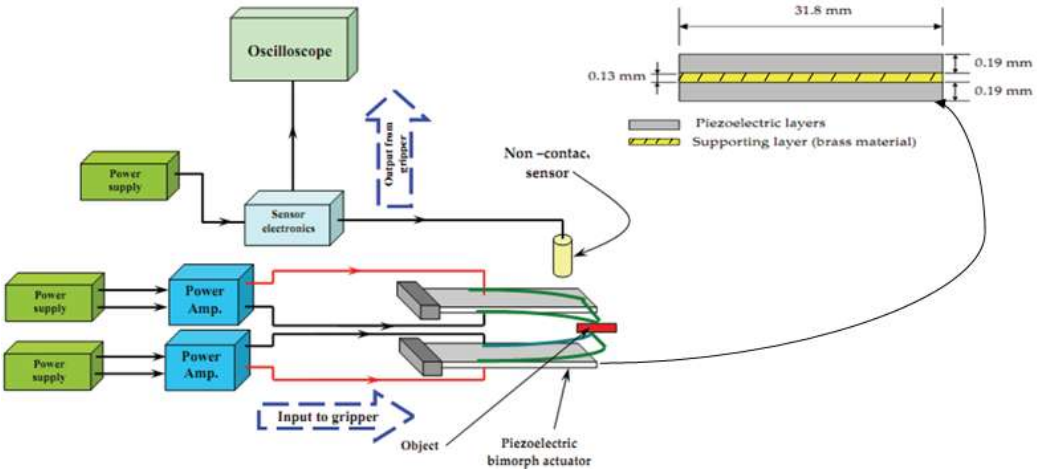

Figure 1.13: (left) Layout of developed microgripper showing the components of the gripping system and (right) cross sectional of the bimorph actuator (El-Sayed *et al*., 2013)

- *Monolithic microgrippers with localized deformation*

In this type, the whole assembly, actuator, amplification and finger tips are carried out in a massive piezoelectric plate while the electrodes are distributed on each face of ceramics to extent and contract locally a flexible structure by elastic hinges (Agnus J, 2005)**.** A monolithic compliant-flexure-based microgripper shown in Figure 1.14 was proposed by Nah (Nah and Zhong, 2007). Micro-wired electrode discharge machining was used in manufacturing the microgripper and a maximum stroke of 170 µm was achieved. Typical lead–zirconate–titanate (PZT) piezoelectric actuator was used and according to a previous study, piezoelectric actuation performed a movements with resolution on the order of a nanometer (Goldfarb and Celanovic, 1999).

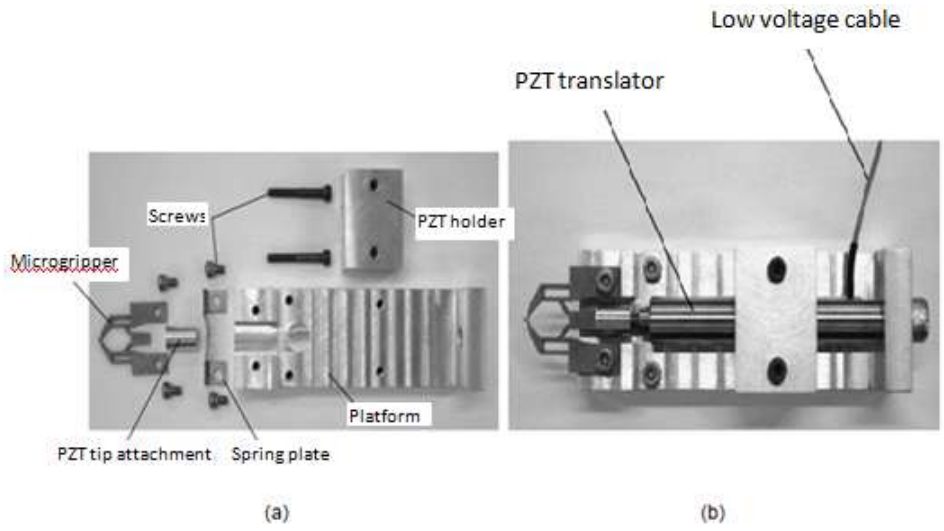

Figure 1.14:.The microgripper designed and fabricated (a) components of gripper device, (b) prototype of gripping device with a PZT translator (Nah and Zhong, 2007)

A later study by Zubir *et al.* proposed a microgripping mechanism in order to deliver high precision and accurate manipulation of micro objects (Zubir *et al*., 2009). The authors used a wire Electro-Discharge Machining (EDM) technique to fabricate the monolithic structure of the gripper mechanism. This design was tested numerically using Finite Element Analysis (FEA) and validated experimentally. The piezoelectric actuation force is transformed into rotational motion by the amplification mechanism. The bias spring will help in achieving a large deflection within elastic region and ensuring precise opening and closing manipulation. A maximum output force and displacement of 0.95 N and 350 µm, respectively, was achieved corresponding to 100 V applied voltage. This device was tested by grasping a 76.2 µm diameter wire. Figure 1.15 shows a prototype of the fabricated microgripper.

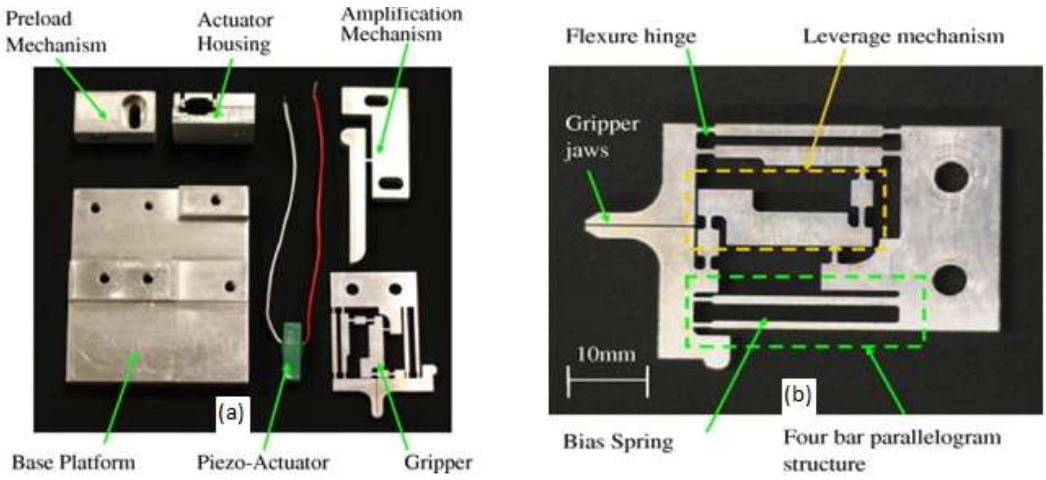

Figure 1.15: (a) Individual component of gripper mechanism, (b) Microgripper prototype (Zubir *et al.*, 2009)

A recent study reported a microgripper monolithic compliant mechanism is actuated by a stack piezoelectric ceramic actuator (SPCA) with integrated sensors for gripping force and tip displacement as in Figure 1.16 (Wang *et al*., 2013). A displacement of the microgripper was found at a magnification of 16x with respect to SPCA was achieved.

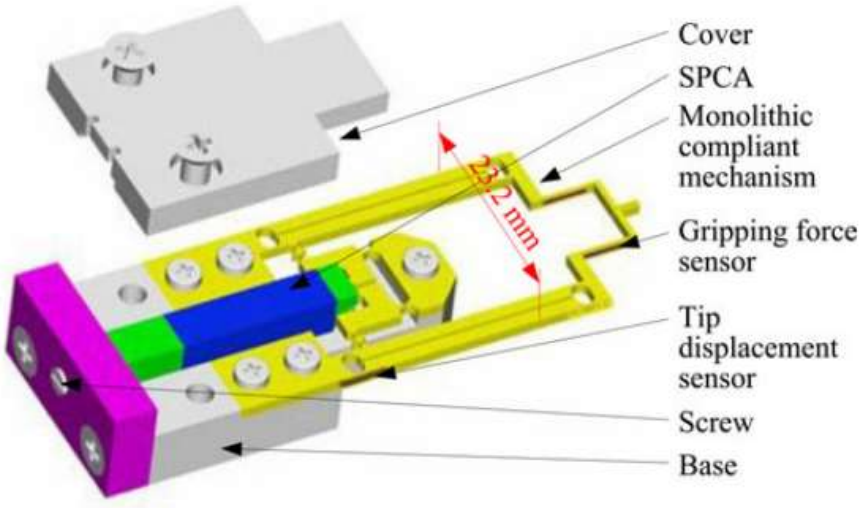

Figure 1.16: Piezoelectrically driven microgripper (Wang *et al*., 2013)

Piezoelectric actuation has been used extensively by researchers due to the advantage of their great speed and overall a high resolution (Agnus J, 2005) but, piezoelectric microgrippers suffer from limited total displacement (Menciassi *et al*., 1997). Another drawback of such technique is the high operating voltage. For example, 100 V is needed to achieve a deflection of only 4µm (Sekhar and Uwizeye, 2012).

1.3.5 Magnetic Microgrippers

This type of microgrippers uses the magnetic actuation principle. The actuating magnetic field is established by passing the current through the coil that is wounded around the core and the gripper arms open or close as a response to the magnetic field. Giourodi *et al.* developed a microgripper that was actuated electromagnetically. The microgripper's fingers and tips were fabricated using a magnetically soft iron alloy (VITROVAC 7505) which exhibits excellent soft magnetic and mechanical properties (Giouroudi *et al*., 2008). The core was crystalline FeSi sheet wounded by a double layer coil. This core was cut using EDM technology. Figure 1.17 shows the layout of the device where the normal state of the tip before actuation is open and the two tips are 250 µm apart. The opening and closing of the fingers is controlled by the applied DC current. The microgripper was tested in atmospheric conditions to pick and place optical fibers (125 µm in diameter) and bonding wires (50 µm in diameter). The maximum gripping force was 130 µN under a maximum operation DC current of 600 mA.

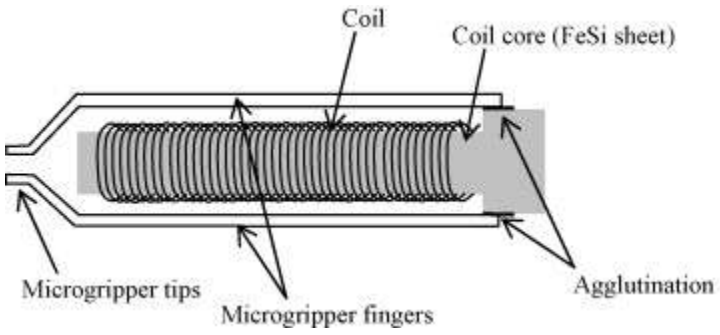

Fig. 1.17: Schematic of the developed microgripper where the tips actuated by passing the current through the wounded coil around the core (Giouroudi *et al*., 2008).

Another device based on giant magnetostrictive material (GMM) was proposed recently (Qinghua *et al*., 2010). The driving force was supplied by the expansion and contraction of GMM in magnetic field. The conceptual drawing of the microgripper is illustrated in Figure 1.18. The operation principle of this microgripper is that when current is passing through coil the to produce magnetic field, GMM will stretch and this stretch will promote the jaws around the flexible hinge towards the direction of palate producing the displacement to grip objects. However, a negative influence on the microgripper was reported due to the generated heat from the coil which induces thermal deformation of magnetostrictive rod.

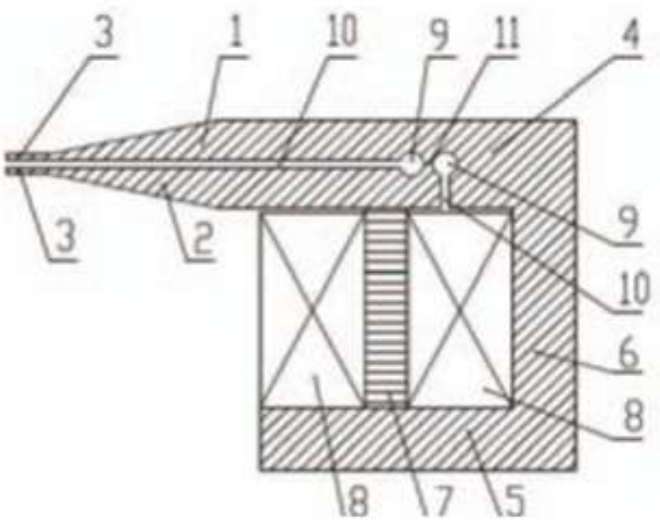

Fig. 1.18: Conceptual drawing of the microgripper, (1) Plate, (2) Microripper jaw, (3) Jaw, (4) Upper suspension arm, (5) Suspension arm, (6) Linker arm, (7) GMM rod, (8) Electromagnetic coil, (9) Circular hole, (10) Slice, and (11) Flexure hinge (Qinghua *et al*., 2010).

In fact and although such actuation source has a large output force and displacement, their performance is also limited because of the thermal dissipation by the conductive materials with significant currents passing through. Furthermore, down scaling of magnetic actuators will lead to a sharp decrease in the output performance of such actuators. Also, the presence of magnetic field becomes problematic in biological environments (Reyne, 2002).

1.3.6 Chemical Microgrippers

This type of microgripper depends mainly on converting the chemical energy into mechanical response (Biener *et al*., 2009). A microgripper actuated chemically was proposed by Randhwa *et al.* (Randhawa *et al*., 2008). Opening and closing procedures were triggered by chemicals. Adding the acetic acid (CH_3COOH) to the water will lead to dissolving of the polymer that restricts the joints to bend, and the gripper closes. Adding hydrogen peroxide (H_2O_2) to the aqueous acetic acid will dissolve the Cu layer, leading to straightening the Cr joint and consequently reopening the gripper, as shown in Figure 1.19. The proposed device demonstrated a manipulation of 200-µm diameter tubes and beads.

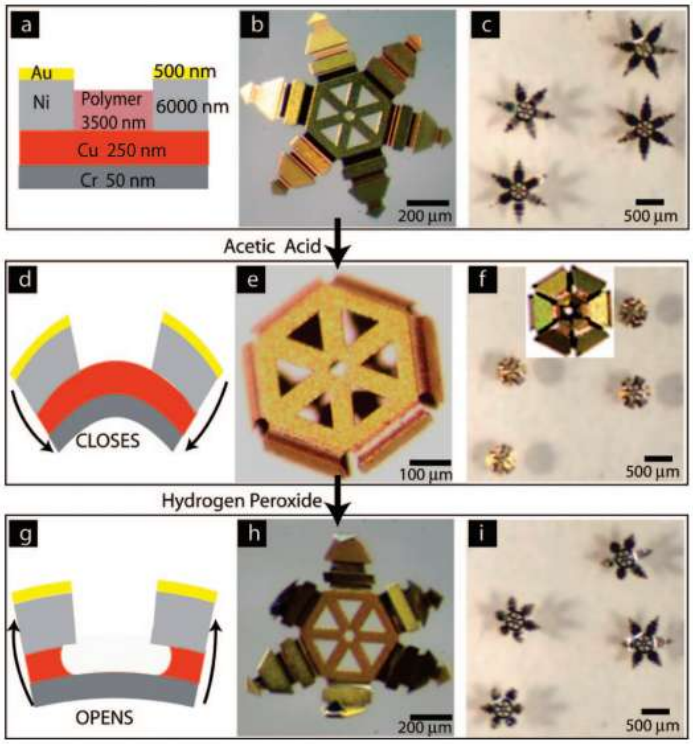

Figure 1.19: (a) Schematic diagram of the trilayer hinge joint between two Au coated Ni phalanges. Optical microscopy image of (b) a single microgripper and (c) many microgrippers in water. (d) Schematic diagram of the microgripper closing when acetic acid dissolves the polymer layer within the hinge. Optical microscopy image of (e) a single microgripper and (f) many microgrippers closing on addition of acetic acid (inset shows the view from the bottom of a closed microgripper). (g) Schematic diagram of the microgripper opening when H_2O_2 dissolves the Cu layer within the hinge. Optical microscopy image of (h) a single microgripper and (i) many microgrippers opening upon addition of H_2O_2 (Randhawa *et al*., 2008).

1.3.7 Fluidic Microgrippers

These devices *(pneumatic when using air and hydraulic when using any other fluid)* use the pressure of fluid to generate elastic deformation in flexible parts which can then return to their original configuration when the pressure is removed. Fluidic microactuators can be divided into three major categories (DeVolder M, 2010):

- Elastic fluidic microactuators

These comprise at least one component that deforms elastically under the applied pressure. Elastic fluidic actuators are common in MEMS since they are relatively easy to fabricate and are not subjected to leakage. These actuators can be sub-classified into membrane, balloon, bellows, and artificial muscles, according to the configuration of the elastic elements, as shown in Figure 1.20.

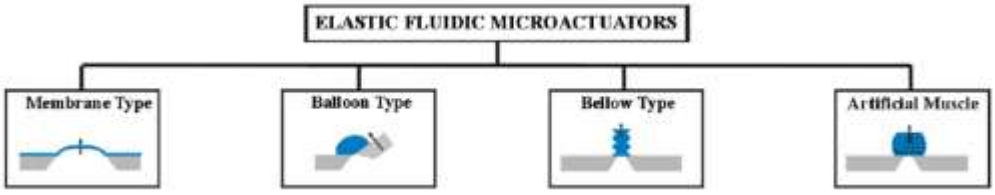

Figure 1.20: Classification of elastic actuators (DeVolder M, 2010)

- *Membrane microgripper*

These are the most widely applied fluidic actuators at the microscale. They consist of a flat or corrugated membrane that is deflected by the driving pressure. Reports on these actuators and their integration in MEMS were published as early as 1980 due to their ease in fabrication using basic silicon processing (Van De Pol *et al*., 1989, Van de Pol *et al*., 1990). However, the main limitation of membrane actuators is their limited stroke because part of the force output will be consumed by the membrane stiffness (DeVolder M, 2010), although several researchers have

presented on corrugated membrane designs to enhance the stroke of these actuators. For example, Ding *et al.* describe a square – sided boron-doped silicon corrugated diaphragm of 3 μm thickness and 1mm side that achieved 33 μm deflection at 101 KPa compared with a planar membrane of the same size, which only achieved 18 μm at the same pressure (Ding, 2002). In a separate study, a corrugated polyimide diaphragm produced similar results (Van Mullem *et al*., 2002).

- *Balloon microgripper*

These are similar to membrane actuators except that they rely on a 3D balloon to generate a bending motion. Due to the 3D shape of these actuators, their adoption in MEMS devices was a little later where it was first reported in 1999. The first balloon MEMS actuator had a diameter of 1 mm and a length of 6 mm and was fabricated by μEDM (micro-electro-discharge-machining) (Song *et al*., 1999). Achieving bending angle of 40° and a bending moment of 20 μNm at a driving pressure of 100 KPa. A similar device has been fabricated using a lithographic approach and multiple actuated joints series were added (Konishi *et al*., 2001). Another balloon microgripper was proposed by Jeong *et al.* illustrated in Figure 1.21 in which the whole structure was made of PDMS using two layers with different stiffness's to induce a bending motion under pressurization (Jeong *et al*., 2006). Each finger is 0.8 mm wide and 7 mm long achieving a bending angle of 130° at 200 KPa. Okayasu *et al.* have described a five degree of freedom flexible manipulator driven by hydraulic balloon actuators applicable to medical interventions such as neurosurgery. A certain amount of hydraulic fluid leakage was reported, but this was not harmful since the actuator was driven by using saline (Okayasu *et al*., 2003).

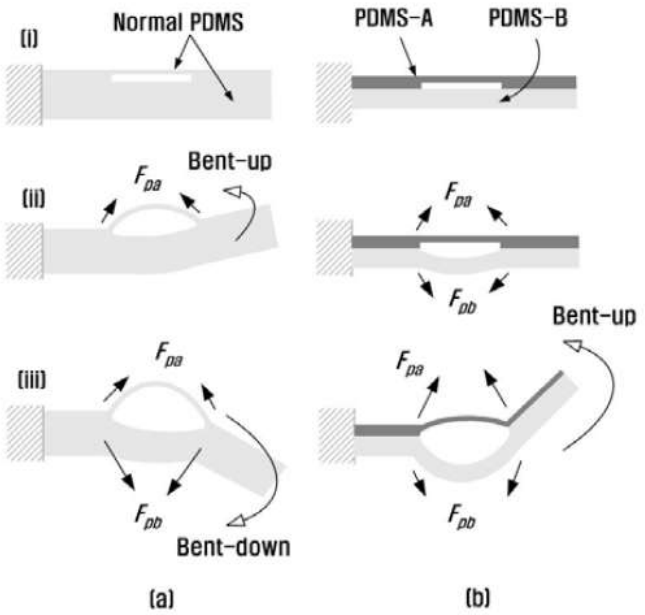

Figure 1.21: Working principle of all PDMS micro finger with balloon actuator. (a) normal PDMS structure, (b) unusual PDMS structure, [i] initial state, [ii] under low pressure, [iii] under high pressure (Jeong *et al*., 2006)

- *Bellow microgrippers*

These are again similar to membrane micro grippers except that the expansion of the membrane is focused on the corrugation in one direction rather than the isotropic expansion of the balloons used in the devices described in the previous section. Butefisch *et al.* demonstrated a Pyrex-silicon-Pyrex sandwich gripper of this kind as shown in Figure 1.22. Two Pyrex layers at the top and the bottom provide the pneumatic seal while the silicon inter-layer contains air ducts, pistons, springs, flexure hinges and cantilevers for the grippers (Bütefisch *et al*., 2002). The bellows are 6.6x5x1.5 mm^3 each, achieving a displacement of 600 µm at 12 KPa input pressure.

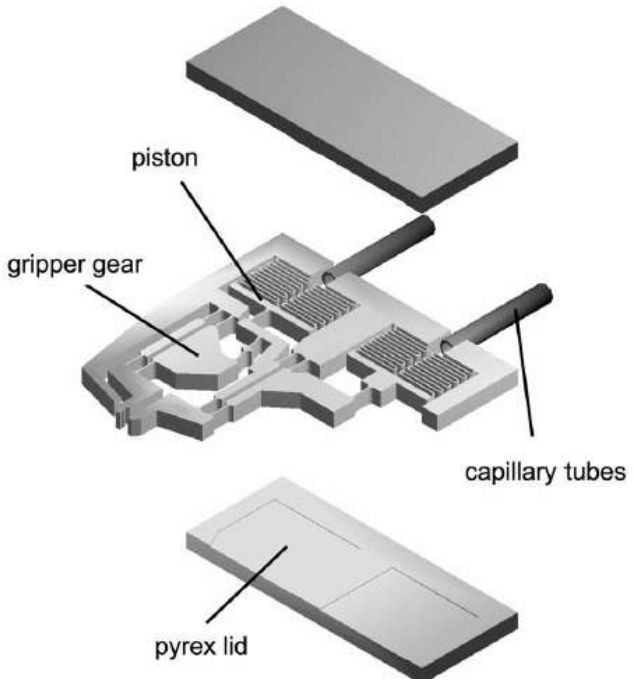

Fig. 1.22: Pneumatically driven micro-gripper showing the main component of the device (Bütefisch *et al*., 2002)

Another study developed microgripper driven by a new type of bellows-shaped micro-actuator using micro-stereolithography (MSTL) technology. This approach was demonstrated by the fabrication of two kinds of micro grippers, a two—tip microgripper and three-tip microgripper as shown in Figure 1.23 (a) and (b), respectively (Kang *et al*., 2006). Displacement up to 300 µm was achieved at a pressure of 600 KPa for one single fold.

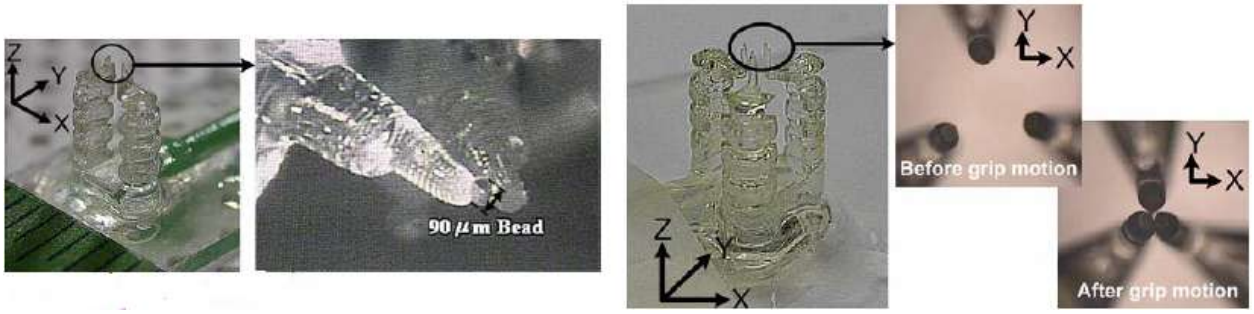

(a) **(b)**

Figure 1.23: (a) Two-tip micro-gripper, (b)Three-tip micro-gripper (Kang *et al*., 2006).

- *Artificial muscles microgripper*

The actuation principle of these micro grippers is similar to biological muscles, where a flexible balloon is equipped with embedded fibers that transform the expansion of the balloon into a contraction force (DeVolder M, 2010). McKibben actuators are of the most popular artificial muscle actuators and are well-known in large scale robotic devices because their force-stroke characteristics are similar to those of biological muscles (Colbrunn et al., 2001, Klute and Hannaford, 2000). They comprise an expandable bladder inside covered by nonelastic tabular mesh. De Volder *et al*. have reported one of the smallest McKibben actuators to date with an outside diameter of 1.5 mm and a length of 22 mm illustrated in figure 1.24 (De Volder *et al*., 2011). A major disadvantage of McKibben Muscles is the limited displacement and the needed energy to deform the elastic membrane or tube, which consequently lowers the output force (Daerden and Lefeber, 2002).

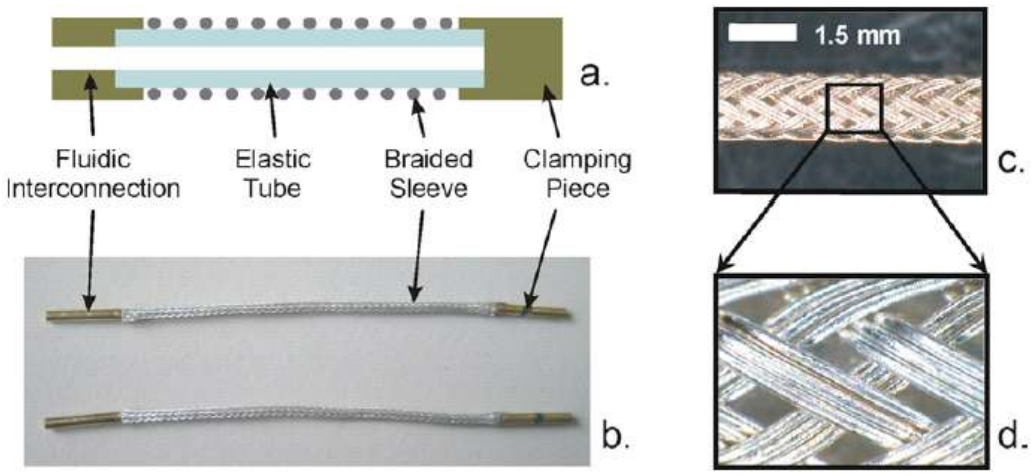

Figure 1.24: a) schematic cross-section of the actuator,b) overview of the actuator, c&d) close-up the actuator (De Volder *et al*., 2011)

- Piston-cylinder fluidic actuators

They are the most common types of large-scale actuator because they can develop high actuation forces and strokes. They are rarely used in microsystems, mainly because they require low friction microseals which are challenging to fabricate. Martinez and Panepucci proposed a microgripper actuated by this principle to manipulate structures in the range of 5 to 50 µm as illustrated in Figure 1.25 (Martinez and Panepucci, 2007). Pushing and pulling the backbone will result in opening and closing of the gripping elements.

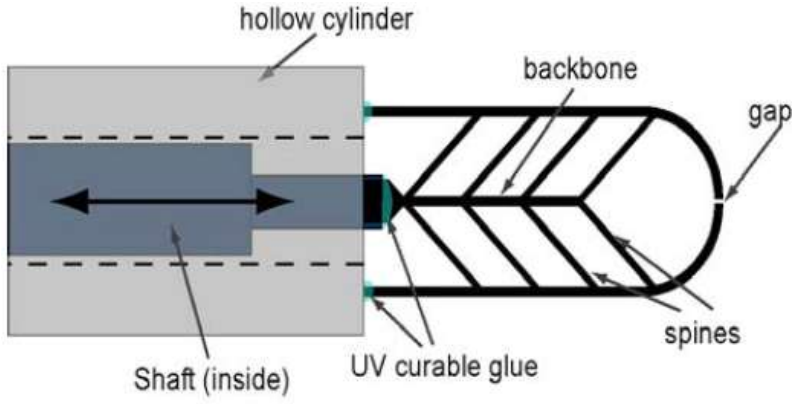

Figure 1.25: Microgripper diagram, where the moving shaft pushs and pulls the backbone to open and close the gripper (Martinez and Panepucci, 2007).

- Drag-based fluidic actuators

This type of actuator uses the drag force exerted by flowing fluids, such as in turbines. This viscous force is usually used for both driving and bearing the actuator, resulting in a smooth actuation motion. Nevertheless, the actuation force of these actuators is usually low in comparison with the former two actuator configurations and they are again difficult to fabricate at the microscale.

1.4 Research Objectives

In the foregoing, a range of studies on a variety of designs have been reviewed in the field of handling microparts. One of the most important factors in comparing devices to each other is the actuation method used. For example, studies on fluidic actuation have shown promise in a number of different aspects. Despit this, fluidic microactuators with their large forces and power densities are still neglected in MEMS although they have been studied extensively over the past 20 years for applications in microfluidics and micro total analysis systems (μTAS) (DeVolder M, 2010). It has been demonstrated that such actuators produce among the highest force and power densities available at the microscale (DeVolder M, 2010). Low fabrication cost and straightforward fabrication processes compared with other actuators make them an attractive prospect for the application in this thesis. Selection of driving fluid plays an important role in the performance of a micro gripper, high compressibility and low viscosity being the main difference between pneumatics and hydraulics, which gives the advantage to hydraulic systems in achieving more accurate positioning. On the other hand, higher flow rates can be generated when using pneumatic systems due to their compressibility. Also, pneumatic systems are lighter than hydraulics and have different leakage implications to hydraulics.

In this thesis, a range of controllable, pneumatically-driven microgrippers are designed, fabricated, and tested with the target for bio-manipulation.

Characterization of the devices is carried out to obtain a scalable design for the opening of the jaws of the microgripper and assessment of the gripping force. The overall aim is the development of a design approach for families of scalable microgrippers for biological manipulation including tactile feedback. Hence, the main objectives for this study are to develop a series of low-cost microgrippers to prototype stage with the following features:

- Scalable design
- Easy to fabricate
- Controllable in terms of output force and displacement
- Compatible with biological environment
- Able to operate in aqueous media

For the above mentioned demands, PMMA was the best choice for prototyping of the developed microgrippers as it is low cost, widely available, easy in laser cutting, and its compatibility with biological environment.

1.5 Outline

The thesis contains 7 chapters and organized as follows:

Chapter 1 presents a general introduction to the manipulation techniques used so far and the advantages and disadvantages of each technique. Also, a review of the state-of-art of microgrippers and their categorization according to their actuation mechanism is presented in this chapter as well.

Chapter 2 describes the experimental techniques that have been implemented during the processes of fabrication and characterization of the proposed devices.

Chapter 3 reports on the design, fabrication and testing of a scalable, pneumatic, syringe-actuated polymeric microgripper.

Chapters 4 and 5 cover the design, fabrication and testing of a pneumatically-driven micro-cantilever. This cantilever design forms the basis of a series of grippers for micro-manipulation (Chapter 4) and sensing (Chapter 5).

Chapter 6 presents the realisation and testing of a novel design of compliant mechanism giving true parallel motion at the gripper faces and adapted to the microscale. This design is adapted to fabrication at the microscale and is demonstrated for fine control applications.

Chapter 7 summarizes the main conclusions of this research and discusses the future potential.

1.6 References

AGNUS, J., Nectoux, P., and Chaillet, N. 2005. Overview of microgrippers and design of a micromanipulation station based on a MMOC microgripper. *In Computational Intelligence in Robotics and Automation, 2005. CIRA 2005. Proceedings. 2005 IEEE International Symposium on*, pp. 117-123. IEEE, 2005.

ASHKIN, A. & DZIEDZIC, J. 1987. Optical trapping and manipulation of viruses and bacteria. *Science,* 235**,** 1517-1520.

ASHKIN, A., DZIEDZIC, J., BJORKHOLM, J. & CHU, S. 1986. Observation of a single-beam gradient force optical trap for dielectric particles. *Optics letters,* 11**,** 288-290.

ASHKIN, A., DZIEDZIC, J. & YAMANE, T. 1987. Optical trapping and manipulation of single cells using infrared laser beams. *Nature,* 330**,** 769-771.

BAO, G. & SURESH, S. 2003. Cell and molecular mechanics of biological materials. *Nature materials,* 2**,** 715-725.

BELLOUARD, Y., CLAVEL, R., GOTTHARDT, R., BIDAUX, J. E. & SIDLER, T. 1998. A new concept of monolithic shape memory alloy micro-devices used in micro-robotics. In *Proc. Actuator*, vol. 98, pp. 499-502. 1998.

BIENER, J., WITTSTOCK, A., ZEPEDA-RUIZ, L., BIENER, M., ZIELASEK, V., KRAMER, D., VISWANATH, R., WEISSMÜLLER, J., BÄUMER, M. & HAMZA, A. 2009. Surface-chemistry-driven actuation in nanoporous gold. *Nature materials,* 8**,** 47-51.

BUICAN, T. N., SMYTH, M. J., CRISSMAN, H. A., SALZMAN, G. C., STEWART, C. C. & MARTIN, J. C. 1987. Automated single-cell manipulation and sorting by light trapping. *Applied Optics,* 26**,** 5311-5316.

BÜTEFISCH, S., POKAR, G., BÜTTGENBACH, S. & HESSELBACH, J. 2000. A new SMA actuated miniature silicon gripper for micro assembly. *Transducers & Systems (Sensor'99),* 2**,** 321-326.

BÜTEFISCH, S., SEIDEMANN, V. & BÜTTGENBACH, S. 2002. Novel micro-pneumatic actuator for MEMS. *Sensors and Actuators A: Physical,* 97**,** 638-645.

CHAN, H.-Y. and LI, W. J. 2003. A thermally actuated polymer micro robotic gripper for manipulation of biological cells." In *Robotics and Automation, 2003. Proceedings. ICRA'03. IEEE International Conference on,* vol. 1, pp. 288-293. IEEE, 2003.

CHEN G, and Xinhan, H. 2004. Research on vacuum micro-gripper of intelligent micromanipulation robots. In *Robotics and Biomimetics, 2004. ROBIO 2004. IEEE International Conference on,* pp. 279-283. IEEE, 2004.

CHEN T, S. L., CHEN L, RONG W, LI X 2010. A hybrid-type electrostatically driven microgripper with an integrated vacuum tool. *Sensors and Actuators,* 158**,** 320-327.

CHONAN, S., JIANG, Z. W. & KOSEKI, M. 1996. Soft-handling gripper driven by piezoceramic bimorph strips. *Smart Materials and Structures,* 5**,** 407-414.

COLBRUNN, R. W., NELSON, G. M. and QUINN, R. D. 2001. Modeling of braided pneumatic actuators for robotic control. *In Intelligent Robots and Systems, 2001. Proceedings. 2001 IEEE/RSJ International Conference on*, vol. 4, pp. 1964-1970. IEEE, 2001.

DAERDEN, F. & LEFEBER, D. 2002. Pneumatic artificial muscles: actuators for robotics and automation. *European journal of mechanical and environmental engineering,* 47**,** 11-21.

DE VOLDER, M., MOERS, A. J. M. & REYNAERTS, D. 2011. Fabrication and control of miniature McKibben actuators. *Sensors and Actuators A: Physical*, *166*(1), 111-116.

DESAI, J. P., PILLARISETTI, A. and BROOKS, A. D. 2007. Engineering approaches to biomanipulation. *Annu. Rev. Biomed. Eng.,* 9**,** 35-53.

DEVOLDER M, R. D. 2010. Pneumatic and hydraulic microactuators: a review. *Micromechanics Microengineering,* 20**,** 18pp.

DING, X. "Behavior and application of silicon diaphragms with a boss and corrugations." In *Solid-State Sensor and Actuator Workshop, 1992. 5th Technical Digest., IEEE,* pp. 166-169. IEEE, 1992.

EL-SAYED, A. M., ABO-ISMAIL, A., EL-MELEGY, M. T., HAMZAID, N. A. & OSMAN, N. A. A. 2013. Development of a Micro-Gripper Using Piezoelectric Bimorphs. *Sensors,* 13**,** 5826-5840.

FU, Y., LUO, J., ONG, S., ZHANG, S., FLEWITT, A. & MILNE, W. 2008. A shape memory microcage of TiNi/DLC films for biological applications. *Journal of micromechanics and microengineering,* 18**,** 035026.

FU, Y. Q., LUO, J. K., FLEWITT, A. J. & MILNE, W. I. 2012. Smart Microgrippers for BioMEMS Applications. *In:* VASUDEV, S. B. A. A. (ed.) *MEMS for Biomedical Applications.* 1ST ed.: WOODHEAD PUBLISHING.

GIOUROUDI, I., HÖTZENDORFER, H., KOSEL, J., ANDRIJASEVIC, D. & BRENNER, W. 2008. Development of a microgripping system for handling of microcomponents. *Precision Engineering,* 32**,** 148-152.

GOLDFARB, M. & CELANOVIC, N. 1999. A flexure-based gripper for small-scale manipulation. *Robotica,* 17**,** 181-187.

GRAYSON, A. R., SHAWGO, R. S., JOHNSON, A. M., FLYNN, N. T., LI, Y., CIMA, M. J. & LANGER, R. 2004. A BioMEMS review: MEMS technology for physiologically integrated devices. *Proceedings of the IEEE,* 92**,** 6-21.

HOCHE, J. H., BUETTGENBACH, S., PITTSCHELLIS, R. & HESSELBACH, J. Silicon microgripper for microassembly realized by photolithography and fast anisotropic silicon etching." In *Photonics East (ISAM, VVDC, IEMB)*, pp. 13-21. International Society for Optics and Photonics, 1998.

HOCHMUTH, R. M. 2000. Micropipette aspiration of living cells. *Journal of biomechanics,* 33**,** 15-22.

HUNG, E. S. & SENTURIA, S. D. 1999. Extending the travel range of analog-tuned electrostatic actuators. *Journal of Microelectromechanical Systems,* 8**,** 497-505.

JAGER, E. W., INGANÄS, O. & LUNDSTRÖM, I. 2000. Microrobots for micrometer-size objects in aqueous media: potential tools for single-cell manipulation. *Science,* 288**,** 2335-2338.

JEONG, O. C., KUSUDA, S., SAKAKIBARA, T., KONISHI, S. & NOKATA, M. 2005. Pneumatic micro finger as end effecter of robot. In *Micro-NanoMechatronics and Human Science, 2005 IEEE International Symposium on* (pp. 145-148). IEEE

JIA, Y. & XU, Q. 2013. MEMS microgripper actuators and sensors: the state-of-the-art survey. *Recent Patents on Mechanical Engineering,* 6**,** 132-142.

JÖNSSON, H., HOLM, C., NILSSON, A., PETERSSON, F., JOHNSSON, P. & LAURELL, T. 2004. Particle separation using ultrasound can radically reduce embolic load to brain after cardiac surgery. *The Annals of thoracic surgery,* 78**,** 1572-1577.

JUAN, M. L., RIGHINI, M. & QUIDANT, R. 2011. Plasmon nano-optical tweezers. *Nature Photonics,* 5**,** 349-356.

KANG, H. W., LEE, I. H. & CHO, D. W. 2006. Development of a micro-bellows actuator using micro-stereolithography technology. *Microelectronic Engineering,* 83**,** 1201-1204.

KHARE, P., MADHAB, G. B., KUMAR, C. S. & MISHRA, P. K. Optimizing Design of Piezoelectric Actuated Compliant Microgripper Mechanism. 2007. *In:* 13th National Conference on Mechanisms and Machines, 2007 Bangalore, India.

KIM, D.-H., WONG, P. K., PARK, J., LEVCHENKO, A. & SUN, Y. 2009. Microengineered platforms for cell mechanobiology. *Annual review of biomedical engineering,* 11**,** 203-233.

KLUTE, G. K. & HANNAFORD, B. 2000. Accounting for elastic energy storage in McKibben artificial muscle actuators. *Journal of dynamic systems, measurement, and control,* 122**,** 386-388.

KOHL, M., JUST, E., PFLEGING, W. & MIYAZAKI, S. 2000. SMA microgripper with integrated antagonism. *Sensors and actuators A: Physical,* 83**,** 208-213.

KÖNIG, K., LIANG, H., BERNS, M. & TROMBERG, B. 1996. Cell damage in near-infrared multimode optical traps as a result of multiphoton absorption. *Optics letters,* 21**,** 1090-1092.

KONISHI, S., KAWAI, F. & CUSIN, P. 2001. Thin flexible end-effector using pneumatic balloon actuator. *Sensors and Actuators A: Physical,* 89**,** 28-35.

KOZUKA, T., YASUI, K., TUZIUTI, T., TOWATA, A. & IIDA, Y. 2008. Acoustic standing-wave field for manipulation in air. *Japanese Journal of Applied Physics,* 47**,** 4336-4338.

KYUNG, J. H., KO, B. G., HA, Y. H. & CHUNG, G. J. 2008. Design of a microgripper for micromanipulation of microcomponents using SMA wires and flexible hinges. *Sensors and Actuators A: Physical,* 141**,** 144-150.

LANG, M. J. & BLOCK, S. M. 2003. Resource Letter: LBOT-1: Laser-based optical tweezers. *American journal of physics,* 71**,** 201-215.

LEE, A. P., CIARLO, D. R., KRULEVITCH, P. A., LEHEW, S., TREVINO, J. & NORTHRUP, M. A. 1996. A practical microgripper by fine alignment, eutectic bonding and SMA actuation. *Sensors and Actuators A: Physical,* 54**,** 755-759.

LEE, S., CHA, H., LEE, S. & KIM, Y. 1994. Development of cell-grabber by using piezo actuator. *In:* Engineering in Medicine and Biology Society, 1994. Engineering Advances: New Opportunities for Biomedical Engineers. Proceedings of the 16th Annual International Conference of the IEEE, 1994. IEEE, 1021-1022.

LEVSKY, J. M. & SINGER, R. H. 2003. Gene expression and the myth of the average cell. *Trends in cell biology,* 13**,** 4-6.

LI, X., CHEAH, C. C., HU, S. & SUN, D. 2013. Dynamic trapping and manipulation of biological cells with optical tweezers. *Automatica, 49 (6),* p: 1614-1625.

MACKENZIE, M. H., AN, N. M., GIERE, M. D., STORI, J. A. & WRIGHT, P. J. 1996 . Experiences with shape memory alloy: robot grippers for submillimeter hard disk drive components." In *Photonics East'96*, pp. 25-36. International Society for Optics and Photonics

MARTINEZ, J. & PANEPUCCI, R. 2007. Design, Fabrication, and Characterization of a Microgripper Device. *In:* Florida Conference on Recent Advances in Robotics, 2007 Florida.

MENCIASSI, A., CARROZZA, M., RISTORI, C., ROSSI, V., TIEZZI, G. & DARIO, P. 1997. Microgrippers with piezoelectric actuators for a micromanipulation workstation. In *2nd Italian Conference on Sensors and Microsystems. Artificial and Natural Perception* (pp. 333-337).

NAH, S. K. & ZHONG, Z. W. 2007. A microgripper using piezoelectric actuation for micro-object manipulation. *Sensors and Actuators A: Physical,* 133**,** 218-224.

OK, J., LU, Y. W. & KIM, C. J. 2006. Pneumatically driven microcage for microbe manipulation in a biological liquid environment. *Journal of Microelectromechanical Systems,* 15**,** 1499-1505.

OKAYASU, H., OKAMOTO, J., FUJIE, M. G., UMEZU, M. & ISEKI, H. 2003. Development of a hydraulic-driven flexible manipulator for neurosurgery. In*International Congress Series* (Vol. 1256, pp. 607-612). Elsevier

PETERSSON, F., NILSSON, A., HOLM, C., JÖNSSON, H. & LAURELL, T. 2005. Continuous separation of lipid particles from erythrocytes by means of laminar flow and acoustic standing wave forces. *Lab on a Chip,* 5**,** 20-22.

PETROVIC D, E. A. 2002. Gripping tools for handling and assembly of microcomponents." In *Proc. 23rd International Conference on Microelectronics (Miel 2002),* vol. 1, pp. 247-50.

PIGGEE, C. 2008. Optical tweezers: not just for physicists anymore. *Analytical Chemistry,* 81**,** 16-19.

POLLA, D. L., ERDMAN, A. G., ROBBINS, W. P., MARKUS, D. T., DIAZ-DIAZ, J., RIZQ, R., NAM, Y., BRICKNER, H. T., WANG, A. & KRULEVITCH, P. 2000. Microdevices in Medicine 1. *Annual review of biomedical engineering,* 2**,** 551-576.

QINGHUA, C., QUANGUO, L., JIANWU, Y. & DEHUI, L. 2010. Design of new microgripper based on GMM. In *2010 International Conference on Mechanic Automation and Control Engineering* (pp. 3694-3697).

RANDHAWA, J. S., LEONG, T. G., BASSIK, N., BENSON, B. R., JOCHMANS, M. T. & GRACIAS, D. H. 2008. Pick-and-place using chemically actuated microgrippers. *Journal of the American Chemical Society,* 130**,** 17238-17239.

REYNE, G. 2002. Electromagnetic actuation for MOEMS, examples, advantages and drawbacks of MAGMAS. *Journal of magnetism and magnetic materials,* 242**,** 1119-1125.

RUSSELL, R. A. 1994. A robotic system for performing sub-millemetre grasping and manipulation tasks. *Robotics and autonomous systems,* 13**,** 209-218.

SATO, M., LEVESQUE, M. J. & NEREM, R. M. 1987. Micropipette aspiration of cultured bovine aortic endothelial cells exposed to shear stress. *Arteriosclerosis, Thrombosis, and Vascular Biology,* 7**,** 276-286.

SEKHAR, P. K. & UWIZEYE, V. 2012. Review of sensor and actuator mechanisms for bioMEMS. *In:* BHANSALI, S. & VASUDEV, A. (eds.) *MEMS for biomedical applications.* Elsevier.

SEKI, H. 1992. Modeling and impedance control of a piezoelectric bimorph microgripper. In *Intelligent Robots and Systems, 1992., Proceedings of the 1992 lEEE/RSJ International Conference on* (Vol. 2, pp. 958-965). IEEE.

Smith, W. R. 1976. Basics of the SAW interdigital transducer. *Wave Electronics, 2,* 25-63.

SOLANO, B. & WOOD, D. 2007. Design and testing of a polymeric microgripper for cell manipulation. *Microelectronic Engineering*, 84**,** 1219-1222.

SONG, X., REYNAERTS, D., MEEUSEN, W. & VAN BRUSSEL, H. 1999. Micro-EDM for silicon microstructure fabrication. In *Design, Test, and Microfabrication of MEMS/MOEMS* (pp. 792-799). International Society for Optics and Photonics.

VAN DE POL, F. C. M., VAN LINTEL, H. T. G., ELWENSPOEK, M. & FLUITMAN, J. H. J. 1990. A thermopneumatic micropump based on micro-engineering techniques. *Sensors and Actuators A: Physical,* 21**,** 198-202.

VAN DE POL, F. C. M., WONNINK, D. G. J., ELWENSPOEK, M. & FLUITMAN, J. H. J. 1989. A thermo-pneumatic actuation principle for a microminiature pump and other micromechanical devices. *Sensors and Actuators,* 17**,** 139-143.

VAN MULLEM, C. J., GABRIEL, K. J. & FUJITA, H. 1991. Large deflection performance of surface micromachined corrugated diaphragms. *In*, Proceedings of the Transducers '91: Dig. Tech. Papers, International Conference on Solid-State Sensors and Actuators, San Francisco, pp. 1014-1017

VELAZQUEZ, R., PISSALOUX, E., HAFEZ, M. & SZEWCZYK, J. 2005. A low-cost highly-portable tactile display based on shape memory alloy micro-actuators. In *Virtual Environments, Human-Computer Interfaces and Measurement Systems, 2005. VECIMS 2005. Proceedings of the 2005 IEEE International Conference on* (pp.121-126). IEEE.

VOLDMAN, J. 2006. Electrical forces for microscale cell manipulation. *Annu. Rev. Biomed. Eng.,* 8**,** 425-454.

VOLDMAN, J., GRAY, M. L. & SCHMIDT, M. A. 1999. Microfabrication in biology and medicine. *Annual review of biomedical engineering,* 1**,** 401-425.

WANG, D., YANG, Q. & DONG, H. 2013. A monolithic compliant piezoelectric-driven microgripper: Design, modeling, and testing. *Mechatronics, IEEE/ASME Transactions on*, *18*(1), 138-147.

WANG, X., CHEN, S., KONG, M., WANG, Z., COSTA, K. D., LI, R. A. & SUN, D. 2011. Enhanced cell sorting and manipulation with combined optical tweezer and microfluidic chip technologies. *Lab on a Chip,* 11**,** 3656-3662.

YI, C., LI, C.-W., JI, S. & YANG, M. 2006. Microfluidics technology for manipulation and analysis of biological cells. *Analytica Chimica Acta,* 560**,** 1-23.

YUN, H., KIM, K. & LEE, W. G. 2013. Cell manipulation in microfluidics. *Biofabrication,* 5**,** 022001.

ZEMAN M, B. V., KNOPF G 2006. Design, kinematic modeling and performance testing of an electro-thermally driven microgripper for micromanipulation applications. *Micromechanics and Microengineering,* 16**,** 1540-1549.

ZESCH W, B. M., WEBER A. 1997. Vacuum tool for handling microobjects with a nanorobot. In *Robotics and Automation, 1997. Proceedings., 1997 IEEE International Conference on* (Vol. 2, pp. 1761-1766). IEEE.

ZHANG, H., BELLOUARD, Y., SIDLER, T. C., BURDET, E., POO, A. N. & CLAVEL, R. 2001. Monolithic Shape Memory Alloy microgripper for 3D assembly of tissue engineering scaffolds. In *Intelligent Systems and Advanced Manufacturing* (pp. 50-60). International Society for Optics and Photonics.

ZHANG, H. & LIU, K.-K. 2008. Optical tweezers for single cells. *Journal of the Royal Society interface,* 5**,** 671-690.

ZHANG, W.-M., MENG, G. & CHEN, D. 2007. Stability, nonlinearity and reliability of electrostatically actuated MEMS devices. *Sensors,* 7**,** 760-796.

ZHENG, X., CHEN, X., KIM, J.-K. & LEE, D.-W. 2011. Analysis on microfinger with grooved patterns and its application in electric–thermal microgripper. *The International Journal of Advanced Manufacturing Technology,* 56**,** 505-513.

ZUBIR, M. N. M., SHIRINZADEH, B. & TIAN, Y. 2009. A new design of piezoelectric driven compliant-based microgripper for micromanipulation. *Mechanism and Machine Theory,* 44**,** 2248-2264.

Chapter 2: Experimental Techniques

The experimental techniques involved in this research are to fabricate, characterize, and demonstrate the gripping devices. In this chapter, the different procedures involved in fabricating the devices are presented. Also, new approaches have been developed to characterize the prototype devices, and these are explained in this chapter. The various readout techniques, which play a crucial role in characterizing any cantilever system, and other aspects of instrumentation involved in demonstrating the devices are also presented in this chapter.

2.1 Fabrication of Microgrippers

Two different techniques of fabrication were used in this research, laser (light amplification by stimulated emission of radiation) cutting and photo-etching technology.

2.1.1 Laser Micro- Machining

Laser micromachining was an essential tool in the design, development, and fabrication of many parts of actuators and microgrippers reported in this thesis. Laser machining is one of the most widely used means for complex machining processes. It is applicable for almost a whole range of materials (Dubey and Yadava, 2008). Moreover, due to its precision and high intensity, laser machining has a wide application in fine cutting without affecting the machined parts (Choudhury and Shirley, 2010). Also, because it is a subtractive technique, laser cutting can be used on bulk-produced materials thus offering a better control over structural properties such as strength and elastic modulus and the potential for low defect contents.

- *Carbon dioxide (CO2) laser*

Carbon dioxide lasers ($CO2_)$, with wavelength of 10 µm, is one of the most widely used types among different types of laser machining (Dubey and Yadava, 2008). They are the highest power continuous wave lasers and it was found that for fine cutting of sheet metals, CO2 lasers are more suitable to be used. Also, other advantages such as the high average of beam power and quality, and the better efficiency should be considered (Tabata *et al*., 1996). $CO2_, N_2$, and He are the gases comprising CO2 lasers. They are mixed and led into a discharge tube and travel through the tube and pumped out of the other end by a mechanical forepump. While the left full mirror is fully reflective, the right one is partially transmitting creating a laser radiates at 10.6 microns.

Fabrication of the prototype of microgripper in chapter 3 was performed using a maskless laser microfabrication procedure. Polymethyl-methacrylate (PMMA) sheet was cut using a TROTEC Speedy 300^{TM} CO2 laser cutter, shown in Figure 2.1, with a 120W maximum power and a large workspace area. PMMA was used here as it is relatively inexpensive and polymer materials are generally more easily worked by laser cutting (Choudhury and Shirley, 2010). The best parameters were found for the cutting of 1mm thick PMMA was 8 W power and 0.25 mm/s using several passes to ensure clean and precise cut without burning. Under these conditions, the cut can be reproduced with an edge precision of 50 µm. However, despite of its capability of rapid prototyping, such laser cutter is not sufficient for cutting thick metals as high power is required for such procedure.

Figure 2.1: CO2 laser system; (a) TROTEC Speedy 300^{TM} laser system, (b) Control panel of the system, (c) Workspace

- *Picosecond laser*

The picosecond laser is a Trumpf Tru Micro 5x50 as illustrated in Figure 2.2. A solid state laser that is an oscillator that is mode-locked with an amplifier and diode pumped with a thin disk laser. Mode locking is the technique of creating a pulsed laser capable of pulses with an extremely short duration.

It could be operated in three wavelengths, 1064 nm (IR), 532 nm (Green), and 355 nm (UV). 125 µJ and 400 KHz are the maximum pulse energy and repetition rate, respectively, in IR wavelength range therefore creating a 50 W average power. In the green wavelength range, the maximum power is 30 W that makes the pulse energy 75 µJ. in the UV, the maximum power is 14 W with 35 µJ pulse energy. These values are maximum values and can be modified as the modification takes place in the software.

Figure 2.2: Trumpf TruMicro picosecond laser

Positioning the work piece is achieved using three axis linear stages (Aerotech) that are controlled via a software interface as programs could be written to achieve movements in a specific order. These stages are driven by a screw and a servo motor and the accuracy is limited to ± 6µm in Z-axis, ±8µm in Y-axis, and ±16 µm in X-axis. Under these conditions, the cut can be reproduced with an edge precision of 15 µm.

2.1.2 Photoetching Machining

Photoetching, which is also known as photo-chemical machining, is a non-traditional manufacturing procedure combining photoresist imaging and chemical etching (Roy *et al*., 2004). Photoetching is typically producing parts that are thin, flat, and complex. It has the advantage of the fast and cost effective procedure over traditional manufacturing processes and produces high precise parts (Roy *et al*., 2004). This procedure starts by coating a cleaned metal with a photo-resist making the metal photo-sensitive. Then, the coated sheet is exposed to ultraviolet (UV) light. The UV light hits the photo-sensitive resist and hardens. The black photo tool will reflect the UV light and the photo-sensitive resist remains soft. These soft areas are then removed from the developed metal producing areas of bare metal that will be etched away. The remaining areas of photo-resist cover the parts that will remain at the end of the etching process. Etching process takes place after that, where an acid attacks the bare metal. Upon the completion of the etching process, the photo resist is removed leaving a clean etched part. The photo-etching processes are illustrated in the following figure, see Figure 2.3. However, the main disadvantage of this technique is that it is not very effective at creating shapes that are not flat. Moreover, this procedure requires extremely clean operation conditions. In this procedure, a negative photo-resist, dry film, was used to implement this procedure as the adhesion to various substrates for such photo-resists is better than for the positive ones.

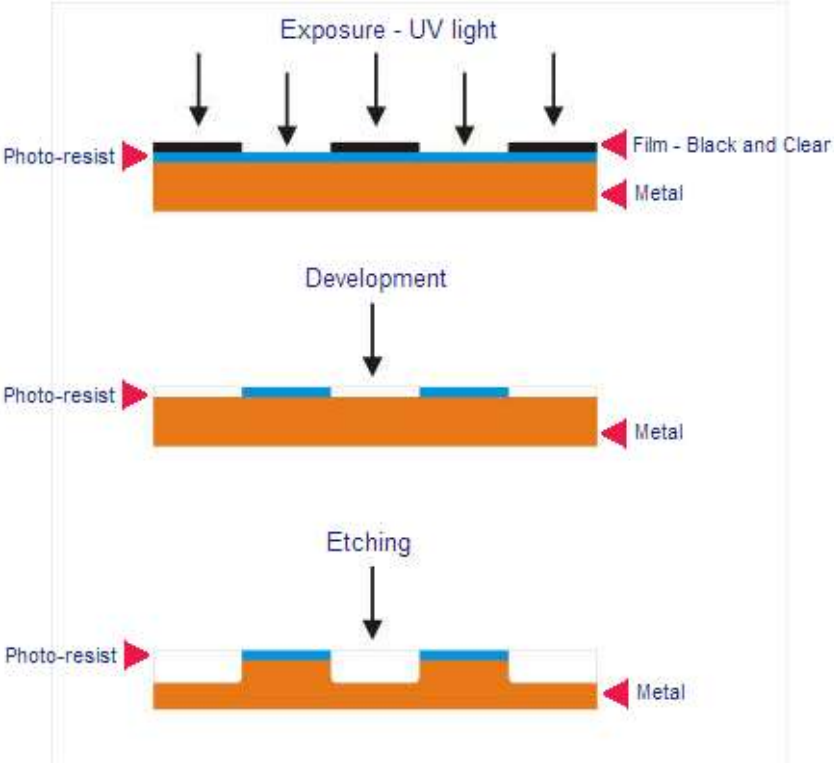

Figure 2.3: Photo-etching procedure

2.2 Characterization of Microgrippers

An important indication of the proposed devices weather they are reliable or not is to characterize the performance of the device. Different instruments and schemes have been implemented to achieve this task. In the following sections, each technique implemented will be presented.

2.2.1 Estimation of Output Force

Due to the nature of biological micro-object, manipulating them requires highly reliable devices. One of the most important factors is the handling, or gripping force. This force has to be controlled in such a way not to damage the manipulated micro-object. Hence, fulfilling this need is highly demanded. Figure 2.4 shows a new approach used to measure the output force for the syringe actuated microgripper in chapter 3 using various sizes of rubber O-ring. The

rubber O-rings were calibrated by holding them in a set of jaws attached to a fixed stage translational device and advancing the O-ring towards the balance to measure the force as a function of the ratio *a/b* thus giving a measure of the O-ring stiffness. Then, each O-ring was picked up by the gripper three times and the ratio *a/b* measured.

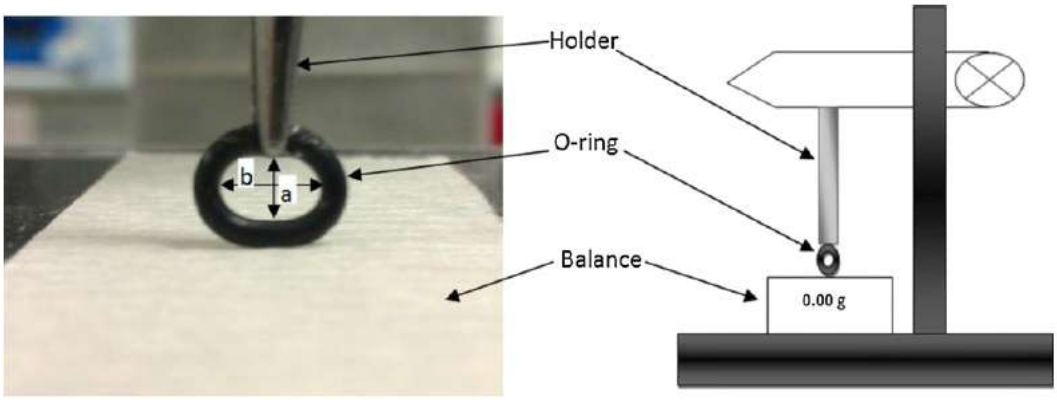

Figure 2.4: Measurement of O-ring stiffness and deformation index a/b (Left) and schematic drawing of experimental procedure for obtaining output force (Right).

Another approach has been implemented to calibrate the output force of the microcantilever-based gripper. A digital scale of up to four decimals has been used to obtain the generated force at the tip of cantilever, see Figure 2.5, where the cantilever tip is in direct contact with a metallic ball to ensure a one point contact between the ball and the cantilever tip.

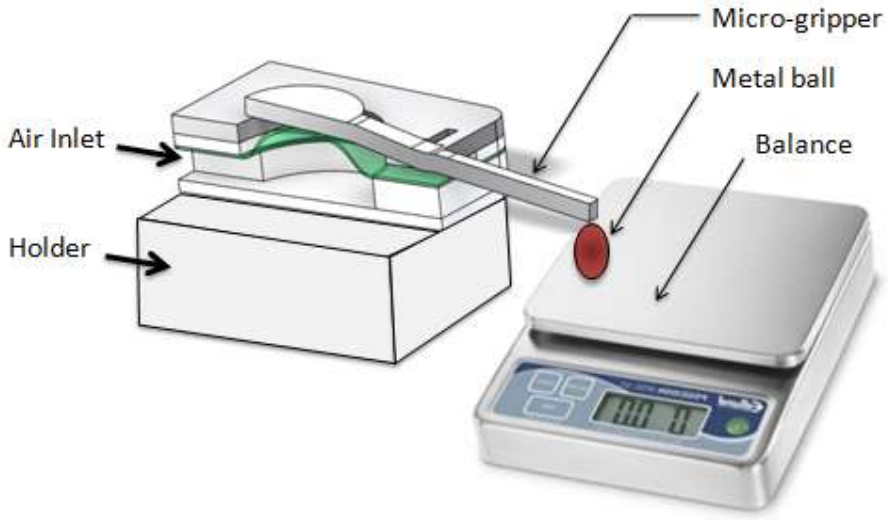

Figure 2.5: Schematic diagram of calibrating output force.

2.2.2 Readout Techniques

A very important aspect of any beam deflection system is the readout techniques. A high-accuracy and real-time measurements in the sub-nanometer range is required. The most commonly readout techniques could be categorizes as optical (Ilic *et al*., 2004), piezoresistive (Lee *et al*., 2005), capacitive (Zhou *et al*., 2006), and metal-oxide semiconductor field-effect transistors (MOSFETs) (Shekhawat *et al*., 2006). Each of these has its advantages and disadvantages as well. But, the most commonly used ones are the optical and the piezoresistive ones.

The working principle of piezoresistive readout techniques depends on detection of changes in the resistivity of the material of the cantilever when a stress is applied (Baselt *et al*., 1997, Minne *et al*., 1995, Tortonese *et al*., 1993, Yu *et al*., 2002). The resistivity of a piezoresistive material will change when such a material incurs a strain. This change in resistivity will be then measured by external devices. However, such readout techniques have their limitations. For example, the sensitivity and resolution of the system will be negatively affected by the built-in noise (Yu *et al*., 2002). Furthermore, it is a challenging task to fabricate a piezoresistive based microcantilever device that incorporates built-in electronics.

The other common observation techniques for the detection of bending in cantilever beams is the optical beam detection system. This system and its data acquisition code was built by Dr. Yifan Liu, a former PhD student in our research group. As shown in Figure 2.6, the main components of the system are: position sensitive photodiode (PSD, Laser Component PSM 1-10), 5mW laser diode (532 nm, ThorLab), data acquisition card (National Instruments BNC-2120), and a computer with LabVIEW support.

Focusing a laser diode on the tip of cantilever which acts as a mirror reflecting the laser beam toward a PSD, Figure 2.6. Throughout the reflection, the detected signal by PSD is then amplified and sent to the computer to analyze and record

the signals. The main advantage of this system is its capability to detect to sub-nanometer ranges (Waggoner and Craighead, 2007). Also, the absence of electrical connection between the cantilever and the system, linear response, ease of setup and use and reliability are other advantages of such detection system.

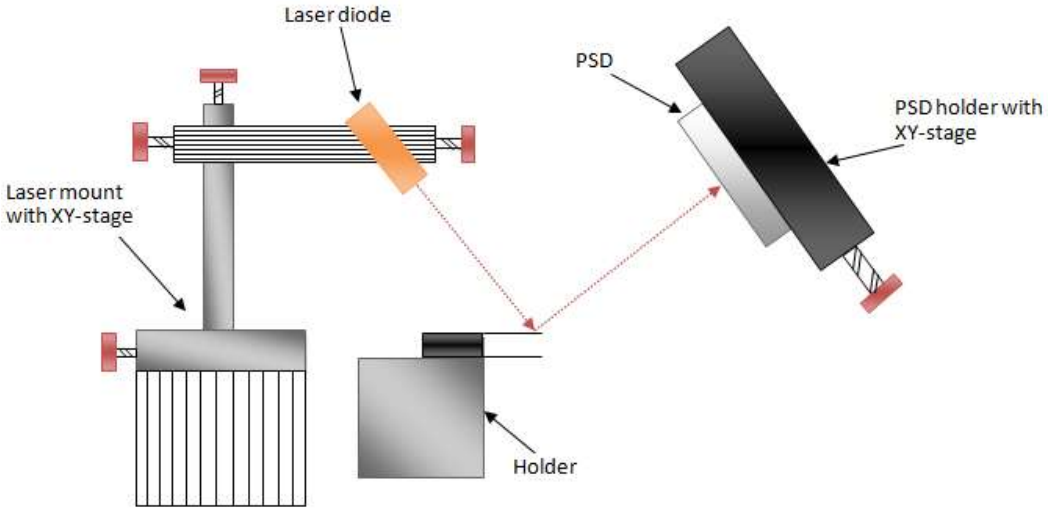

Figure 2.6: Schematic illustration setup of the optical beam detection system for measuring the deflection of microcantilever beam.

The acquired data through the mentioned readout system will appear as in Figure 2.7.

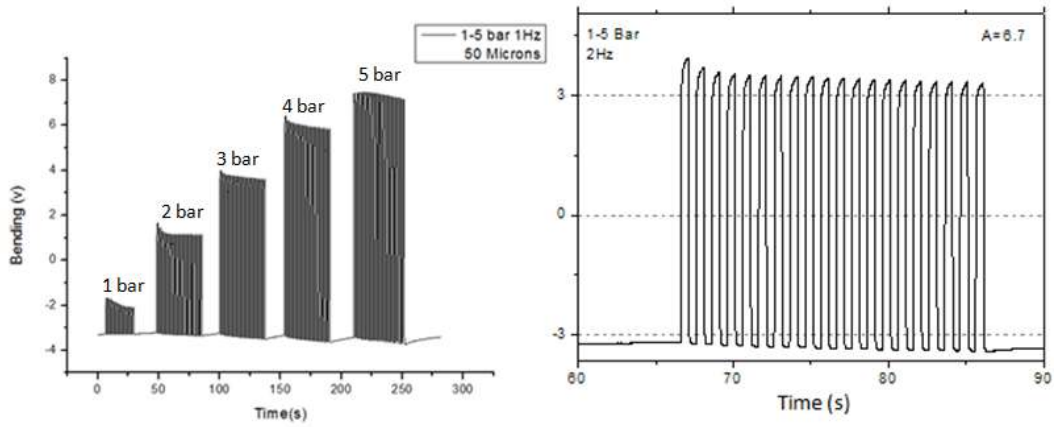

Figure 2.7: Sample raw data from optical beam detection system where the output is the amplitude of the deflection of the cantilever tip in volts.

The used PSD directly and linearly converts the laser spot into two currents (i_A and i_B) from its two ends. These outputs are processed internally through a specified arrangement ending up with signals that can be measured, X, Y, and intensity signals output. As the laser spot reflection moves because of the cantilever deflection, the positional change in Y can be determined to be:

$$\Delta z = \frac{L \times L_{PSD}}{8s}(\Delta V) \tag{2.1}$$

where L is the length of the cantilever, L_{PSD} is the length of PSD area, s is the distance from the cantilever tip to the PSD, and ΔV is the amplitude of the output bending signal in volts.

For calibration of the system and maximization of the readout signal, the laser beam is required to focus on the tip of the cantilever where the most deflection takes place. The laser beam is moved until it is centered on the cantilever tip, and at the same time, ensuring the presence of a reflective signal using the PSD. As a signal is achieved by realizing a positive intensity signal, the laser is then further adjusted to get the optimum combination of the maximum intensity signal while still focusing on the tip of the cantilever. Finally, centering the laser (Y position) to 0 allows maximum possible signal change, although it is not required as the signal is not enough to reach the boundaries, $\pm$10 V.

2.2.3 Programming

The programming and control of the actuation and detection of the microcantilever based microgripper was performed by using LabVIEW 8.5. The inputs into LabVIEW are actuation frequency for the actuation phase and the data acquisition frequency in the detection phase. For the actuation phase, the program is controlling the opening and closing of the valve in the pneumatic circuit which will be further discussed in the next section. The front panel, see Figure 2.8, in this step consists of three variables; pumping cycles, no. of cycles, and the pumping pulse in ms. For example, if the pumping pulse was 1000 ms, it means that the frequency of pumping is 1Hz.

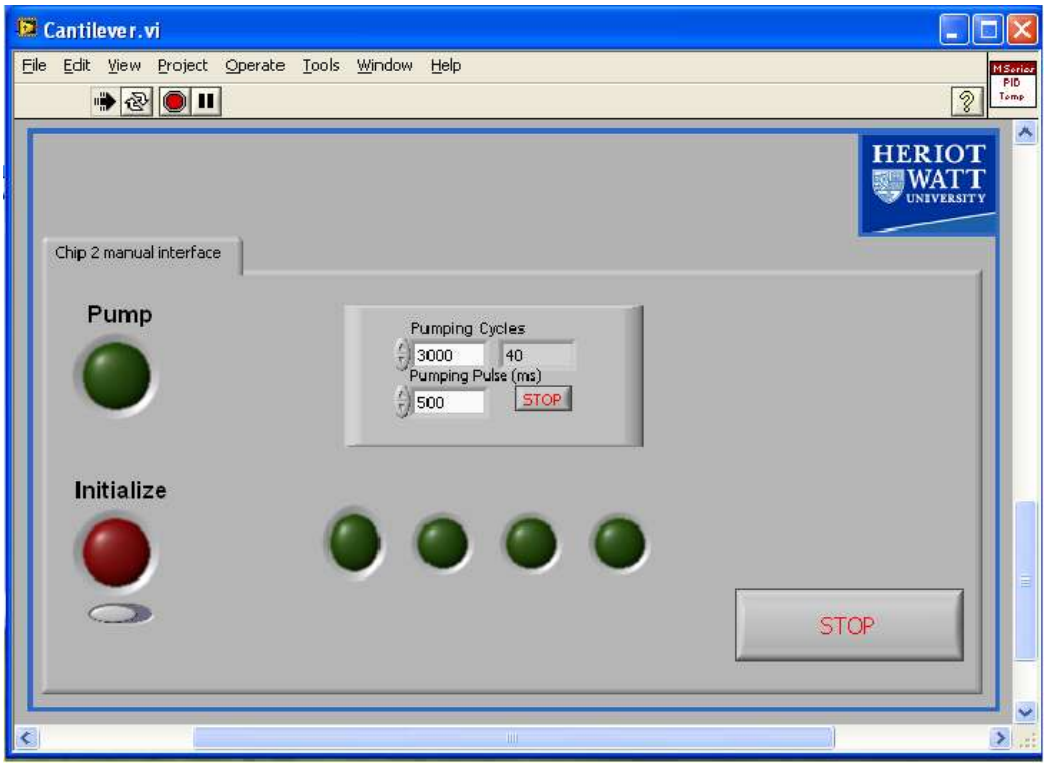

Fig. 2.8: LabView front panel for actuation phase where the actuation frequency can be changed by changing the pumping pulse.

In the detection phase, the program is employed to detect the deflection at the tip of the microcantilever. The front panel, see Figure 2.9, consists of three XY graphs: differential, intensity, and normalized cantilever signal. File saving and data acquisition frequency are represented at the top left of the front panel. Once the program is started, the data will be saved automatically in the specified path as a text file in a spreadsheet format. Data acquisition frequency is controlled by two variables: scan rate, and scans to read at a time. While the scan rate is the frequency in Hz of the speed that the data should be acquired, scans to read at a time determines the number of data points should be read at once before acquiring again. Hence, if the scan rate set to be 300 kHz and the scans to read 100, 300 data point per second will be provided.

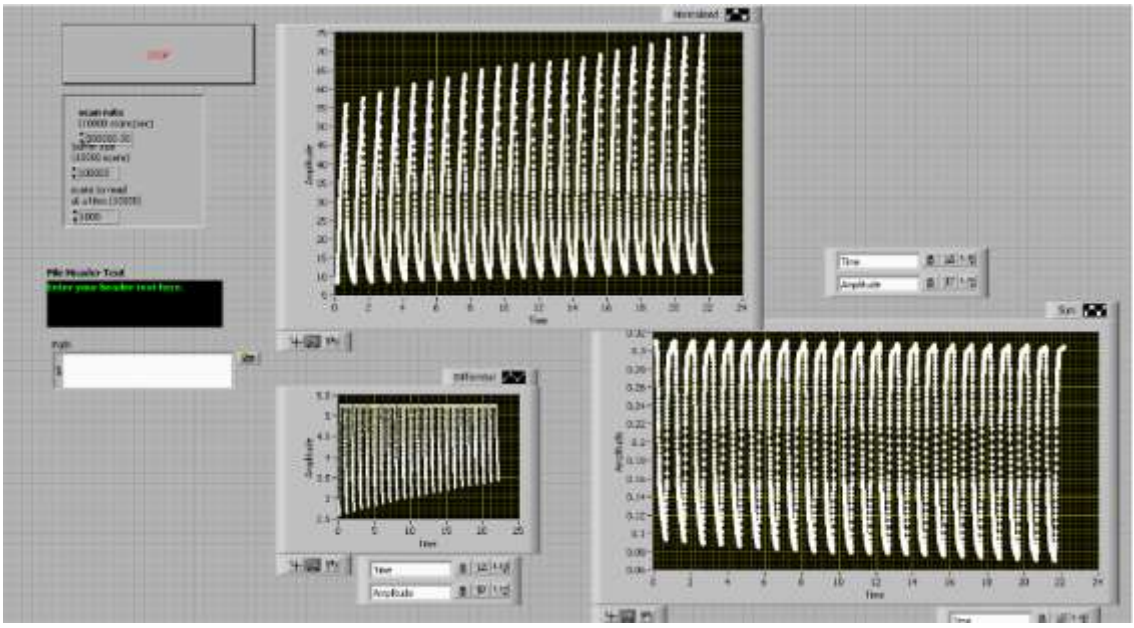

Figure 2.9: LabVIEW front panel for optical detection of cantilever bending

2.2.4 Control of Pneumatic System

The pneumatic circuit consists mainly of four components: pressurized air cylinder, a digital pressure gauge, pumping valve, and the previously mentioned pneumatic control LabVIEW program. As shown in Figure 2.10, the gas released from the gas cylinder passing through the digital pressure gauge to deliver the desired amount of pressure to the system. Then, the valve, which is controlled by the LabVIEW program, opens and shuts according to the input parameters to the program. The control of the valve enhances the dynamic analysis for the sensing and palpation procedure.

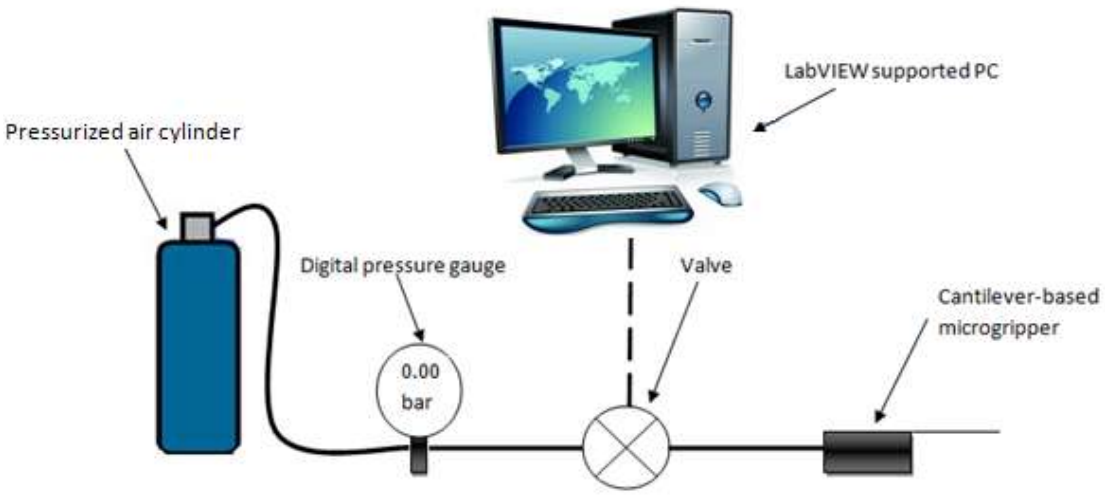

Fig. 2.10: Schematics of the pneumatic system where the pressurized air travels through the delivery tube and adjusted by the pressure gauge, the valve is used to supply the pressurized air under the actuation frequency controlled by the LabVIEW software

2.3 Micro-Manipulation

The processes of micro-manipulation was accomplished using a CNC (Mach3 make) machine. Figure 2.11 shows the set-up used to perform this process. The micro-manipulator is clamped to the moving stage and the positioning is being controlled automatically as Figure 2.12 shows the control screen of the software used to operate the CNC machine.

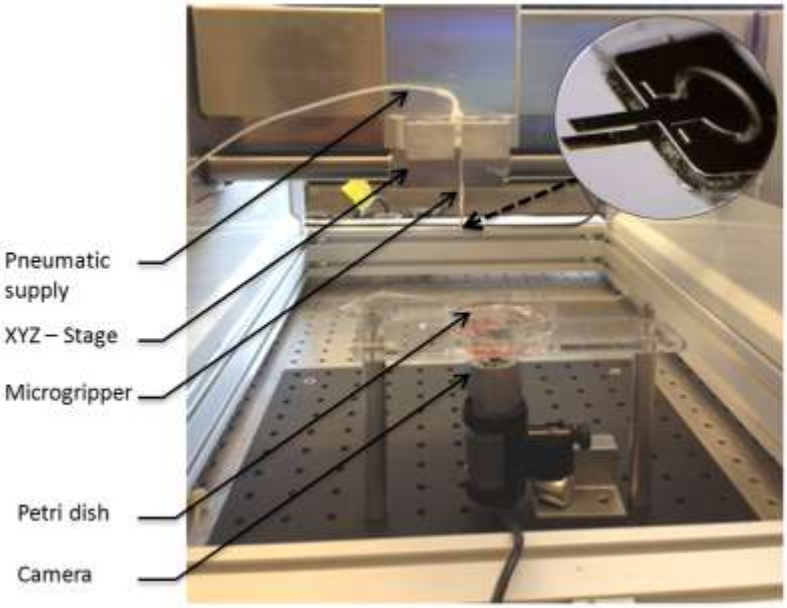

Figure 2.11: Manipulation set-up used to perform an automated controlled micromanipulation of various sizes of micr-objects

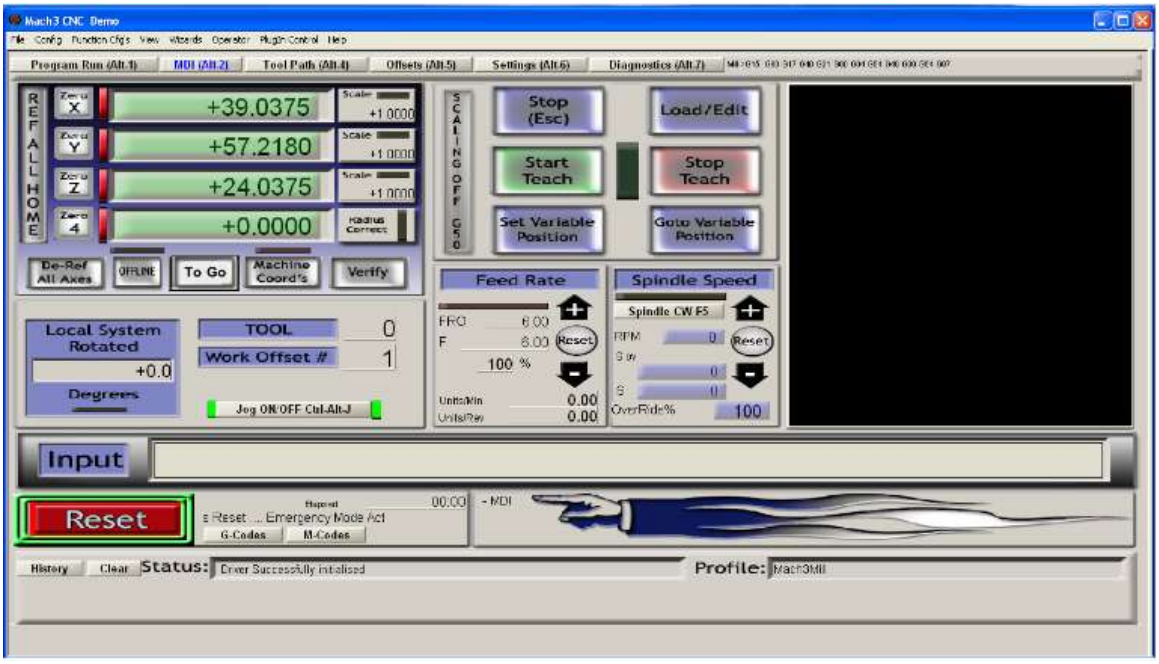

Figure 2.12: Front panel for operating CNC machine used to control the pick-place operation for the micro-cantilever based microgripper.

As seen in Figure 2.12, the top left indicates the exact position of the micro-manipulator very precisely. In the input space, the user types the desired position

to move to using G-CODE. For example, if the user wants to move the manipulator, then he should first define a reference point or a zero point. After that, typing the new position in the form “G0 X1 Y1 Z1”, so the manipulator will move directly to the point of coordinates (1,1,1) according to the reference point. The precision of the CNC machine allowing manipulation of micro-objects with a spacing between them up to 500 μm.

2.4 Finite Element Modeling

The development of Finite element modeling (FEM) technique was originally in the 1940s to analyze complex problems in aeronautical and civil engineering. The working principle of FEM technique is basically dividing a pre-defined structure into a set of appropriate finite elements connected to each other at points called nodes. System inputs like force, temperature, and current are applied as loads to each of these elements and the boundary conditions are applied as well. Determining an accurate response of the system modeled with FEM is the main objective of this technique. Also, FEM helps in validating the experimental results and to understand the behavior and the influence of each parameter. Furthermore, a sufficient understanding of the performance of the system will be enabled using FEM before investing in its fabrication.

In this thesis, ABACUS 6.10 has been used in all finite element analysis.

2.5 References

BASELT, D. R., LEE, G. U., HANSEN, K. M., CHRISEY, L. A. & COLTON, R. 1997. A high-sensitivity micromachined biosensor. *Proceedings of the IEEE,* 85**,** 672-680.

CHOUDHURY, I. & SHIRLEY, S. 2010. Laser cutting of polymeric materials: An experimental investigation. *Optics & Laser Technology,* 42**,** 503-508.

DUBEY, A. K. & YADAVA, V. 2008. Laser beam machining—a review. *International Journal of Machine Tools and Manufacture,* 48**,** 609-628.

ILIC, B., YANG, Y. & CRAIGHEAD, H. 2004. Virus detection using nanoelectromechanical devices. *Applied Physics Letters,* 85**,** 2604-2606.

LEE, J. H., HWANG, K. S., PARK, J., YOON, K. H., YOON, D. S. & KIM, T. S. 2005. Immunoassay of prostate-specific antigen (PSA) using resonant frequency shift of piezoelectric nanomechanical microcantilever. *Biosensors and Bioelectronics,* 20**,** 2157-2162.

MINNE, S., MANALIS, S. & QUATE, C. 1995. Parallel atomic force microscopy using cantilevers with integrated piezoresistive sensors and integrated piezoelectric actuators. *Applied Physics Letters,* 67**,** 3918-3920.

PPD Ltd *http://www.ppdltd.com/web_site_3/The_Process.html* [Online]. [Accessed 18 october 2013].

ROY, R., ALLEN, D. & ZAMORA, O. 2004. Cost of photochemical machining. *Journal of materials processing technology,* 149**,** 460-465.

SHEKHAWAT, G., TARK, S.-H. & DRAVID, V. P. 2006. MOSFET-embedded microcantilevers for measuring deflection in biomolecular sensors. *Science,* 311**,** 1592-1595.

TABATA, N., YAGI, S. & HISHII, M. 1996. Present and future of lasers for fine cutting of metal plate. *Journal of materials processing technology,* 62**,** 309-314.

TORTONESE, M., BARRETT, R. & QUATE, C. 1993. Atomic resolution with an atomic force microscope using piezoresistive detection. *Applied Physics Letters,* 62**,** 834-836.

WAGGONER, P. S. & CRAIGHEAD, H. G. 2007. Micro-and nanomechanical sensors for environmental, chemical, and biological detection. *Lab on a Chip,* 7**,** 1238-1255.

YU, X., THAYSEN, J., HANSEN, O. & BOISEN, A. 2002. Optimization of sensitivity and noise in piezoresistive cantilevers. *Journal of Applied Physics,* 92**,** 6296-6301.

ZHOU, F., SHU, W., WELLAND, M. E. & HUCK, W. T. 2006. Highly reversible and multi-stage cantilever actuation driven by polyelectrolyte brushes. *Journal of the American Chemical Society,* 128**,** 5326-5327.

Chapter 3: A Scalable Syringe-Actuated Polymeric Microgripper for Biological Manipulation

Microdevices with dimensions from 1 μm to 1 mm have been developed or envisaged recently for a range of different biological and medical purposes. Consequently, handling and manipulation tools to aid this rapid development are urgently required (Dario P, 2000, Sun J, 2002). As mentioned in Chapter 1, fluidic actuation has been overlooked in MEMS despite its satisfactory output in the micro-scale (DeVolder M, 2010). A common type of such actuators as have been published uses the deformation of an elastic component to actuate the integrated system (Jeong et al., 2006, Bütefisch et al., 2002, Yoshida et al., 2005), so-called elastic fluidic actuators. Membrane based actuators are widely applied at the microscale due to their relatively easy fabrication and the absence of leakage issues (DeVolder M, 2010).

This chapter describes the development of a family of low-cost, polymer based compliant microgrippers that can be actuated manually using pneumatic forces (e.g. via a syringe). The design, fabrication and demonstration of such a pneumatically actuated microgripper capable of scaling to the level of manipulating a single biological cell is reported in detail. The main design challenge is to provide control over the opening and closing displacements and the gripping force, which is achieved by a compliant gripper design and two-way actuation.

3.1 Microgripper Design

The device design comprises of two main parts; the actuation mechanism and the gripper arms**.** The actuator is essentially a flexible membrane suspended across one end of a delivery tube and applies a force to the base of the gripper when a pneumatic pressure is applied to it. The microgripper is mainly a compliant structure actuated by the actuation mechanism. Compliant structures are the structures that achieve an output displacement from the elastic deformation of one

or more flexible members within the structure (Howell, 2001). Such structures have the advantage of reducing the number of parts required for accomplishing a specific task, which consequently will reduce the cost and increase the performance of the whole system (Howell, 2001). At the micro-scale, compliant structures become highly appreciated as they avoid the problems accompanied in assembling such microstructures (Kota *et al*., 2001).

3.1.1 Actuation Mechanism

The actuation is achieved by using a flexible membrane fixed to one end of a 'delivery' tube. The membrane will expand and contract as air pressure in the tube rises and falls, by means of a pneumatic source. A schematic diagram of the pneumatic actuation is illustrated in Figure 3.1. The resulting change in vertical displacement of the membrane will provide the means of actuation for the gripping arms.

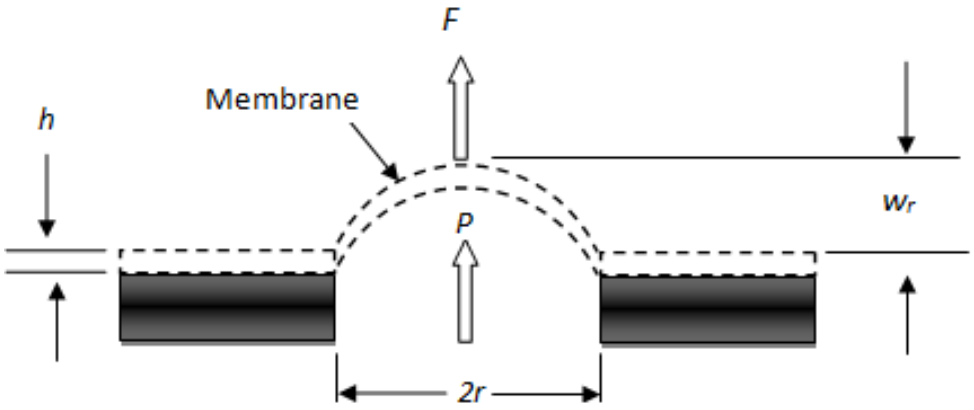

Figure 3.1: Schematic diagram of pneumatic actuation where the deflection of the membrane is used to exert an input force on the microgripper.

To understand the operation of the gripper a mathematical model is derived to describe each stage of the actuation process. The force acting on the membrane can be calculated from equation (3.1), where r is equal to the radius of the membrane and P is the applied pressure.

$$F = P \times \pi r^2 \tag{3.1}$$

The second stage of actuation relates to the deflection in the circular membrane of radius r caused by the increase in pressure. The governing formula for determining the deflection in a plate under an applied pressure in case of large deflections is given by (Timoshenko *et al*., 1959):

$$\frac{d^3w}{dr^3} + \frac{1}{r}\frac{d^2w}{dr} - \frac{1}{r^2}\frac{dw}{dr} = \frac{12}{h^2}\frac{dw}{dr}\left[\frac{du}{dr} + v\frac{u}{r} + \frac{1}{2}\left(\frac{dw}{dr}\right)^2\right] + \frac{1}{Dr}\int_0^r \Pr\, dr \qquad (3.2)$$

Where u is the radial displacement of a point in the plane of the plate, and D represents the flexural rigidity of the plate, and w is the perpendicular displacement to the plane of the plate. In the case of very thin plates, it can be treated as a flexible membrane and the general equation for such a membrane is obtained from equation (3.3) and following equation was obtained (Timoshenko *et al*., 1959):

$$w_r = 0.662\, r \sqrt[3]{\frac{Pr}{Eh}} \qquad (3.3)$$

where "*E"* is Young's modulus of the membrane and "*h"* represents the thickness of the membrane.

3.1.2 Gripper Design

The microgripper consists of two fixed legs and two compliant arms, actuated by a central platform to which the actuation force is applied, as shown in Figure 3.2. The sizes of biological cells are usually in the range from 5 to 150 μm, so the outer dimensions were chosen at the higher end to demonstrate the design principles while maintaining scalability. To assess the performance, five design variables were investigated using Finite Element Analysis (FEA); thickness of gripping arm (T1), thickness of linkage arm (T2), thickness of actuation arm (T3), length of gripping arm (L), and inclination angle of linkage arm (θ). These were varied by ±25% around a set of reference dimensions; T1= 1mm, T2= 1mm, T3= 0.5mm, L= 5mm and θ= 20°

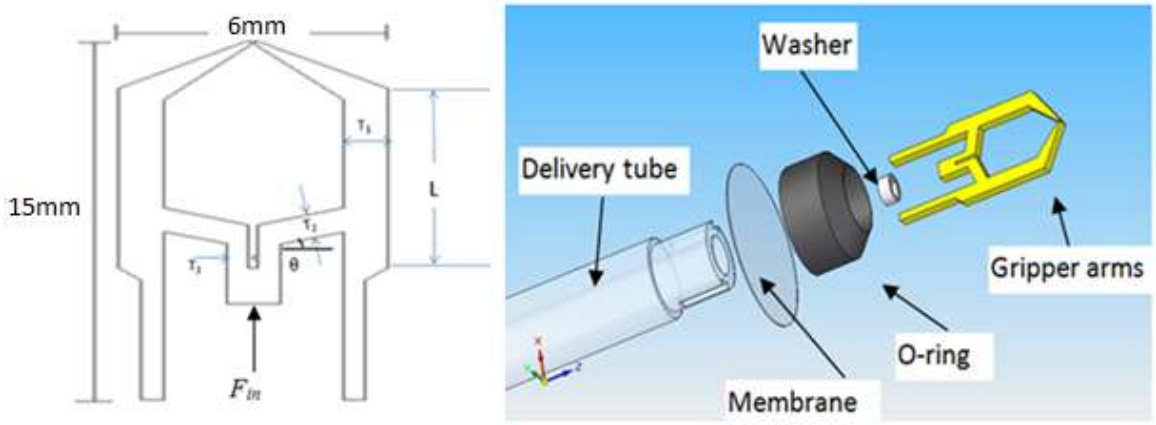

Figure 3.2: Design variables of the microgripper (Left), and conceptual design of the device showing the assembling steps (Right)

3.1.3 Finite Element Analysis

The microgripper design was analyzed using finite element in ABAQUS 6.10. The analysis used the properties of PMMA which exhibits a good elastic response (Young's Modulus of 1.8 GPa and Poisson's ratio of 0.35) at low strain rates (Rittel, 2000). A seed size of 0.045 was used when meshing the part. The total number of elements was 418725 and the number of nodes was found to be 461604. The model legs were constrained and the actuation force increased until the tensile strength of the PMMA was reached at some point in the model. The distribution of stress over the microgripper is shown in figure 3.3.

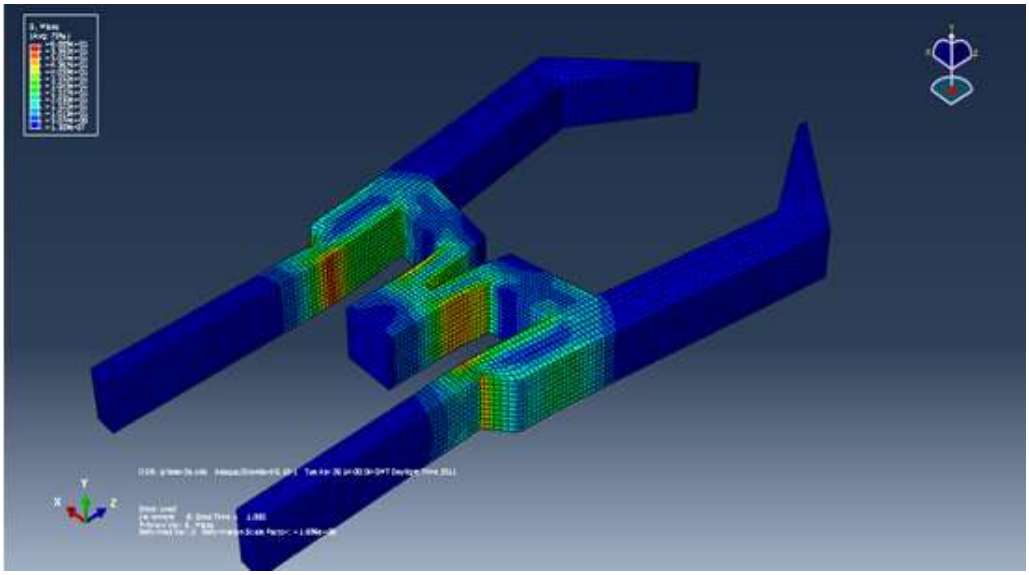

Fig. 3.3: Stress distribution over the microgripper showing the areas where maximum stress is occurring.

Figures 3.4a and b show the effect of the sensitivity analysis to T1, T2, T3 and L, and to θ, respectively.

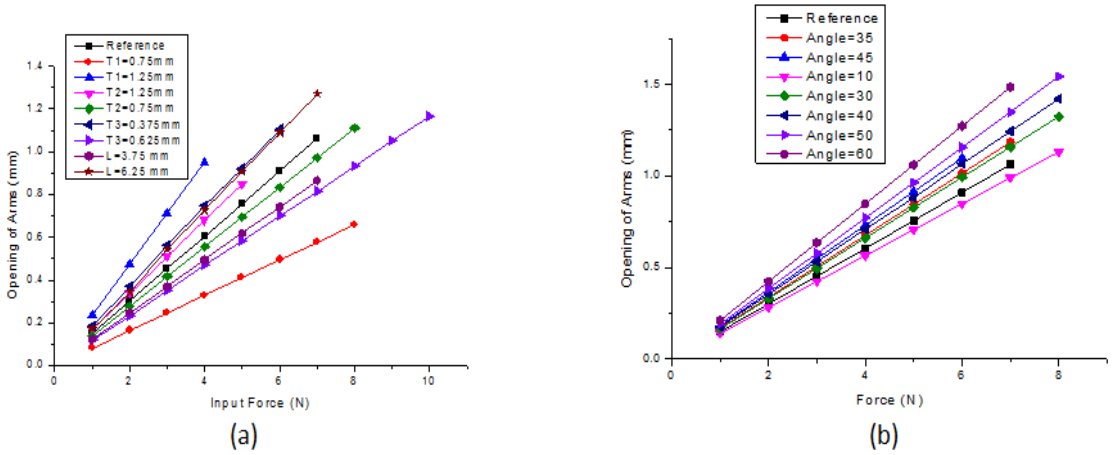

Figure 3.4: Sensitivity analysis of opening of one arm over range of design variables (a) effects of T1, T2, T3 and L and (b)effect of θ.

As might be expected, T1 has the largest effect on opening as it controls the bending stiffness of the part of the gripper arm below the point where the hinge

joins; it also affects the passive gripping force for a given degree of jaw opening. The angle θ also has a significant effect as it affects the bending length of the gripper arm. On the other hand, T2 has the lowest effect on the total stiffness of the system among the design parameters.

The results in Figures 3.4a and 3.4b were re-plotted as in Figure 3.5 to observe the curve of stiffness of the gripper (*K*) for each design variable. As can be seen, the curve of the stiffness of the gripper is almost linear for all the parameters, whereas it shows a higher order dependence for T1.

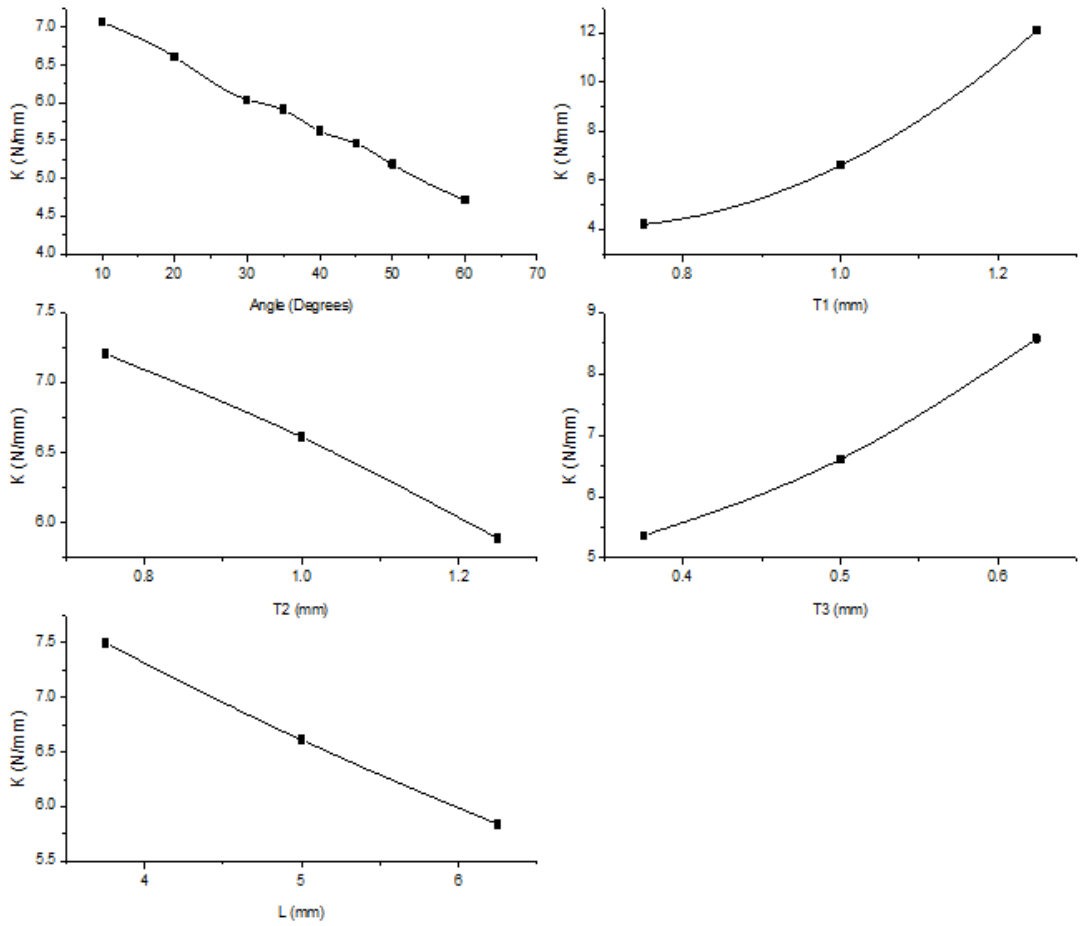

Fig. 3.5: Sensitivity analysis for calculated gripper stiffness when changing the variables, all the curves are linear except T1 shows a higher order of dependance

In Figure 3.5, the effect of each parameter on the stiffness of the system is presented. It is obvious that the parameter T1 has the highest effect on the stiffness among the other parameters while T2 is the lowest. The curve of T2 illustrates that the total stiffness of the device is 5.5, 6.6, and 7.2 N/mm for the values of T2 of 1.25, 1, and 0.75 mm, respectively.

The main conclusion of Figure 3.5 is that the stiffness of the device is proportional to T1 and T3, while it is inversely proportional to θ, T2, and L.

3.2 Fabrication and Assembly

A gripper was fabricated to the reference dimensions using a maskless laser microfabrication procedure. It was cut from 1 mm thick polymethyl-methacrylate (PMMA) sheet using a TROTEC Speedy 300^{TM} CO_2 laser cutter operating with the power and speed adjusted to 9 W and 0.6 mm/sec, respectively, using several passes to ensure a clean and precise cut without burning. Under these conditions, the cut can be produced with an edge precision of 50μm. The diameter at one end of the delivery tube was reduced and slots made in its wall to allow the gripper arms to be fixed to the outside of the delivery tube and over the top of the membrane. A combination of a washer and rubber O-ring was used to form an air tight seal around the membrane and hold the gripper arms in place. Epoxy resin was used to bond the gripper arms to the membrane and also sealing the washer and O-ring to the delivery tube. Upon completion of the assembly a syringe was attached to the other end of the delivery tube to act as a pneumatic air source as shown in Figure 3.6.

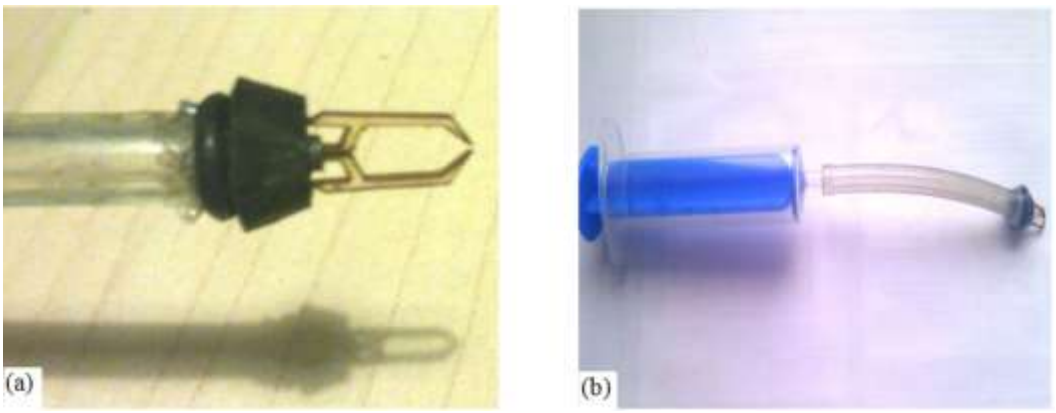

Fig. 3.6: (a) Assembled gripper, (b) Complete final prototype (with syringe).

3.3 Calibration of Output Force

An important indicator of the performance of the device is its output force as it is essential to control the gripping force that might cause damages to the manipulated objects. Hence, the new approach illustrated in chapter 2, Figure 2.4 was used to measure the output force using various sizes (3, 3.5, and 4 mm outer diameter) of rubber O-ring, which are sufficiently compliant to provide a measurable deformation when picked up by the gripper. The O-rings were first calibrated by holding them in a set of jaws attached to a fixed stage translation device and advancing the O-ring toward the balance to measure the force as a function of the ratio *a/b*, Figure 3.7, thus giving a measure of the O-ring stiffness. Then, each O-ring was picked up by the gripper three times and the ratio a / b measured. The ratio could then be used to determine the gripping force for each of the O-rings, each of which held the jaws open by a different amount, thus yielding a measurement of gripping force versus jaw opening. The device was able to generate an output force of up to 8mN with a resolution of ±.01 mN. The measured and calculated stiffness curves are shown in Figure 3.8 and, as can be seen, the agreement is excellent.

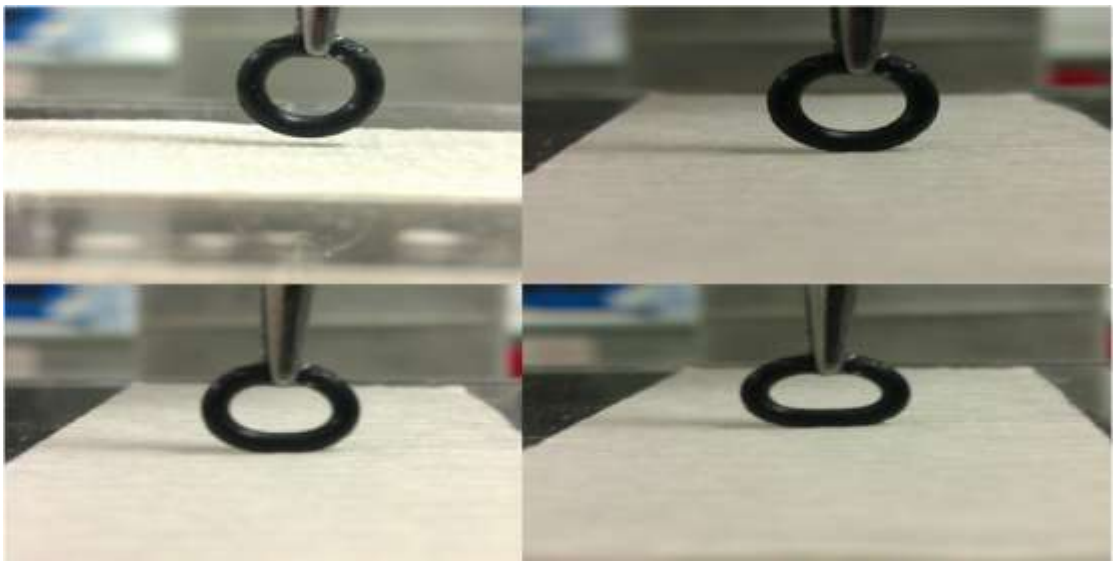

Fig. 3.7: Procedure of obtaining the stiffness of O-ring by observing and calibrating the deformation of the O-ring

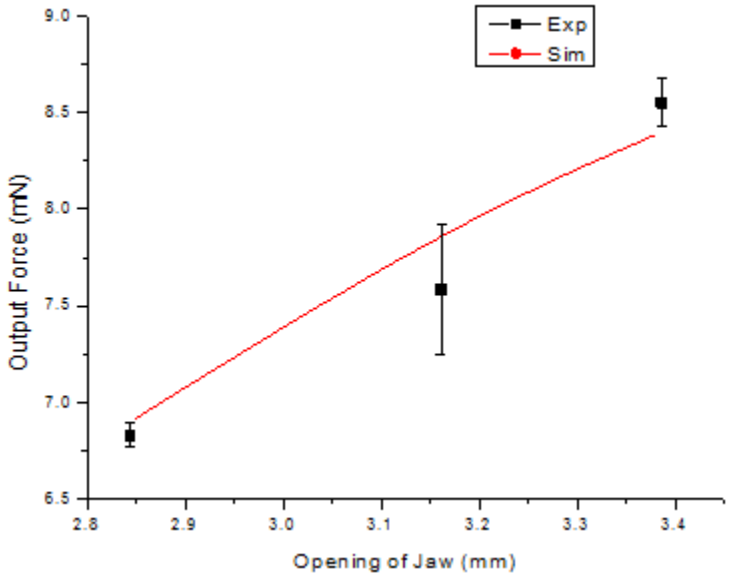

Fig. 3.8: Measured and calculated gripper stiffness

Finally, to verify the ability of the device to perform pick and place operations, a range of tests were conducted on objects of known size. The gripping actuation was controlled using the pneumatic pressure exerted by a syringe. A positive pressure from the syringe will open the gripper and the release of the pressure will

close the gripper. Figure 3.9 shows the simple actuation mechanism can precisely manipulate a range of objects with the sizes down to 200 µm in thickness. It is expected this approach can be further scaled down, by shrinking the dimension of the gripping arm, to manipulate single biological cells in liquid environment.

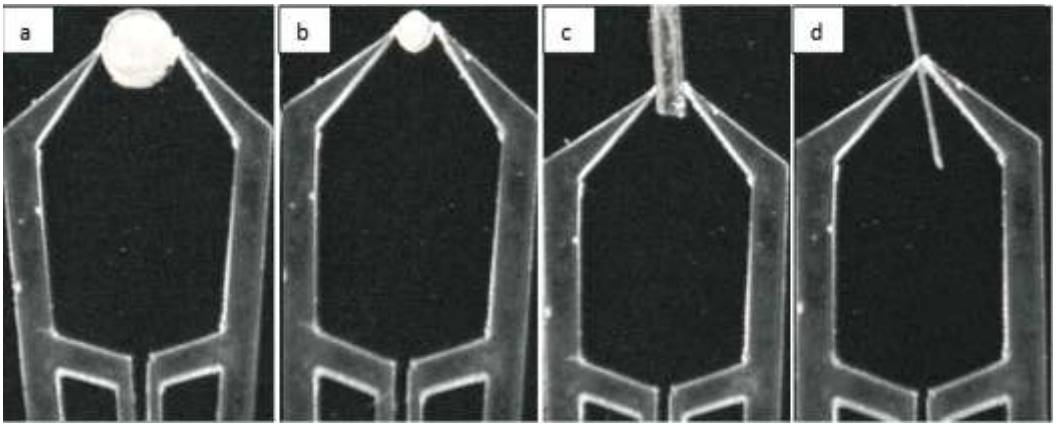

Fig. 3.9: Demonstration of the grasping of (a) 2 mm, (b) 1 mm, (c) 500 µm, and (d) 200 µm diameter samples

3.4 Discussion

Different microfabrication techniques could be implemented to fabricate the proposed device such as laser cutting, photolithography, and microinjection moulding (µIM) techniques. All of them have a great potential in the scope of microfabrication. However, photolithography and µIM techniques are more expensive and are, relatively speaking, more complicated since they need more setup equipment and more fabrication steps (Pimpin and Srituravanich, 2011, Giboz *et al*., 2007). Moreover, due to its precision and high intensity, laser cutting has a wide application in fine cutting of sheet metals without affecting the quality of the machined parts (Choudhury and Shirley, 2010). Also, because it is a subtractive technique, laser cutting can be used on bulk-produced materials thus offering greater control over structural properties, such as strength and elastic modulus and the potential for low defect contents.

The range of available materials depends somewhat on the fabrication technique and, for this particular prototype, silicon, SU-8, or a polymeric material such PMMA could have been chosen. PMMA was used here as it is relatively inexpensive and polymer materials are generally more easily worked by laser cutting (Choudhury and Shirley, 2010). To use other structural materials, such as stainless steel or titanium, a more powerful laser would be required and there could be attendant problems with distortion and the quality of the cut edge. With such materials, chemical etching can be a useful alternative.

The device is scalable in principle using a planar configuration with a channel on the fluid side as illustrated in Figure 3.10. Such configuration will help to overcome the difficult manual assembly which would escalate as the device becomes smaller. The effect of overall dimension on the gripping force can be overcome to an extent by increasing member stiffness's (changes in material, length or second moment of area), so, in principle, the design is flexible to deliver a range of performance parameters depending on the delicacy of the gripping task and the control envelope.

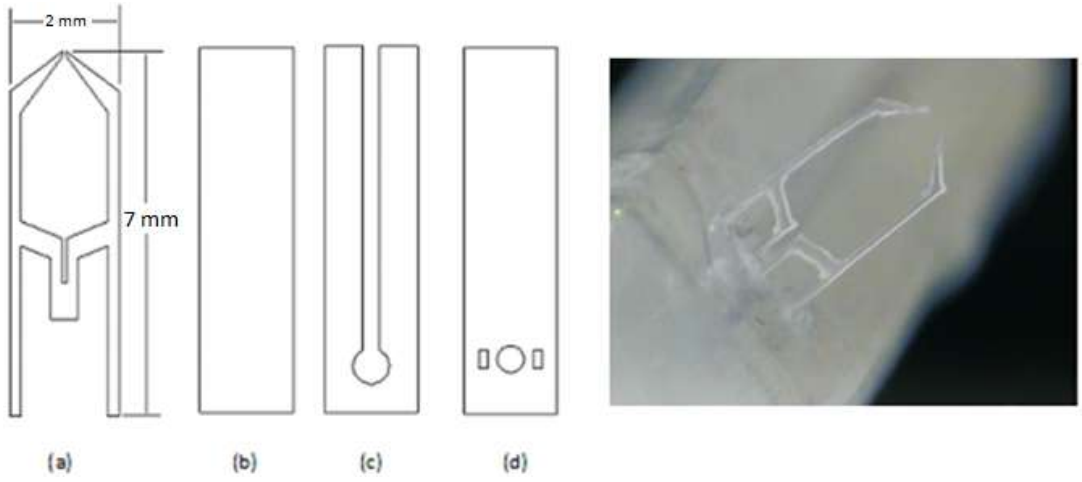

Fig. 3.10: (a) microgripper, (b) bottom layer, (c) middle layer, (d) top layer, (Right) assembled microgripper

3.5 Conclusion

A pneumatically actuated microgripper was designed, fabricated, simulated and tested. The gripper can be actuated using the pneumatic pressure exerted by a syringe. The output force of the gripper was obtained experimentally and theoretically and the match between them was satisfactory. The gripper has shown to be effective in manipulating a number of objects ranging from 200 μm to 2 mm. The design is scalable in principle, with the gripper arms being limited only by the acuity of laser cutting and the minimum defect size in the machined material. The membrane actuator is similarly scalable provided that a planar configuration is used with a channel on the fluid side. This procedure will help to overcome the difficult manual assembly when miniaturizing. The main challenge in further miniaturization is to make the connection to a delivery tube at the smallest possible size.

3.6 References

BÜTEFISCH, S., SEIDEMANN, V. & BÜTTGENBACH, S. 2002. Novel micro-pneumatic actuator for MEMS. *Sensors and Actuators A: Physical,* 97**,** 638-645.

CHOUDHURY, I. & SHIRLEY, S. 2010. Laser cutting of polymeric materials: An experimental investigation. *Optics & Laser Technology,* 42**,** 503-508.

DARIO P, C. A., BENVENUTO A, MENCIASSI A 2000. Micro-systems in biomedical applications. *Micromechanics and Microengineering.,* 10**,** 235-244.

DEVOLDER M, R. D. 2010. Pneumatic and hydraulic microactuators: a review. *Micromechanics Microengineering,* 20**,** 18pp.

GIBOZ, J., COPPONNEX, T. & MÉLÉ, P. 2007. Microinjection molding of thermoplastic polymers: a review. *Journal of micromechanics and microengineering,* 17**,** R96.

HOWELL, L. L. 2001. *Compliant mechanisms,* Wiley-Interscience.

JEONG, O. C., KUSUDA, S., SAKAKIBARA, T., KONISHI, S. & NOKATA, M. Year. Pneumatic micro finger as endeffecter of robot. *In*, 2006. IEEE, 145-148.

KOTA, S., JOO, J., LI, Z., RODGERS, S. M. & SNIEGOWSKI, J. 2001. Design of compliant mechanisms: applications to MEMS. *Analog Integrated Circuits and Signal Processing,* 29**,** 7-15.

PIMPIN, A. & SRITURAVANICH, W. 2011. Review on micro-and nanolithography techniques and their applications. *Engineering Journal,* 16**,** 37-56.

RITTEL, D. 2000. A Note on the Dynamic Failure of PMMA. *International journal of fracture,* 106**,** 3-8.

SUN J, Z. Z. 2002. Finite element analysis of a new PZT actuator for hard disk drives. *Sensors and Actuator A: Physical,* 100**,** 257-263.

TIMOSHENKO, S., WOINOWSKY-KRIEGER, S. & WOINOWSKY, S. 1959. *Theory of plates and shells,* McGraw-Hill New York.

YOSHIDA, K., PARK, J.-H., YANO, H., YOKOTA, S. & YUN, S. 2005. Study of valve-integrated microactuator using homogeneous electro-rheological fluid. *Sensors and Materials,* 17**,** 97-112.

Chapter 4: Micro-Tweezers: A Pneumatically Driven Microcantilever Based Microgripper for Micromanipulation

Cantilevers, beams that are free at only one end, have been applied in the field of MEMS since the early sixties, initially as electromechanical resonators (Wilfinger et al., 1968). More recently, microcantilevers have been proposed as biosensors (Madzhi et al., 2010), gripping force sensors (Chang and Cheng, 2009, Bharanidaran and Ramesh, 2013), and microgrippers (Xu, 2012, El-Sayed et al., 2013, Rakotondrabe and Ivan, 2011). This chapter reports the design and testing of a novel pneumatically actuated micro-gripper capable of scaling to the level of manipulating a single biological cell. The reported device was designed in such a way as to eliminate the manual assembly difficulties associated with miniaturizing the design reported in the previous chapter. The microgripper consists of two microcantilevers pneumatically actuated by a deflected flexible membrane. The main design challenge was again to achieve accurate control over the opening and closing states of the gripper, along with the gripping forces.

4.1 Microgripper Design

The micro-gripper described here is pneumatically actuated and is designed to be operated in a range of environments, including air and liquid, at a range of scales. It comprises two main parts; the actuation mechanism and the flexible gripper arms, see Figure 4.1. The design of the active part of the microgripper is shown in Figure 4.2. The actuator is essentially a flexible membrane that applies a force to the gripper pad when the air inlet is pressurized. The gripper plate was cut from stainless steel sheet using photo-etching technology to give an outer envelope, which was sandwiched between two PMMA layers with a specific arrangement explained in the next section. When pressure is applied to the pad, the arms pivot around a torsional spring consisting of a bar-shaped ligament of the gripper plate. The arms themselves are designed to be flexible so that the gripping force can, in principle, be monitored by measuring the strain at the pivot end of the arm or the

slope at its free end. The design can be operated in with two arms closing together when actuated (as shown in Figure 4.1) or can be operated so that the jaws are opened by actuators on the opposite sides of the gripper plates using the spring force and compliance of the arm to offer the gripping force, limited, if necessary, by the air pressure. The whole design is scalable by controlling the dimensions of the components of the gripper, in particular the arms and torsion bars.

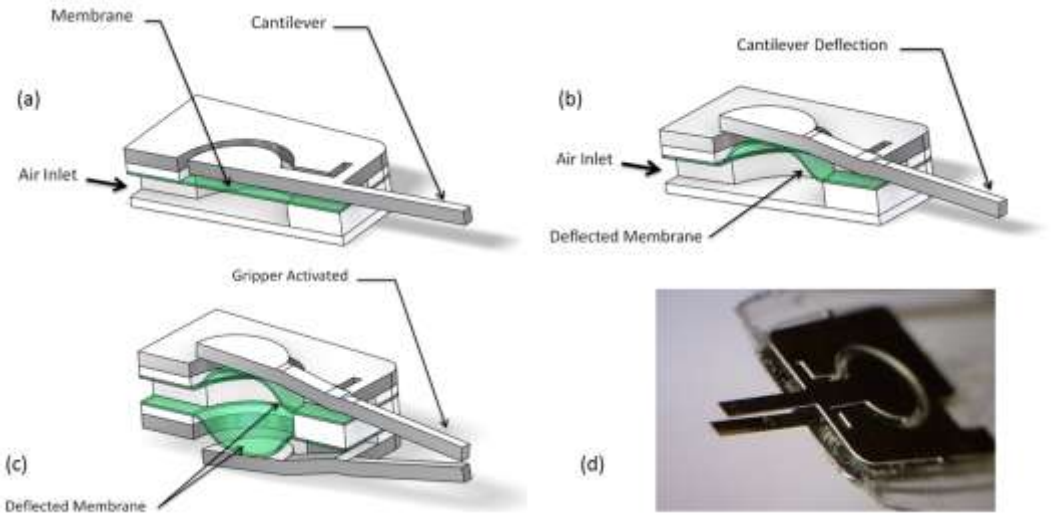

Figure 4.2: Schematic drawings of working principle of the gripper device (a-c), and picture of assembled microgripper (d).

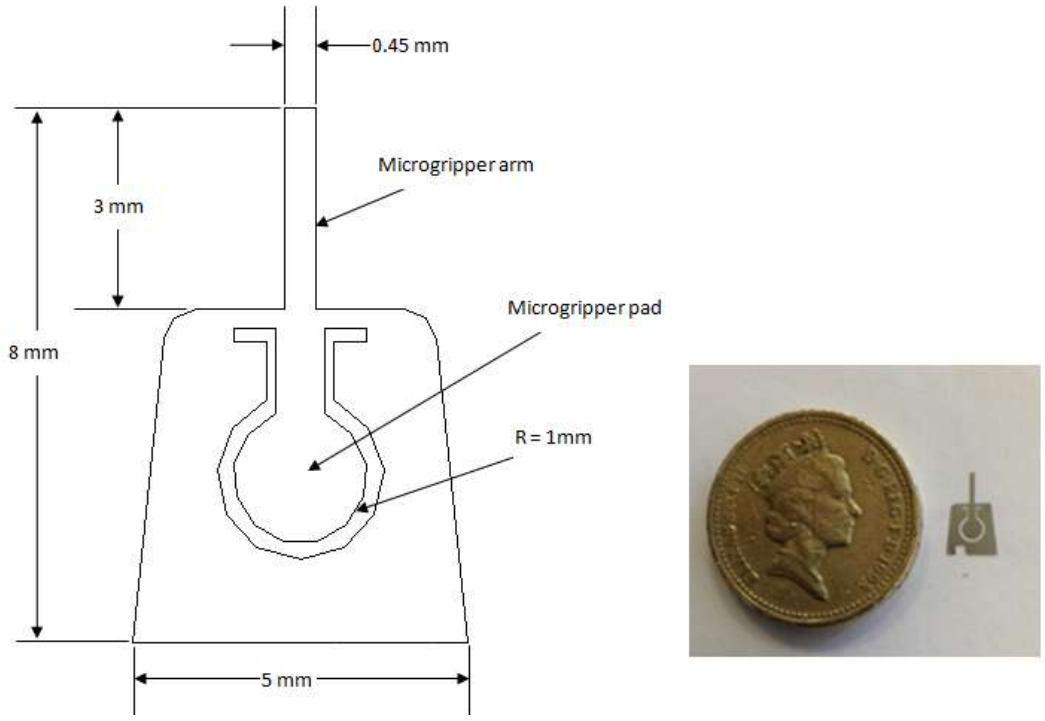

Fig. 4.1: Design of the active part of the microgripper

4.2 Fabrication and Assembly

The body of the gripper is assembled using 3 layers of laser cut PMMA 200µm thick: bottom, mid, and top layer. The mid-layer is laser cut into a shape with 50 microns thick transfer adhesive layers attached to both sides. These layers of transfer adhesive themselves were laser cut to define micro-channels before attaching them to the mid-layer. Two silicone membranes, 65 micron thick each, are then applied to the adhesives. Two microgrippers are then fixed over each membrane and then the two layers of PMMA, with the transfer adhesive on both sides, are attached as the bottom and top layers over the membranes and the microgrippers. An inlet hole should be present within all layers of the assembly apart from the bottom membrane and the bottom PMMA layer. This will allow air to enter the microchannel and inflate/expand the membrane layers. To ensure that the membranes do not slip and that there are no leaks in the set up, the micrpgripper assembly is laminated between two 75 micron thick layers of

laminate sheet. The underside of the assembly is attached to a laminate, that is laser cut allow the microgripper arm to flex, using the transfer adhesive already in place. The top layer of the laminate is laser cut to expose the inlet hole in the device and to allow the gripper arm to flex. This layer is then attached to the topside of the assembly again using the transfer adhesive that is already in place. The entire device is then laminated at 130 degrees on heavy gauge at a feed speed of 1mm/sec. The assembling steps are illustrated in Figure 4.3, and a picture of an assembled microgripper is also shown in Figure 4.2 (d). The active part of the microgripper was fabricated using a photo-etching technology as described in chapter 2.

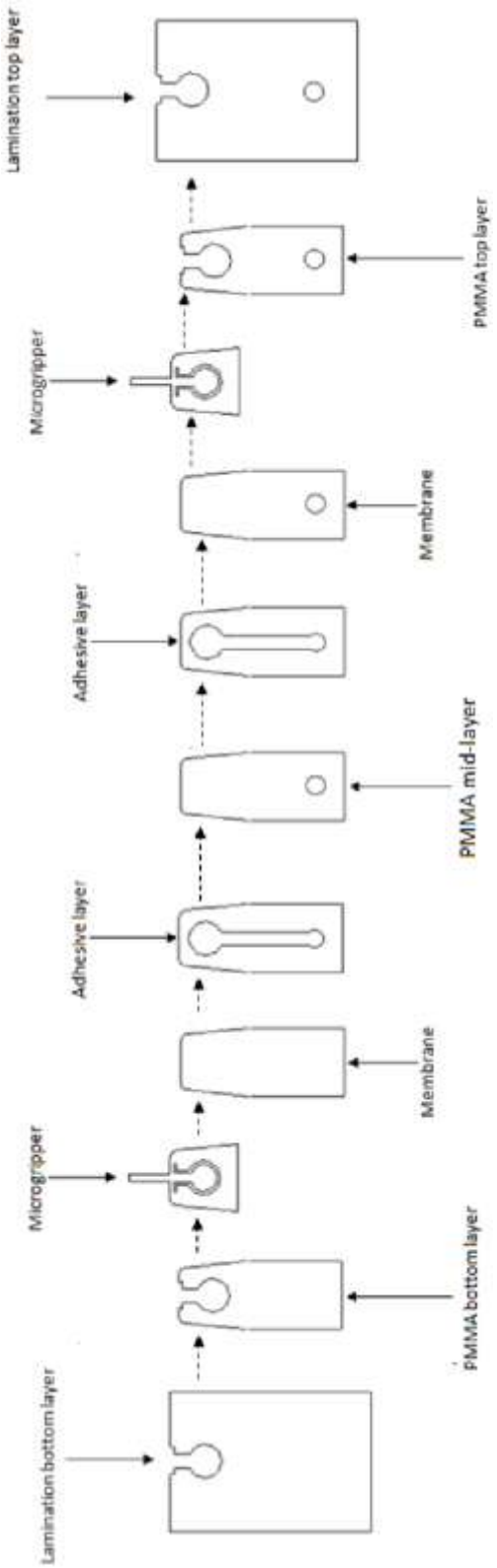

Fig. 4.3: Steps of assembling microgripper device illustrating the sequence of assembly of the different layers of the device.

4.3 Performance of Prototype Device

To validate the above-mentioned design principle, a prototype device was realised in 50 µm thick stainless steel sheet with a pad diameter of 2 mm, arms of length 3 mm and breadth 0.45 mm, and torsion bars of breadth 0.3 mm and length 0.625 mm. The performance of the device was evaluated using two tests; a dynamic test where the feed air pressure was pulsed at a range of frequencies and pressures and the tip displacement with no loading was measured, and a static test where the input load and output load were measured.

For the dynamic test, an optical sensor was used to obtain the deflection at the cantilever tip using a similar approach to an AFM where a laser beam at a fixed angle is reflected from the end of the cantilever and the position of the spot on a photdetector recorded as mentioned in chapter 2, see Figure 2.7. Deflection data were acquired using a LabView control interface at a rate of 300 samples per second for a record length of around 20 cycles (e.g. Figure 4.5) whilst the pressure was pulsed from zero to 1, 2, 3, 4, and 5 bar at frequencies of 1, 2, 4, 8, 20, 50, 100, and 300 Hz.

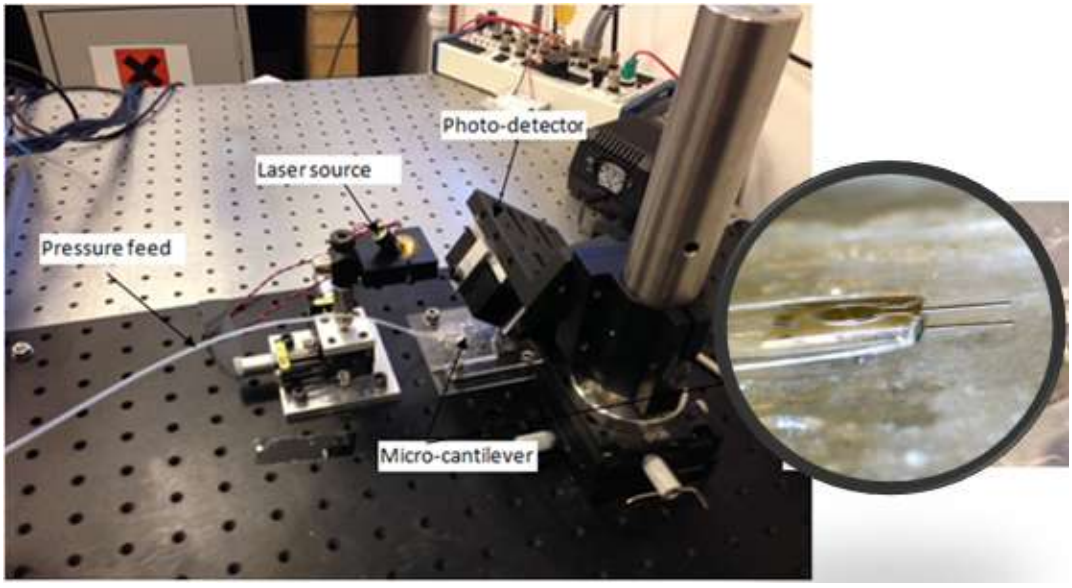

Figure 4.4: Dynamic test set-up with optical sensor where the laser spot is reflcted by the cantilever tip, and the deflection is recorded by the photo-detector

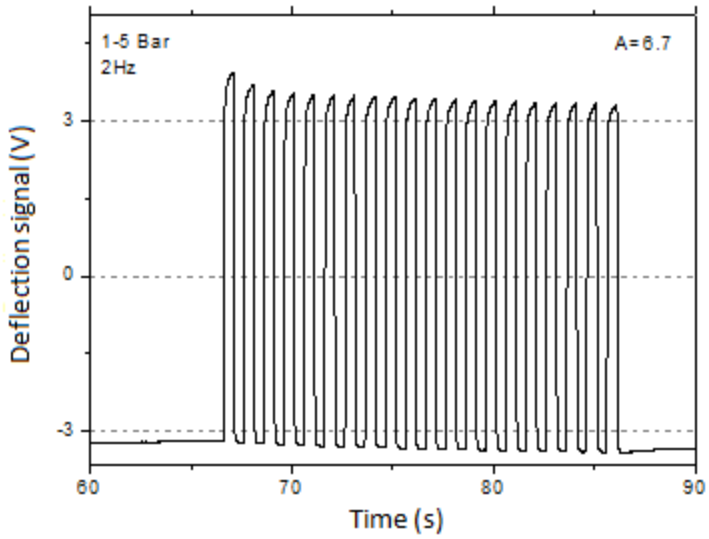

Figure 4.5: Sample raw data from dynamic test showing the amplitude of deflection of cantilever tip in volts.

4.3.1 Cantilever Tip Bending

Utilizing the signal from the PSD requires quantifying the acquired data into an actual cantilever tip bending. PSD is used to detect the reflected laser from the tip of the cantilever. Focusing and aligning the laser diode with the tip of the cantilever is very crucial in this procedure since the PSD captures the reflective signal, as the cantilever bends, to measure the laser position. As shown in Figure 4.5, the output of this step is the bending of the tip of the cantilever in volts (v) and the aim is to obtain the bending in millimeters (mm).

This step was implemented under different pressures 1, 2, 3, 4, and 5 bar and different frequencies 1, 2, 4, 8, 20, 50, 100, and 300 Hz. The acquired data will appear as in Figure 4.6.

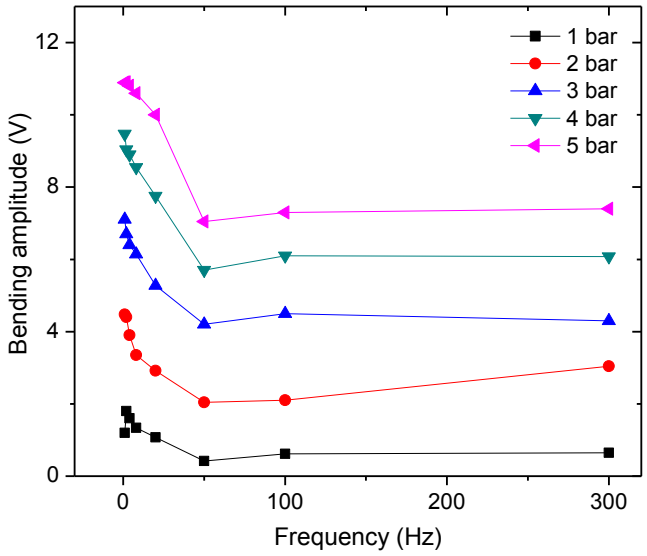

Figure 4.6: Amplitude of tip displacement in dynamic tests for different pulsed pressures and frequencies

The used PSD linear that directly and linearly converts the laser spot into two currents (i_A and i_B) from its two ends. These outputs are processed internally through a specified arrangement ending up with signals that can be measured, X, Y, and intensity signals output. As the laser spot reflection moves because of the cantilever deflection, the positional change in Y can be determined to be:

$$\Delta z = \frac{L \times L_{PSD}}{8s}(\Delta V) \qquad (4.1)$$

Where L is the length of the cantilever, L_{PSD} is the length of PSD area, s is the distance from the cantilever tip to the PSD, and ΔV is the amplitude of the output bending signal in volts. Therefore, the cantilever deflection of ΔZ can then be calculated.

For calibration of the system and to maximize the readout signal, the laser beam is required to focus on the tip of the cantilever where the most deflection takes place. The laser beam is moved until it centered on the cantilever tip, and at the same time, ensuring the presence of a reflective signal using the PSD. As a signal is achieved by realizing a positive intensity signal, the laser is then further

adjusted to get the optimum combination of the maximum intensity signal while still focusing on the tip of the cantilever. Finally, centering the laser (Y position) to 0 allows maximum possible signal change, although it is not required as the signal is not enough to reach the boundaries, ±10 V.

The relation between the deflection of the microgripper pad and microgripper tip is an important design consideration since it is related the torsional stiffness of the pivot bars. This relation was measured using a modification of the dynamic set-up shown in Figure 4.4, where the deflection of the pad and the tip were measured in separate experiments for pressure pulses set at 0.17, 0.35, 0.56, and 0.75bar at a frequency of 1Hz. Figure 4.7 shows the mean and standard deviation of the amplitudes of tip displacement and pad displacement for each of the pressures plotted against each other.

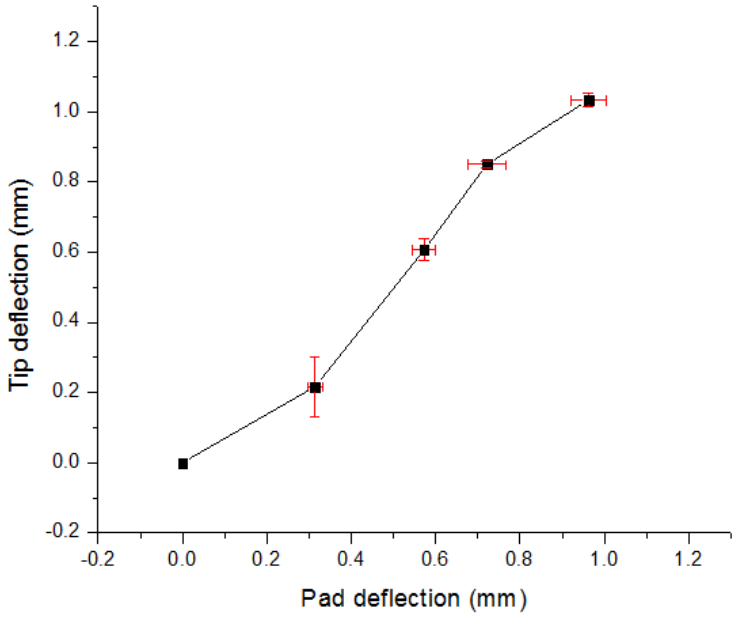

Figure 4.7: Relation between pad deflection and tip deflection

4.3.2 Output Force

As mentioned above, an important indicator of the performance of the device is the output force. For the static test, a digital scale of up to four decimals was used to measure the generated force at the tip of cantilever, illustrated in chapter 2 in Figure 2.5, where the cantilever tip is in direct contact with a metallic ball to ensure a one point contact between the ball and the cantilever tip. The pressure in the feed line was then increased incrementally to 5 bar, recording the output force at approximately 0.2, 0.3, 0.4, 0.5, and 1 bar, thereafter at 1 bar interval. The results are shown in Figure 4.8 for forward and reverse increments of pressure up to 5 bar using two dwell times (10s and 30s) before the force was recorded. The same procedure was used to determine the input force for a given pressure by applying the membrane directly to the metal ball, Figure 4.10, and recording the force at the same increments of pressure. Figure 4.9 shows the relationship between the input force and the output force for each of the pressure increments.

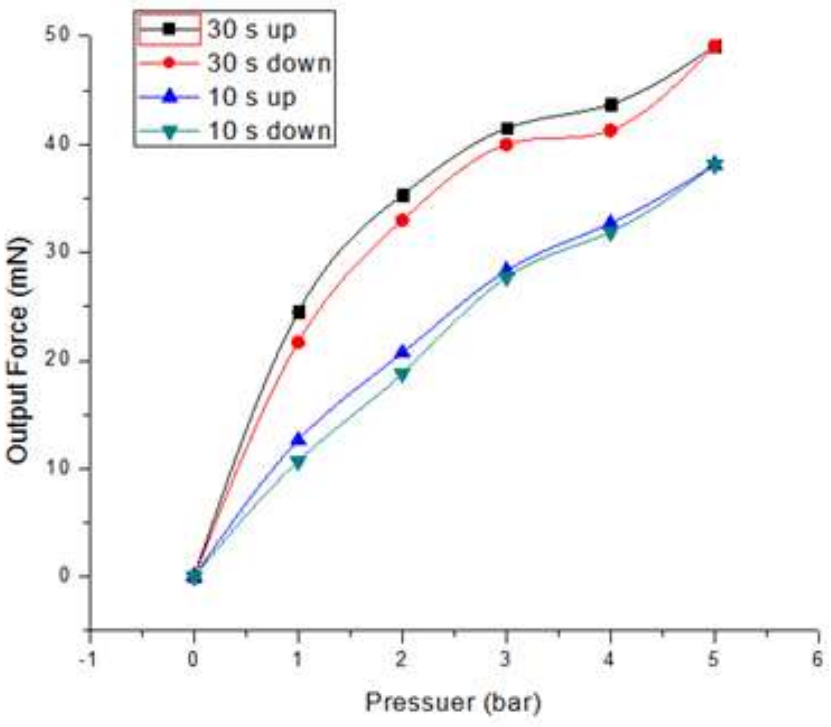

Figure 4.8: Cantilever tip (output) force for a range of input pressure

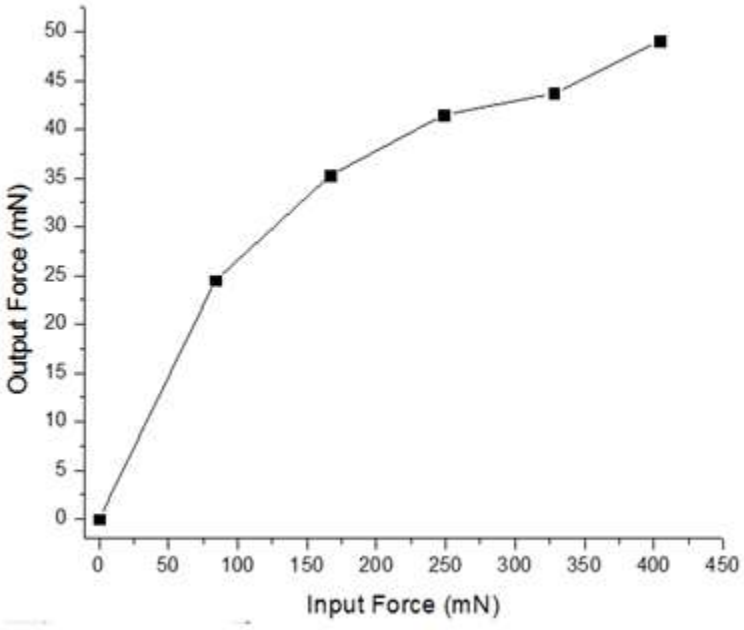

Figure 4.9: Input force and output force at pressures used in Figure 4.8

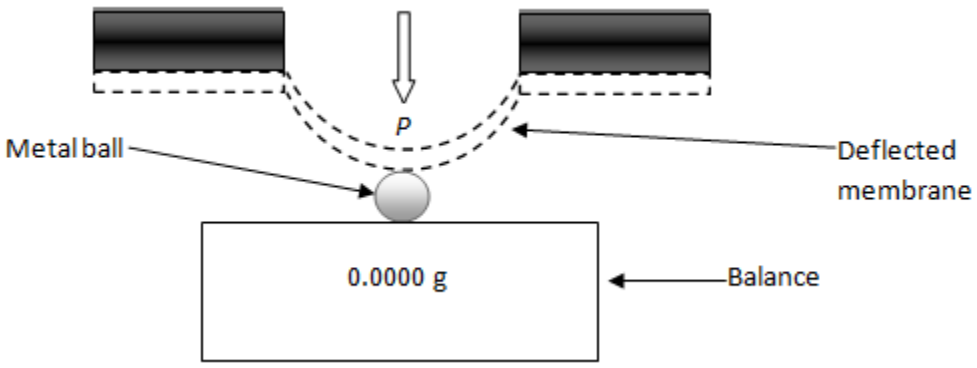

Fig. 4.10: Schematic illustration of input force calibration

4.4 Results and discussion

In order to select appropriate dimensions for a tactile gripper of the type presented, it is useful to have a simple analytical model for the stiffnesses of its key parts. Figure 4.11 shows a simplified mechnical model of the gripper pad-arm plate, with the input force, the output reaction and the torsional springs.

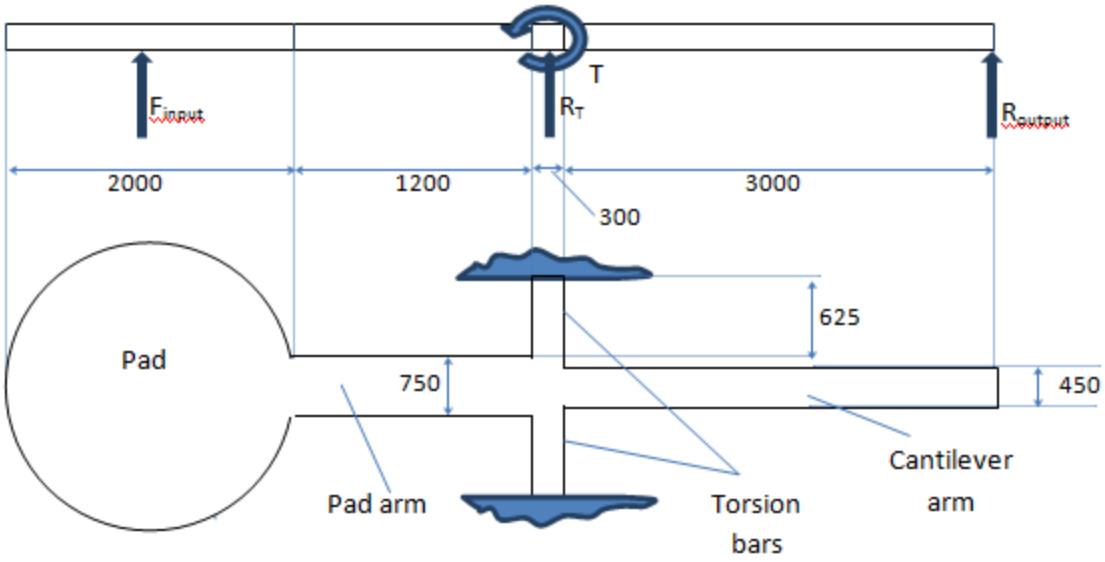

Figure 4.11: Simplified mechanical model of cantilever.

When the cantilever tip is not in contact with an object (R_{output} = 0), the input force determines the reaction torque:

$$T = 2.35F_{input} \tag{4.2}$$

for an input force in N and torque in Nmm.

Thus, for linear elastic materials, the angular displacement at the hinges θ can be written by (Vable, 2012):

$$\theta = \frac{TL}{JG} = \frac{2.35\times0.625}{2ab^3\left[\frac{16}{3} - 3.36\frac{b}{a}\left(1-\frac{b^4}{12a^4}\right)\right]78\times10^3}F_{input} \tag{4.3}$$

where,

L: the length of torsion bar, J: Second moment of area

G: the modulus of rigidity = 78 GPa

and 2a and 2b are the short and long dimensions of the bar cross-section.

2a = 0.3mm, and 2b = 0.05 mm

$$\theta = \frac{TL}{JG} = \frac{2.35 \times 0.625}{2 \times 0.15 \times 0.025^3 \left[\frac{16}{3} - 3.36\frac{0.025}{0.15}\left(1 - \frac{0.025^4}{12 \times 0.15^4}\right)\right] 78 \times 10^3} F_{input}$$

$$= \frac{2.35 \times 0.625}{2 \times 0.15 \times 0.025^3 \left[\frac{16}{3} - 0.56\right] 78 \times 10^3}$$

$$\theta = \frac{TL}{JG} = 0.841 F_{input} \qquad r^2 \qquad (4.4)$$

The expected tip displacement for a given angle is

$$\delta_{arm} = l_{arm} \tan\theta = l_{arm} \tan\left(0.841 F_{input}\right) mm \qquad (4.5)$$

and, for a simple torsion pivot, the displacements at the pad and at the cantilever tip for a given angle (i.e. a given pressure) might therefore be expected to be related

$$\delta_{cantilever,T} = \frac{l_{cantilever}}{l_{pad}} \delta_{pad,T} \tag{4.6}$$

As well as causing the above displacements, a certain amount of bending might be expected in the pad arm (also in the cantilever, if loaded) and this will be a function of applied force. To a first approximation, the pad itself can be assumed not to bend so that the bending component of the pad displacement can be taken as the end deflection of a cantilever of length L where the load plus an additional applied moment $M_{input} = F_{input}\left(L-l\right)$ is applied a distance l from the fixed end. The relevant displacements at the pad are given by

$$\delta_{pad} = \delta_{arm} + slope_{arm}\left(L-l\right) \tag{4.7}$$

so:

$$\delta_{pad,b} = \frac{F_{input}l^3}{3EI} + \frac{F_{input}l^2}{2EI}\left(L-l\right) + \frac{M_{input}l^2}{2EI} + \frac{M_{input}l}{EI}\left(L-l\right)$$
$$= \frac{F_{input}l^3}{3EI} + \frac{F_{input}l^2}{2EI}\left(L-l\right) + \frac{F_{input}l^2}{2EI}\left(L-l\right) + \frac{F_{input}l}{EI}\left(L-l\right)^2$$
$$= \frac{F_{input}}{EI}\left[\frac{l^3}{3} + l^2\left(L-l\right) + l\left(L-l\right)^2\right]$$

$L = l_{pad}$ and $\delta_{cantilever,T} = 3.15\tan\left(0.841F_{input}\right)$, i.e. $F_{input} = \frac{1}{0.841}\tan^{-1}\left(\frac{\delta_{cantilever,T}}{3.15}\right)$

$$\delta_{pad,b} = \frac{1}{0.841}\tan^{-1}\left(\frac{\delta_{cantilever,T}}{3.15}\right)\frac{1}{EI}\left[\frac{l^3}{3} + l^2\left(l_{pad}-l\right) + l\left(l_{pad}-l\right)^2\right]$$
$$= \frac{1}{0.841}\tan^{-1}\left(\frac{\delta_{cantilever,T}}{3.15}\right)\frac{12}{193\times10^3\times0.75\times0.05^3}\left[\frac{1.2^3}{3} + 1.2^2\left(2.2-1.2\right) + 1.2\times\left(2.2-1.2\right)^2\right]$$
$$= 0.789\tan^{-1}\left(\frac{\delta_{cantilever,T}}{3.15}\right)\left[3.22\right] = 2.536\tan^{-1}\left(\frac{\delta_{cantilever,T}}{3.15}\right)$$

Thus, the relationship between pad displacement and tip displacement for an unloaded tip can be expressed as:

$$\delta_{pad} = \delta_{pad,T} + \delta_{pad,b} = \frac{l_{pad}}{l_{cantilever}} \delta_{cantilever,T} + 2.536 \tan^{-1}\left(\frac{\delta_{cantilever,T}}{3.15}\right)$$

$$= \frac{2350}{3150} \delta_{cantilever,T} + 2.536 \tan^{-1}\left(\frac{\delta_{cantilever,T}}{3.15}\right)$$

$$= 0.746\delta_{cantilever,T} + 2.536 \tan^{-1}\left(\frac{\delta_{cantilever,T}}{3.15}\right)$$

$$\delta_{pad} = 0.746\delta_{cantilever} + 2.536 \tan^{-1}\left(\frac{\delta_{cantilever}}{3.15}\right) \quad (4.8)$$

It should be pointed out here that the above relationship is an approximate in that it assumes that both the pad arm and cantilever arm remain straight and also that the effects of compressive and tensile stresses on twisting of the relatively flat bars are negiligible. Figure 4.12 shows the mean data from Figure 4.7 for measured pad and tip displacements for the four increments of pressure. Also, for each of the tip displacements, the corresponding pad displacements have been calculated, firstly assuming the torsion bars to act merely as pivots and, secondly, taking into account the stiffness of the torsion bars. As can be seen, the second calculation is reasonably consistent with the measurements indicating that the analytical model is sufficient for the purposes of sizing the torsion bars. A finite element model of the plate including the outer frame was also built and this was was loaded using the membrane pressure applied over the surface of the pad, but simulated as a point force at the centre of the pad as shown in Figure 4.13 (a). In the simulation, the gripper was analyzed as a 2D model with the material of stainless steel, of which Young's modulus is 200 GPa, and Poisson's ratio is 0.3. The mesh size was 0.1mm for the whole mechanism, but that for the critical regions it was decreased to 0.005mm as they govern the performance of the device as illustrated in Figure 4.13 (b). The total number of elements was 475644 and the number of nodes was found to be 294107.

Figure 4.14 shows the resulting pad and tip displacements for each of the pressures used in the static tests, alongside calculated values of the pad displacement for each of the simulated tip displacements using Equation (4.8).

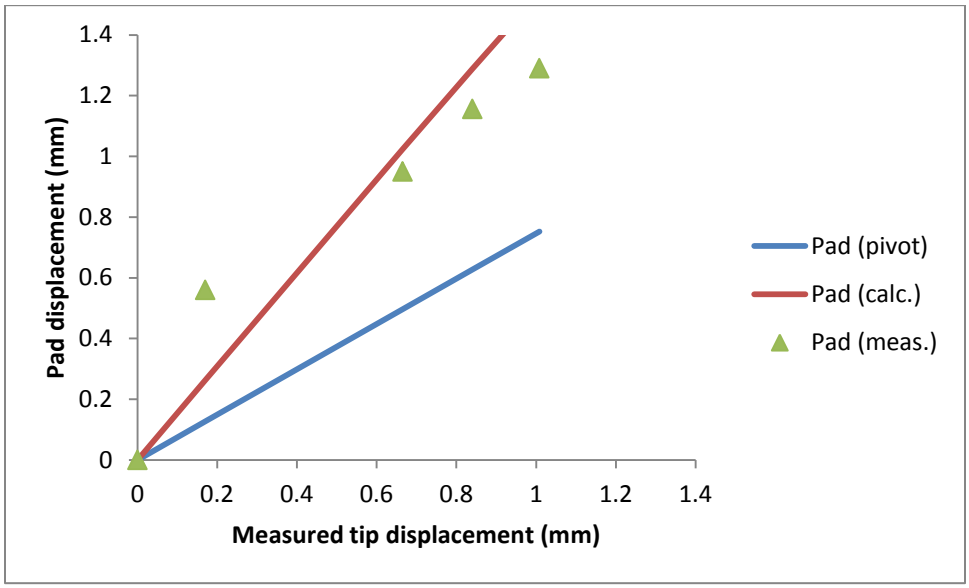

Figure 4.12: Analytical model of cantilever for assessing pad displacment compared with measured values (Figure 4.7).

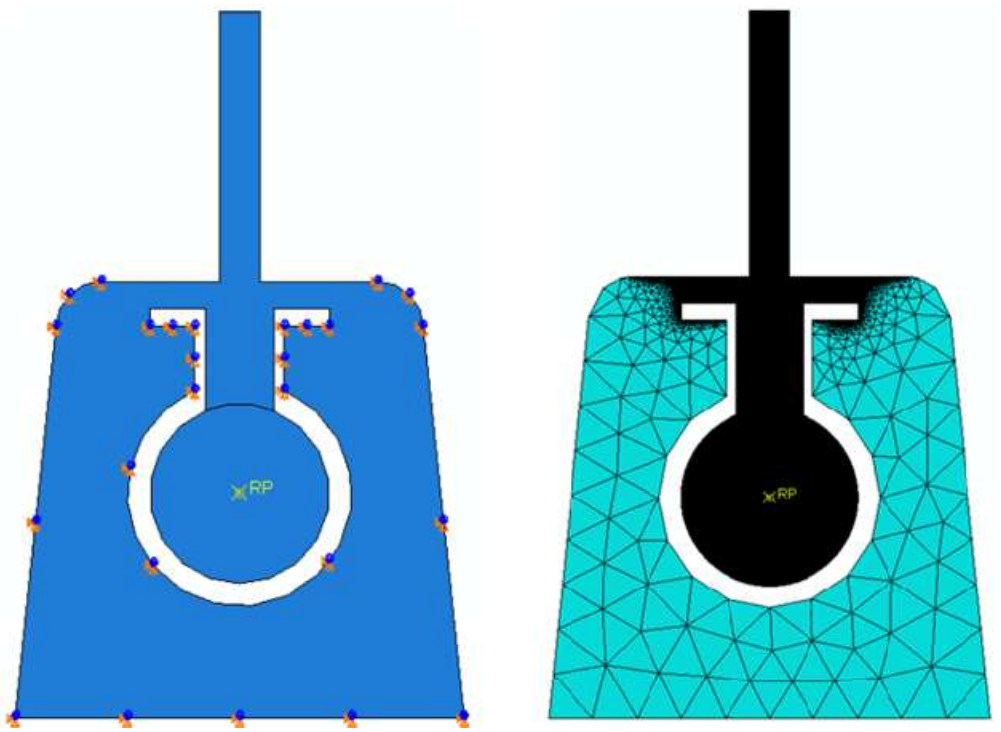

(a) **(b)**

Figure 4.13: FE model of gripper plate for assessing pad and tip displacments for a force applied at RP.

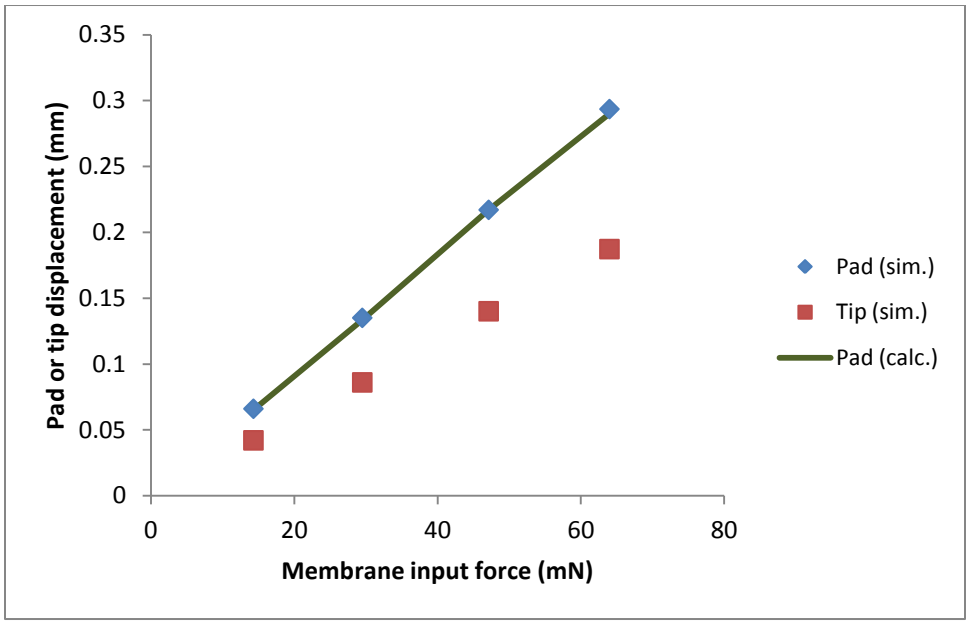

Figure 4.14: Simulated pad and tip displacements for pressure loading of the pad at values shown in Figure 4. Solid line shows calculated pad displacement for each of the simulated tip displacements.

Based on this tentative verification, the analytical model can now be used to assess the input force corresponding to the various pressure amplitudes seen in Figure 4.6. However, Figure 4.6 shows that the maximum tip displacement for the unloaded cantilever depends on actuation frequency of at least up to 50Hz above which the actuator is probably limited by the supply of air. The frequency sensitivity is unlikely to be due to a structural resonance (for example, the natural frequency of the least stiff part of the system, the cantilever, is about 4kHz) nor is it likely, given the data in Figure 4.8, to be due to membrane relaxation or leakage. Figures 4.15 and 4.16 show the variation of maximum tip displacement (as voltage output from the photodetector) with input pressure pulse height at the actuator (data essentially re-plotted from Figure 4.6). The curves are reasonably linear (more so at lower frequencies) and thus an overall compliance (in mm tip deflection per bar) can be determined for the actuator. This is plotted in Figure 4.17 for the whole range of frequency examined, and it can be seen that the compliance changes with frequency over the range 0-50 Hz, and little thereafter. This suggests that the dynamic behaviour of the actuator is affecting the tip displacement and so the most reliable measurement of the system compliance is given by extrapolation to zero frequency (Figure 4.18), i.e. a value of 0.223 mm/bar. Since this is only around 1% different to the value measured using a frequency of 1Hz, the pad and tip measurements shown in Figure 4.7 are unlikely to have been much affected by the actuator dynamic response.

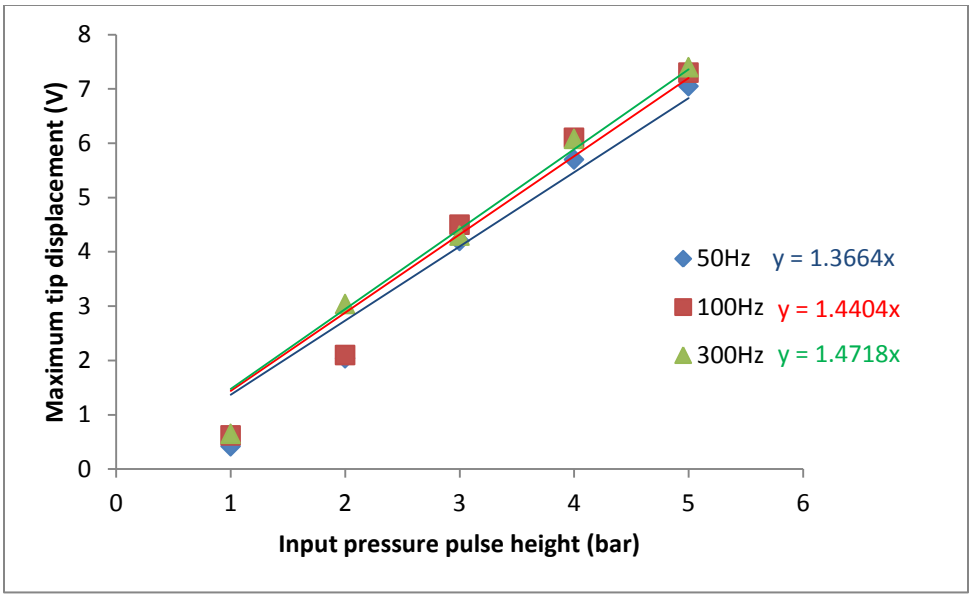

Figure 4.15: Effect of frequency on unloaded cantilever system compliance at higher frequencies (data from Figure 4.6).

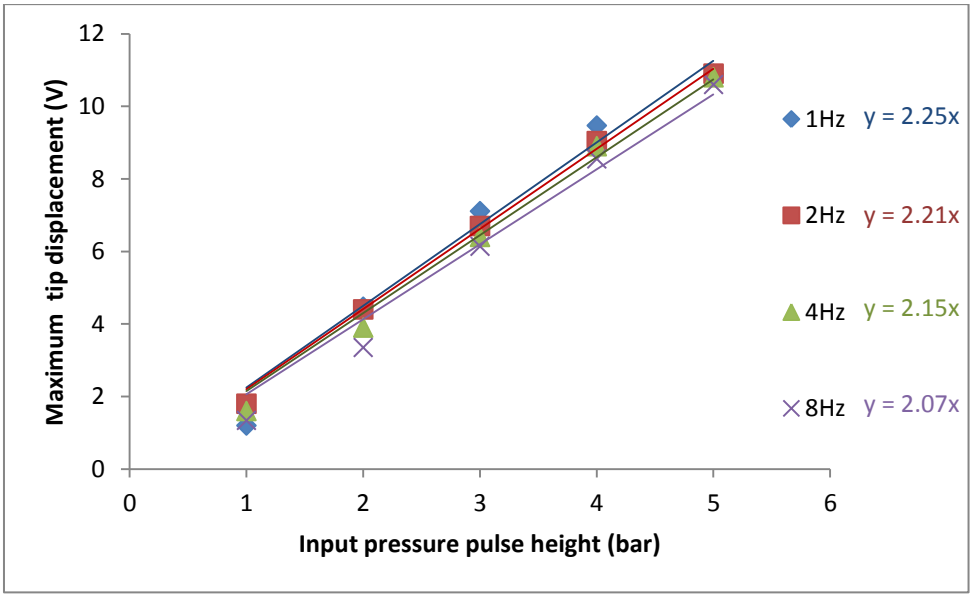

Figure 4.16: Effect of frequency on unloaded cantilever system compliance at lower frequencies (data from Figure 4.6).

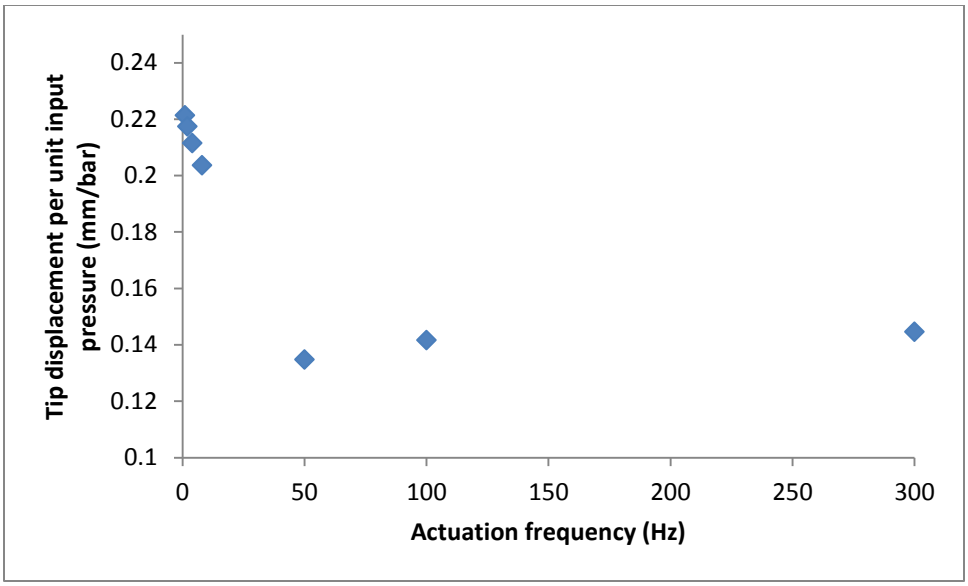

Figure 4.17: Unloaded system compliance over full frequency range.

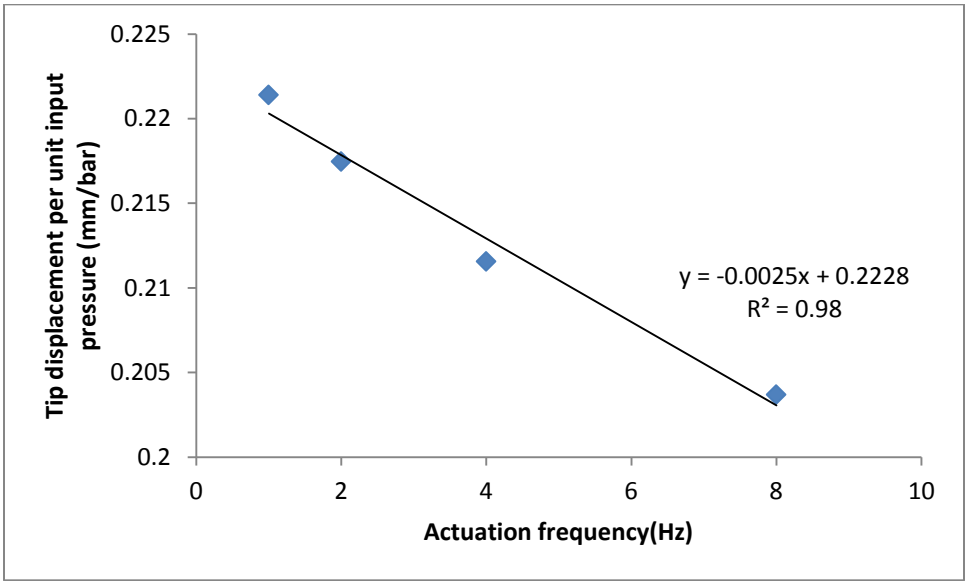

Figure 4.18: Unloaded system compliance at low frequencies 1, 2, 4, and 8 Hz.

The compliance can further be used to determine the input force corresponding to a given input pressure when R_{output} = 0 using the relationship between input force and cantilever displacement:

$$F_{input,R_{output}=0} = \frac{1}{0.841}\tan^{-1}\left(\frac{\delta_{cantilever,T}}{3.15}\right)$$

i.e.

$$F_{input,R_{output}=0} = \frac{1}{0.841}\tan^{-1}\left(\frac{0.223p}{3.15}\right) \qquad (4.9)$$

where the input pressure, *p*, is in bar. When the cantilever is loaded, the force system becomes statically indeterminate which makes an analytical model a bit more tedious and so, for the pruposes of this study, the analytical realtionship between the input pressure and input force equation (4.9) was used in a linear elastic FE simulation of the gripper plate with a loaded cantilever to calculate the output force. The results of this simulation are compared with the measured output forces at 30 s dwell time from the static tests (Figure 4.8) in Figure 4.19 and it can be seen that agreement is good up to a pressure of 1 bar, beyond which the simulated output force is higher than that measured, the discrepancy increasing with increasing pressure. The reason for this can be seen in the finite element elastic stress distribution calcualted at 1 bar input pressure shown in Figure 4.20. Notwithstanding the local stresses, it can be seen that the von Mises stress at the torsion bar end on the input pad arm is about 800MPa, whereas that at the fixed ends of the torsion bars is about 500MPa, both vlaues prevailing across most of the relevant cross-section. These stresses are beyond the yield stress of moderatley cold-worked stainless steel and well beyond yield for annealed stainless steel (Milad *et al*., 2008), so it is likely that the reduction in experimental force output is due to the formation of one or more plastic hinge in the gripper plate. Plastic collapse would invalidate the relationship between input force and pressure equation (4.9) so that the simulation would be in error in terms of the

input as well as in terms of the resulting deflections. At any rate, equations (4.8) and (4.9) can still be used for design purposes so that dimensions of the gripper can be chosen to avoid yield using very simple analytical expressions.

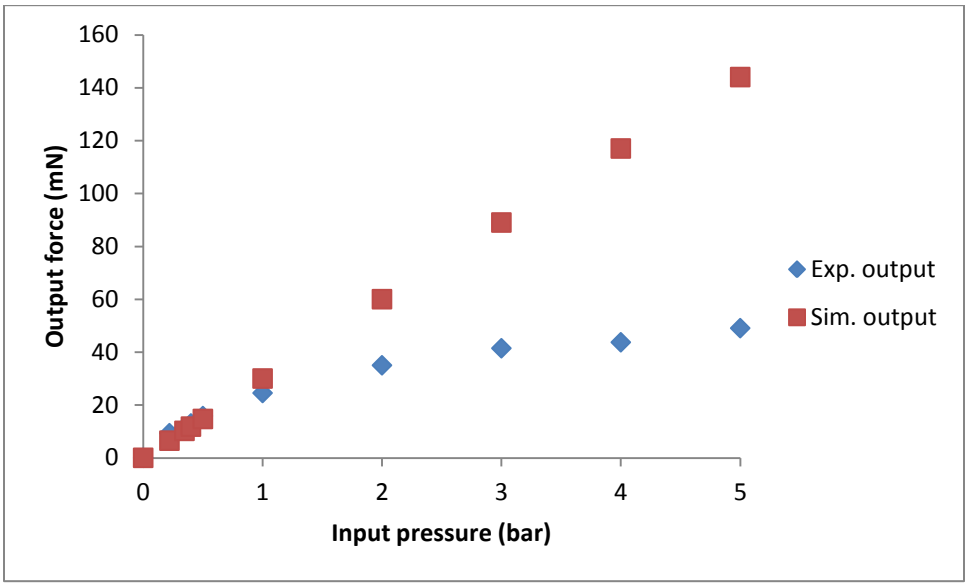

(a)

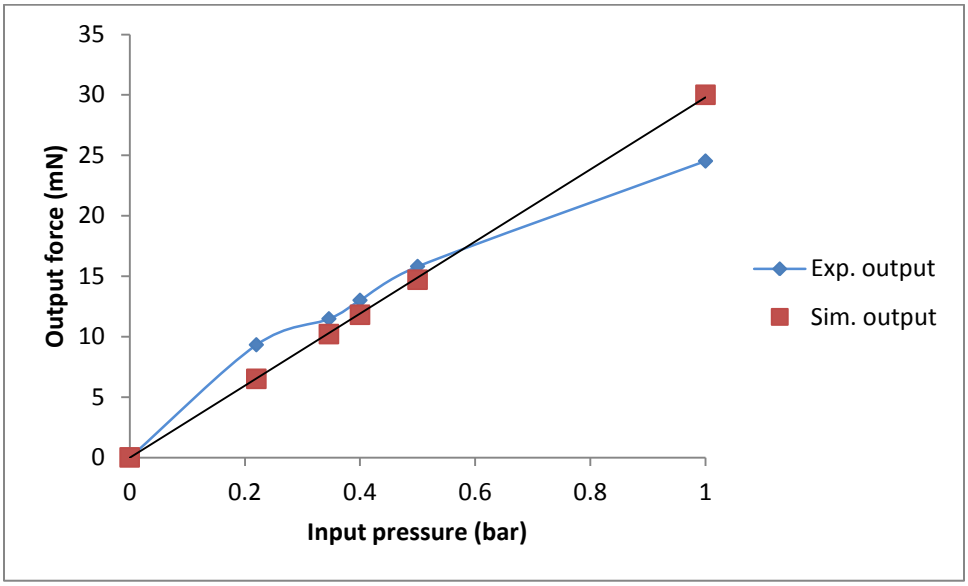

(b)

Figure 4.19: Measured and simulated output forces for a range of input pressures (a) range for 0 to 5bar, (b) range from 0 to 1 bar.

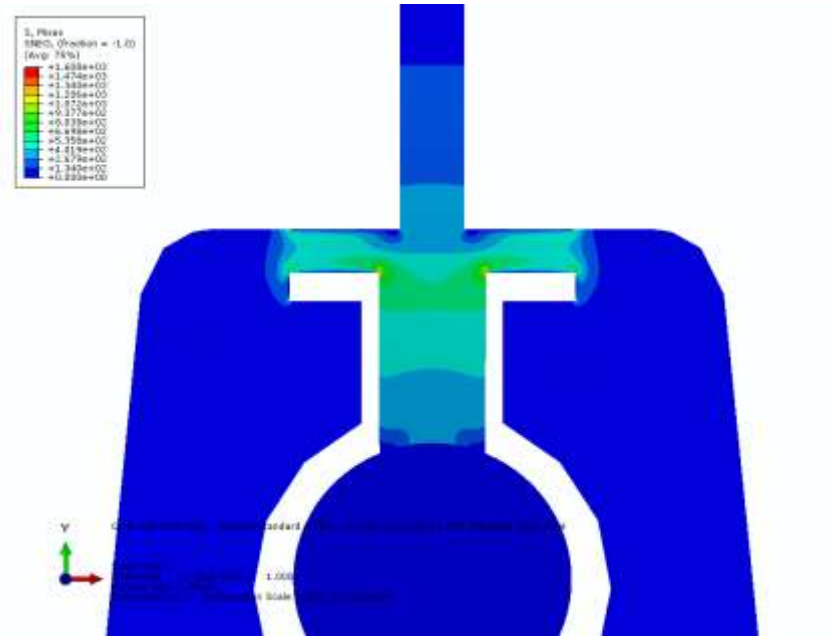

Figure 4.20: Elastic stress analysis for loaded gripper plate with applied pressure of 1 bar.

4.5 Demonstration of Device

A fully-assembled version of the device was used to demonstrate that actuator in pick-and-place mode and also in sensor-gripper mode.

The pick-and-place funcition was demonstrated in air and in water and consisted of manipulating acid washed zirconium microbeads of 200 µm diameter (OPS Diagnostics, Lebanon NJ, USA). The device was mounted on an XYZ stage and the microbeads placed in a petri-dish with a monitoring camera underneath, as illustrated in the micro-manipulation set-up in chapter 2, see Figure 2.11.

Figure 4.21 and 4.22 show the sequence of gripping operation and different patterns that have been constructed using the proposed manipulation technique, respectively.

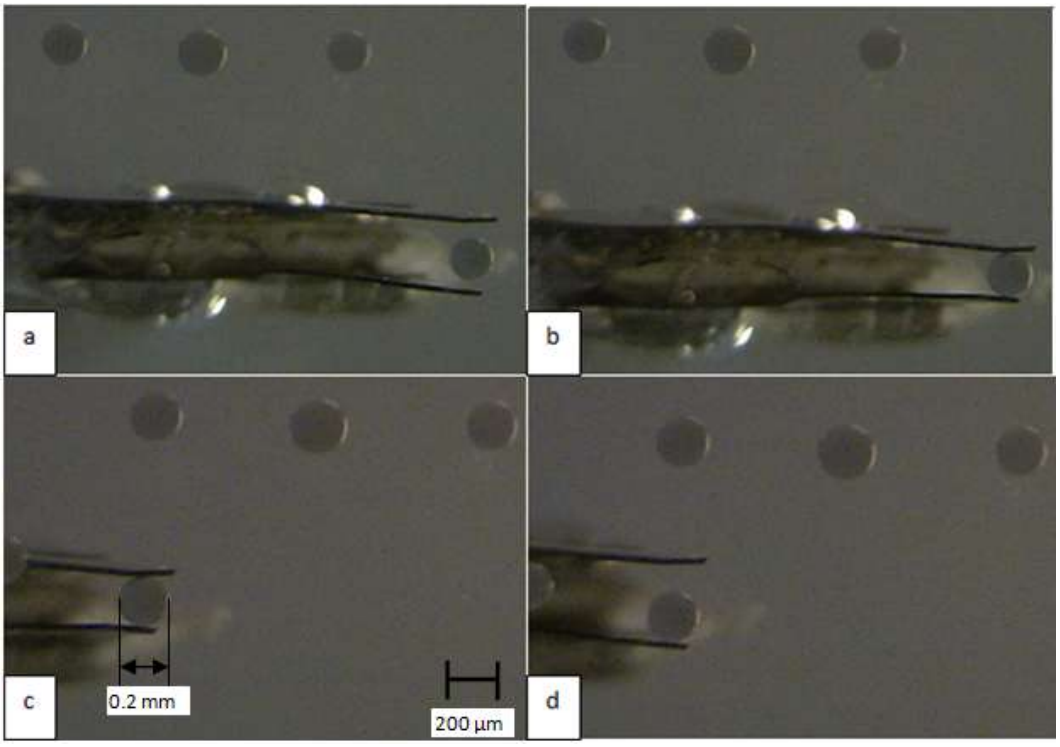

Figure 4.21: Sequence of gripping operation (a) positioning, (b) gripping, (c) placing, and (d) releasing

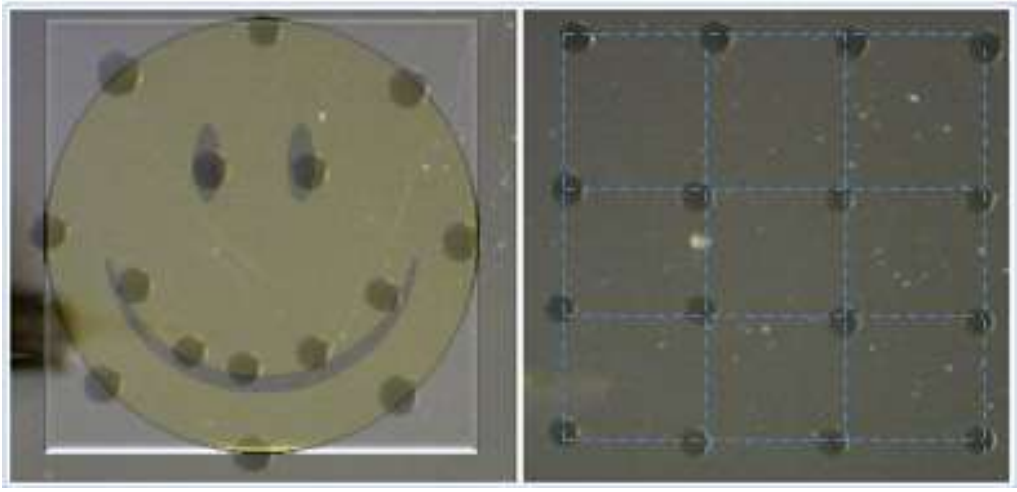

Figure 4.22: 200 microns microbeads used to form a smiley face (left), and 4x4 array (right)

4.6 Conclusion

This chapter has demonstrated the design and fabrication of a simple-to-manufacture gripper with abilities to pick and place micron-sized hard and soft objects.

The design involves a balloon actuator whose pressure-force relationship can be simply measured and controlled in both static and dynamic modes.

Two stainless steel gripper plates can be fabricated in a range of dimensions, chosen to suit the application and a simple analytical or FE model can be used to perform the scaling.

Essentially, two torsion bars can be used with a variety of stiffness between something which behaves almost like a pivot to one where there is considerable down-regulation of the input force (for more delicate tasks).

Besides controlling the input and output forces, the design of the gripper arms can be tuned in order to provide a deflection of the arms, whose measurement can be used to measure the gripping force in operation and can potentially be fed back to control the force or used to assess the gripped object.

4.7 References

BHARANIDARAN, R. & RAMESH, T. 2013. A numerical approach to design a compliant based Microgripper with integrated force sensing jaw. *International Journal of mechanics,* 2 (7), 128-135.

CHANG, R.-J. & CHENG, C.-Y. 2009. Vision-based compliant-joint polymer force sensor integrated with microgripper for measuring gripping force. *In:* Advanced Intelligent Mechatronics, 2009. AIM 2009. IEEE/ASME International Conference on, 2009. IEEE, 18-23.

EL-SAYED, A. M., ABO-ISMAIL, A., EL-MELEGY, M. T., HAMZAID, N. A. & OSMAN, N. A. A. 2013. Development of a Micro-Gripper Using Piezoelectric Bimorphs. *Sensors,* 13**,** 5826-5840.

MADZHI, N. K., AHMAD, A., KHUAN, L. Y. & ABDULLAH, F. 2010. Development and electrical measurements of piezoresistive microcantilever biosensor signal transduction for human stress measurement. *In:* Proceedings of the 9th WSEAS international conference on Electronics, hardware, wireless and optical communications, 2010. World Scientific and Engineering Academy and Society (WSEAS), 72-75.

MILAD, M., ZREIBA, N., ELHALOUANI, F. & BARADAI, C. 2008. The effect of cold work on structure and properties of AISI 304 stainless steel. *Journal of materials processing technology,* 203**,** 80-85.

RAKOTONDRABE, M. & IVAN, I. A. 2011. Development and force/position control of a new hybrid thermo-piezoelectric microgripper dedicated to micromanipulation tasks. *Automation Science and Engineering, IEEE Transactions on,* 8**,** 824-834.

VABLE, M. 2012. *Mechanics of Materials*, Michigan Technological University.

WILFINGER, R., BARDELL, P. & CHHABRA, D. 1968. The resonistor: a frequency selective device utilizing the mechanical resonance of a silicon substrate. *IBM Journal of Research and Development,* 12**,** 113-118.

XU, Q. 2012. A new method of force estimation in piezoelectric cantilever-based microgripper. *In:* Advanced Intelligent Mechatronics (AIM), 2012 IEEE/ASME International Conference on, 2012. IEEE, 574-579.

Chapter 5: Micro-Tweezers for Tactile Detection

Devices that sense such information as shape, softness, temperature, and normal forces by physical interaction can be termed “tactile” sensors or detectors (Tiwana et al., 2012). The implementation of tactile sensing technology has been studied for over 3 decades and researchers have recognised the huge potential and application of tactile detecting in certain areas of robotics (Tiwana et al., 2012, Harmon, 1982, Harmon, 1984, Harmon, 1980). In the surgical and medical fields, the properties of the bio-microobjects and tissues are very important in the assessment of their quality. For example, in clinical practice, assessing the condition of organs and tissues is often carried out by doctors using hand or palm which has its disadvantages (Tiwana et al., 2012). For example, nodules and small lumps are often missed by doctors during clinical practice (Barman and Guha, 2006) and, perhaps more importantly, the result is subjective and, at best semi-quantitative. Thus, there is a need for a reliable, objective and quantitative technique. Sarvazyan *et al.* indicated that an approach has the potential to provide a reliable low-cost technique to detect breast cancer complementing the other available techniques (Sarvazyan et al., 2008). Micro-cantilevers have been used both as biosensors (Madzhi et al., 2010) and sensors for characterizing the force (Chang and Cheng, 2009, Bharanidaran and Ramesh, 2013), so combining these two applications should be feasible.

Displacement-based sensing was suggested by Puangmali *et al.* as the simplest method of tactile sensing of an elastic object, whereby the force, spring constant, and the displacement are the only three variables needed. If the applied force is known and the displacement is accurately measured, then the stiffness of the object is directly obtained (Puangmali et al., 2008).

Another type of tactile sensor is vibration-based, whereby tactile information is obtained from the dynamic response (Puangmali et al., 2008) which can differentiate between different soft materials.

In this chapter, the design, fabrication, assembly, and testing of the micro-tweezers reported in the previous chapter is adapted for tactile detection. The proposed device could be used as a simple displacement-based sensor for the static measurements of an elastic or visco-elastic material. Also, it could be implemented as a vibration-based sensor by observing the dynamic response of the test object, particularly useful for materials which show time-dependent elastic behaviour.

5.1 Detector Design

The design of the detector is much similar to the microgripper presented in Chapter 4, where the main difference is that one of the arms is stationery while the other one is the active one used for the purpose of sensing and palpation as shown in Figure 5.1.

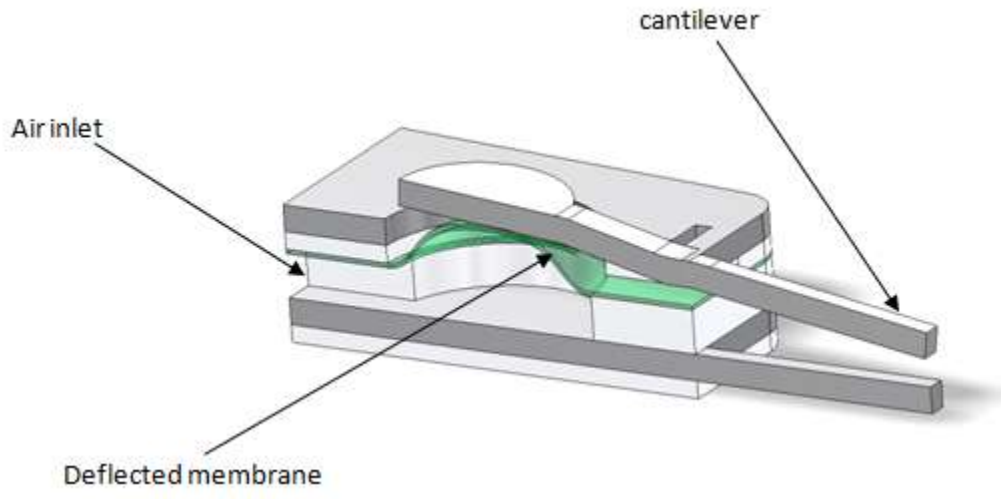

Figure 5.1: Schematic drawing of working principle of tactile detector where the cantilever is moving upon the deflection of the membrane and the lower arm is stationery

5.2 Fabrication and Assembly

The body of the detector was assembled using 2 layers of laser cut PMMA 500 µm thick for the bottom one and 200 µm thick for the top one. A silicone membrane approx 65 microns thick was sandwiched between the layers and are fixed in place using a 50 micron thick transfer adhesive. The first layer is PMMA is laser cut into shape with transfer adhesive attached to the underside. A layer of the transfer adhesive itself was then laser cut to define a microchannel and attached

to the topside of the first PMMA layer. The membrane was then applied to the adhesive over the topside. The sensing arm of the device was fixed over the membrane and then the second layer of PMMA (this time with the transfer adhesive on both sides) was attached as the top layer over the membrane and gripping arm. An inlet hole should be present within all layers of the assembly apart from the bottom PMMA layer. This will allow air to enter the microchannel and inflate/expand the membrane layer. The stationery arm of the detector was then attached to the bottom-side of the bottom-PMMA. To ensure that the membrane does not slip and that there are no leaks in the set up, the detector assembly was laminated between two 75 micron thick layers of laminate sheet. The underside of the assembly was attached to a plain piece of laminate using the transfer adhesive already in place. The top layer of the laminate was laser cut to expose the inlet hole in the device and to allow the detector arm to flex. This layer was then attached to the topside of the assembly again using the transfer adhesive that was already in place. The entire device was then laminated at 130 degrees on heavy gauge at a feed speed of 1mm/sec. The assembling steps are illustrated in Figure 5.2. The two active parts of the tactile detector, sensing and stationery arms, were fabricated using a photo-etching technology as described in Chapter 2.

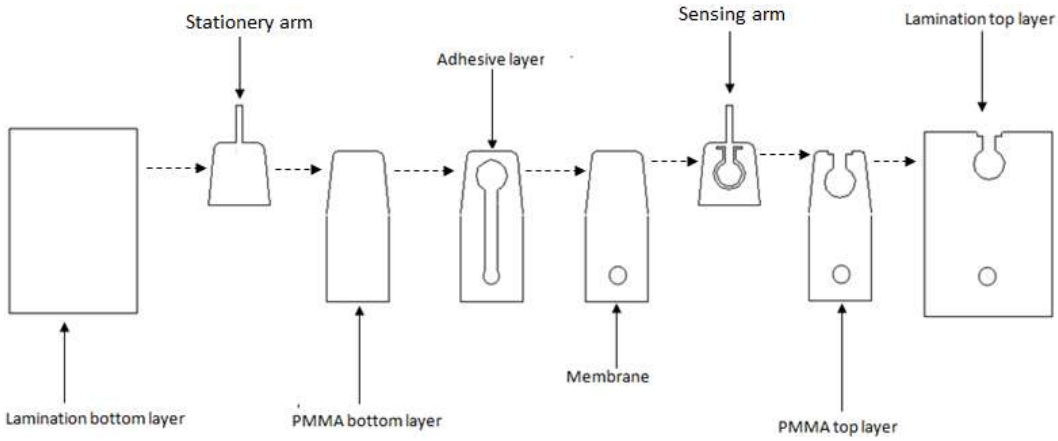

Figure 5.2: Assembling steps of the detector illustrating the sequence of assembling the device.

5.3 Testing of Device

The main application for the proposed device is to probe the mechanical properties of the biological micro-object. The operating principle for the detector is to apply a force which is known in advance on a micro-object and observe the deformation the micro-object undergoes as shown in sensing a 500 µm hydrogel bead, Figure 5.3.

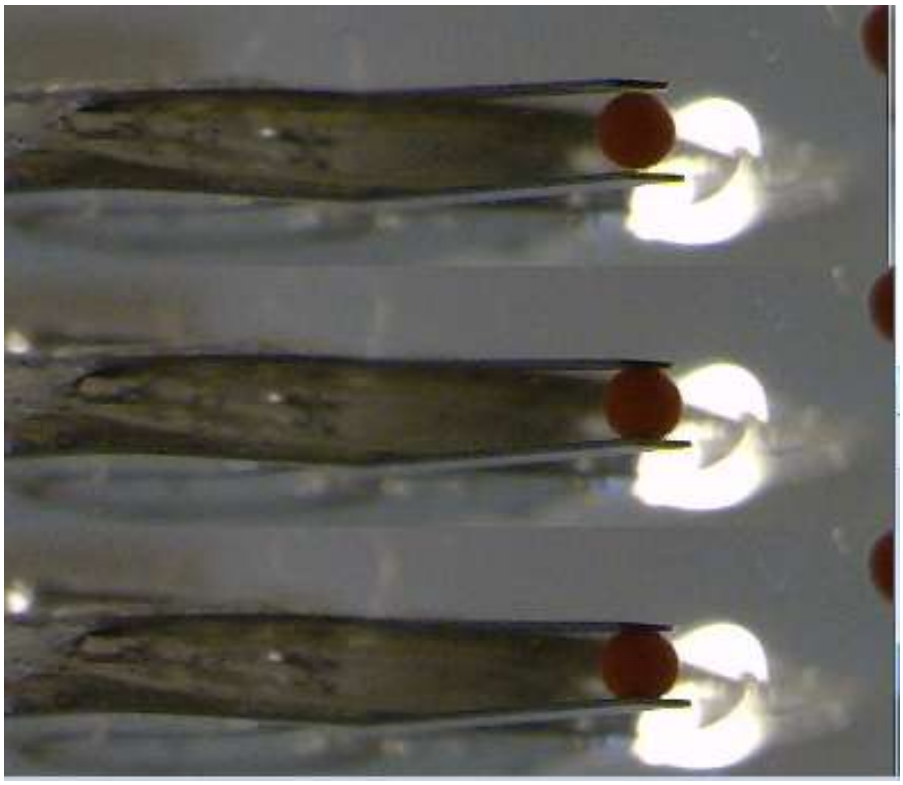

Fig. 5.3: Hydrogel bead sensing sequence in aqueous media where the deformation of the microbead obtaind by measuring the deflection of the micro-cantilever

In order to demonstrate the applicability of the proposed detector, the optical beam detection system mentioned previously has been recalled. A similar set-up that performed in the previous chapter for obtaining the bending of the cantilever tip is being implemented in this chapter as well, Figure 5.4. The optical detection system is performed for this detector in two cases; the first is to observe the bending of the tip while it is free and the second is to observe the bending of the tip while holding a hydrogel bead under the same applied pressure for both cases.

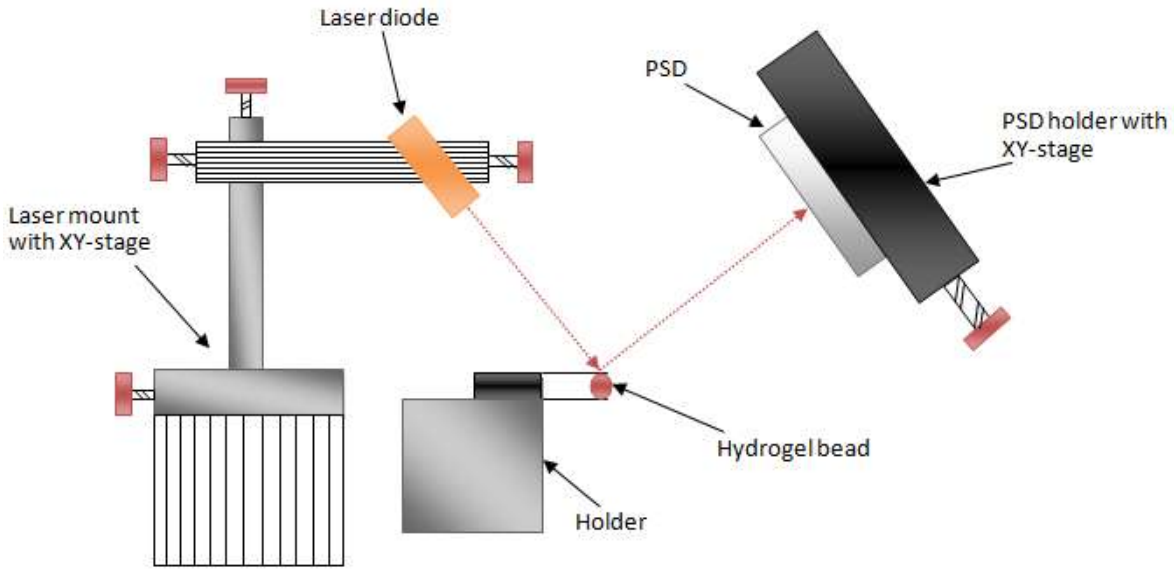

Fig. 5.4: Schematic illustration of the laser beam optical detection system used for sensing hydrogel microbeads

The procedure of sensing hydrogel beads while the bending of the cantilever tip was detected by the means of optical detection system is illustrated in Figure 5.5, where in Figures 5.5 (a) the detector holding the hydrogel bead, and in Figure 5.5 (b) the laser beam is focused to the tip of the cantilever. Figure 5.5 (c) illustrates the deformation that the hydrogel suffers while the force is applied. The amplitude of the bending at the tip of the cantilever is obtained and for the two mentioned previously cases which provides an indication of the stiffness of the hydrogel bead.

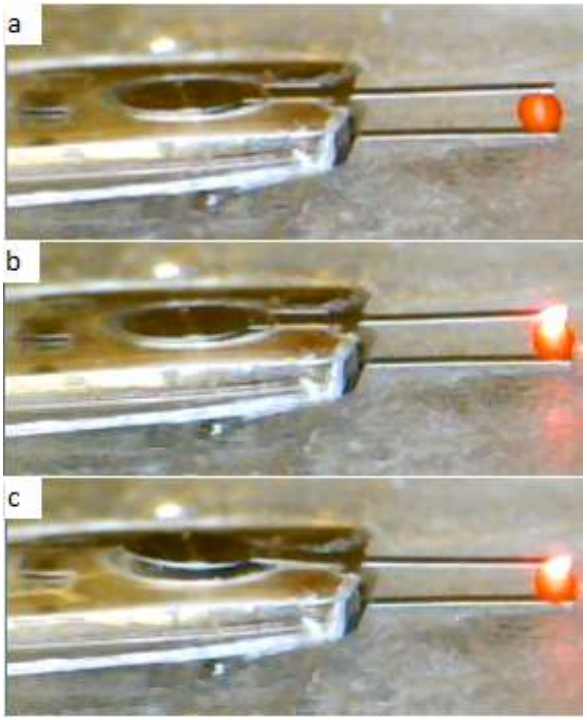

Fig. 5.5: Sequence of sensing hydrogel bead using optical detection system, (a) holding hydrogel bead, (b) focusing laser beam at the tip of cantilever, and (c) applying input force deforming the hydrogel bead.

5.4 Results and Discussion

The test mentioned in the previous section was carried out under an applied pressure of 1 bar and frequencies 1, 2, 4, and 10 Hz. The procedure was repeated twice: vibrating free and holding the hydrogel bead. The amplitude of bending of cantilever tip was obtained as shown in Figure 5.6. Where A1 is the amplitude at frequency of 1 Hz, A2 at 2 Hz, A3 at 4 Hz, and A4 at 10 Hz. The influence of the presence of hydrogel bead under the detector arm could be depicted from this figure where the drop in amplitude under the same conditions is obvious.

This procedure helps to differentiate the stiffnesses of the micro-objects that are being detected by observing the amplitude of the cantilever tip deflection and comparing them to each other to obtain the amplitude ratio (AR). The amplitude ratio could be expressed in the following equation:

$$AR = \frac{A1_1}{A1_2}$$

where $A1_1$ is the amplitude of cantilever tip deflection while detecting object 1, and $A1_2$ is the amplitude while detecting object 2, i.e., if $AR < 1$; that means that object 2 is stiffer than object 1, and vice versa.

For example, form Figure 5.6 and 5.7; the amplitude ratio is between 1.2 for 10Hz and 1.4 for 1Hz. Hence, if a stiffer material sensed instead of a hydrogel bead, a higher amplitude ratio will be obtained, and vice versa.

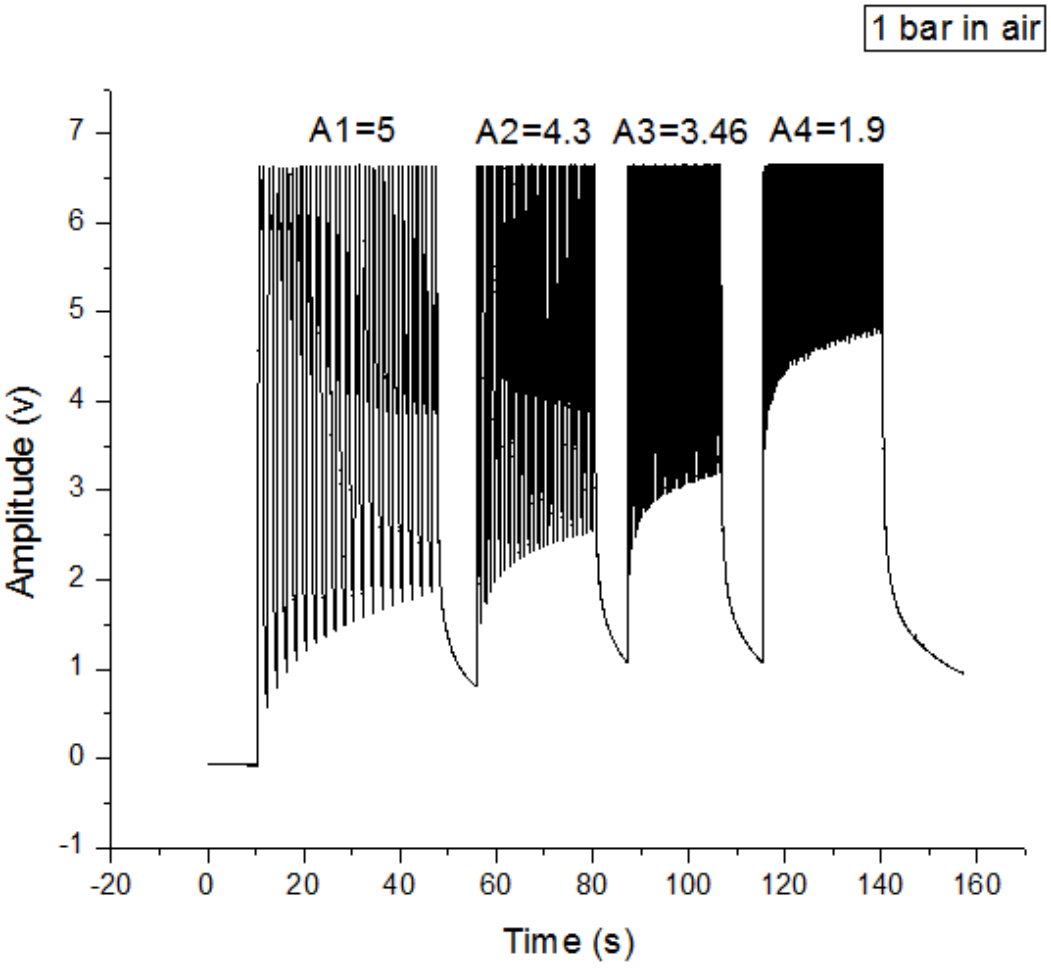

Fig. 5.6: Amplitude of cantilever tip at 1 bar for different frequencies with free end

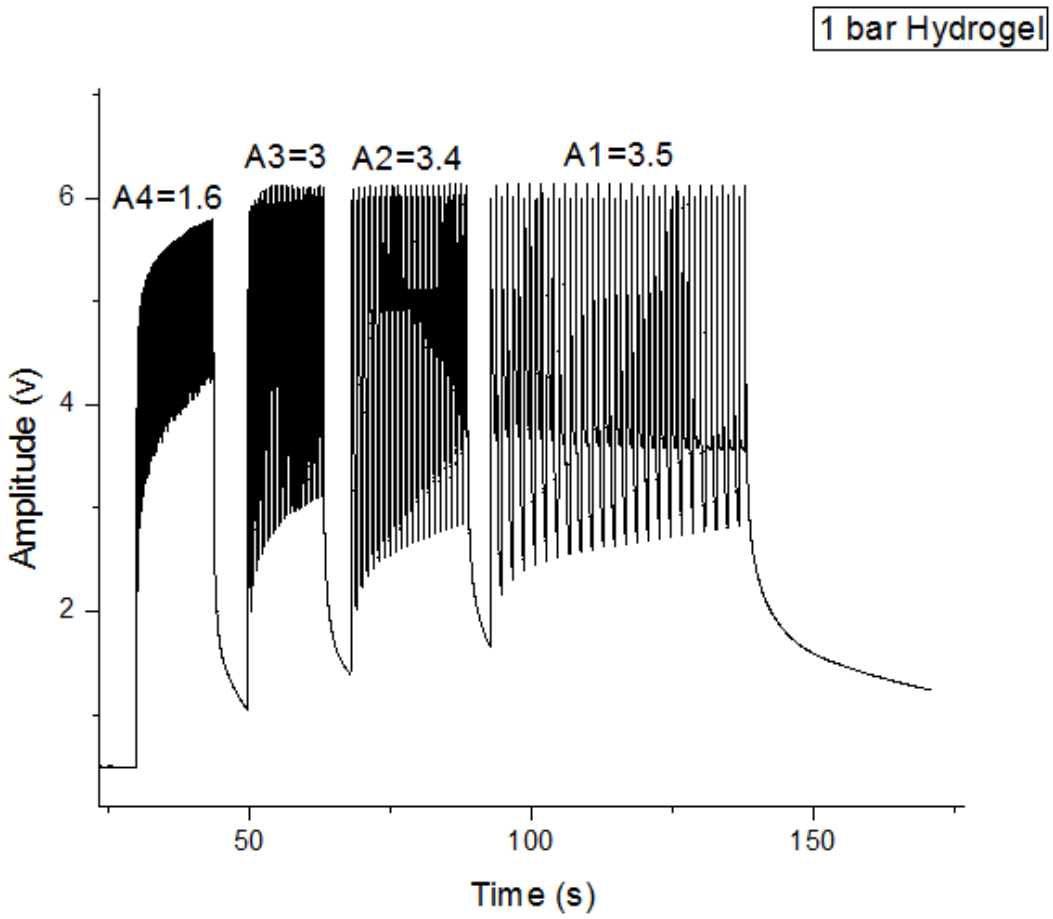

Fig. 5.7: Amplitude of cantilever at 1 bar tip holding hydrogel bead

5.5 Conclusion

In this chapter, a detector for sensing the stiffness of micro-objects has been reported. The proposed sensor could be implemented to investigate and differentiate the stiffnesses of different materials statically and dynamically. It could be used as a displacement-based sensor in case of static measurements, where the applied force is already obtainable as shown in the previous chapter and the displacement could be measured as well. Also, the device could be used as a vibrotactile sensor where the dynamic response of the device will give an indication of the stiffness of each material tested.

5.6 References

BARMAN, I. & GUHA, S. K. 2006. Analysis of a new combined stretch and pressure sensor for internal nodule palpation. *Sensors and Actuators A: Physical,* 125**,** 210-216.

BHARANIDARAN, R. & RAMESH, T. 2013. A numerical approach to design a compliant based Microgripper with integrated force sensing jaw. *International Journal of mechanics,* 2 (7), 128-135.

CHANG, R.-J. & CHENG, C.-Y. 2009. Vision-based compliant-joint polymer force sensor integrated with microgripper for measuring gripping force. *In:* Advanced Intelligent Mechatronics, 2009. AIM 2009. IEEE/ASME International Conference on, 2009. IEEE, 18-23.

HARMON, L. D. 1980. Touch-sensing technology- A review. *Society of Manufacturing Engineers, 1980. 58*.

HARMON, L. D. 1982. Automated tactile sensing. *The International Journal of Robotics Research,* 1**,** 3-32.

HARMON, L. D. 1984. Tactile sensing for robots. *Robotics and Artificial Intelligence.* (pp. 109-157). Springer Berlin Heidelberg.

MADZHI, N. K., AHMAD, A., KHUAN, L. Y. & ABDULLAH, F. 2010. Development and electrical measurements of piezoresistive microcantilever biosensor signal transduction for human stress measurement. *In:* Proceedings of the 9th WSEAS international conference on Electronics, hardware, wireless and optical communications, 2010. World Scientific and Engineering Academy and Society (WSEAS), 72-75.

PUANGMALI, P., ALTHOEFER, K., SENEVIRATNE, L. D., MURPHY, D. & DASGUPTA, P. 2008. State-of-the-art in force and tactile sensing for minimally invasive surgery. *Sensors Journal, IEEE,* 8**,** 371-381.

SARVAZYAN, A., EGOROV, V., SON, J. & KAUFMAN, C. 2008. Cost-effective screening for breast cancer worldwide: current state and future directions. *Breast cancer: basic and clinical research,* 1**,** 91-99.

TIWANA, M. I., REDMOND, S. J. & LOVELL, N. H. 2012. A review of tactile sensing technologies with applications in biomedical engineering. *Sensors and Actuators A: Physical,* 179**,** 17-31.

Chapter 6: Compliant Mechanism Based Parallel Microgripper using Pneumatic Actuation

In Chapters 3 and 4, two different designs of microgrippers were presented, both of which used an angular gripping scheme. Generally, grasping with a pair of jaws can be either angular or parallel, as illustrated in Figure 6.1. Angular gripping may allow slide of the grasped object, especially if this is wet or slippery, while this is avoided with a parallel gripping arrangement. Also, parallel gripping provide an even distribution of the gripping force and reduced stress concentration over the manipulated sample (Nikoobin and Hassani Niaki, 2012).

The overall aim of this chapter is to demonstrate a low cost polymer based compliant microgripper, designed using a parallel gripping scheme, and actuated using pneumatic forces. In this chapter, the design and realisation of such a pneumatically actuated microgripper capable of scaling to the level of manipulating a single biological cell is reported.

Compliant mechanisms, a class of mechanism that achieve an output displacement from the elastic deformation of one or more flexible members within the structure (Howell, 2001), have been extensively used in the field of micromanipulation. Such mechanisms have the advantages of reducing the number of parts within the system, reducing the cost, and increasing the performance of the whole system. Furthermore, at the micro-scale, they become highly favourable as they avoid the difficulties involved in assembling microstructures with moving parts (Kota et al., 2001). These merits have attracted researchers to implement such structures in the field of micromanipulation using a range of actuation methods such as piezoelectric (Xu, 2013, Wang et al., 2013, Zubir et al., 2009), SMA (Kyung et al., 2008, Lin et al., 2009), and pneumatic actuation (Alogla et al., 2013).

Each actuation method has its advantages and disadvantages but fluidic actuation is investigated here for reason already outlined, not least because it gives good

force output at the microscale (DeVolder M, 2010). Again for reasons already outlined, a class of elastic fluidic actuator (Jeong et al., 2006, Bütefisch et al., 2002, Yoshida et al., 2005) with a pressurised membrane (DeVolder M, 2010) has been used.

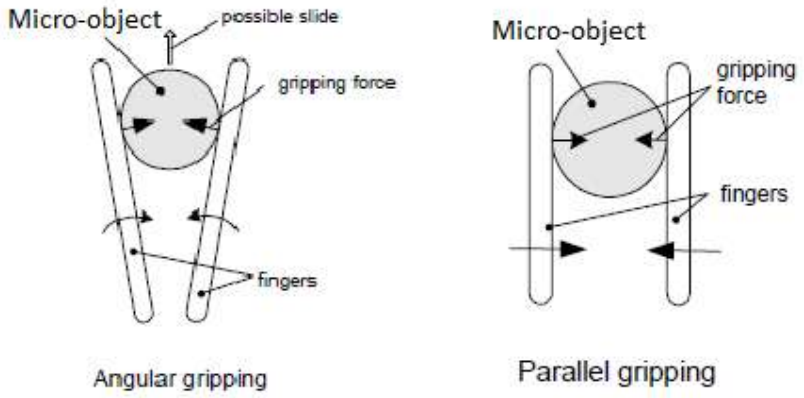

Figure 6.1: Angular and parallel gripping illustrating the possibility of sliding of the grasped micro-object (Wenjie and Wei, 2004)

6.1 Microgripper Design

The microgripper described here is pneumatically actuated and is designed to be operated in a range of environments, including air and liquid, at a range of scales. It comprises of two main parts: the actuation mechanism and the compliant gripper legs. The actuator is essentially a flexible membrane that applies force to the gripper legs when the air inlet is pressurized as shown in Figure 6.2, where a compliant mechanism has been designed to comply with the input force delivered through a membrane at the gripper legs, achieving an output displacement at the gripper jaws.

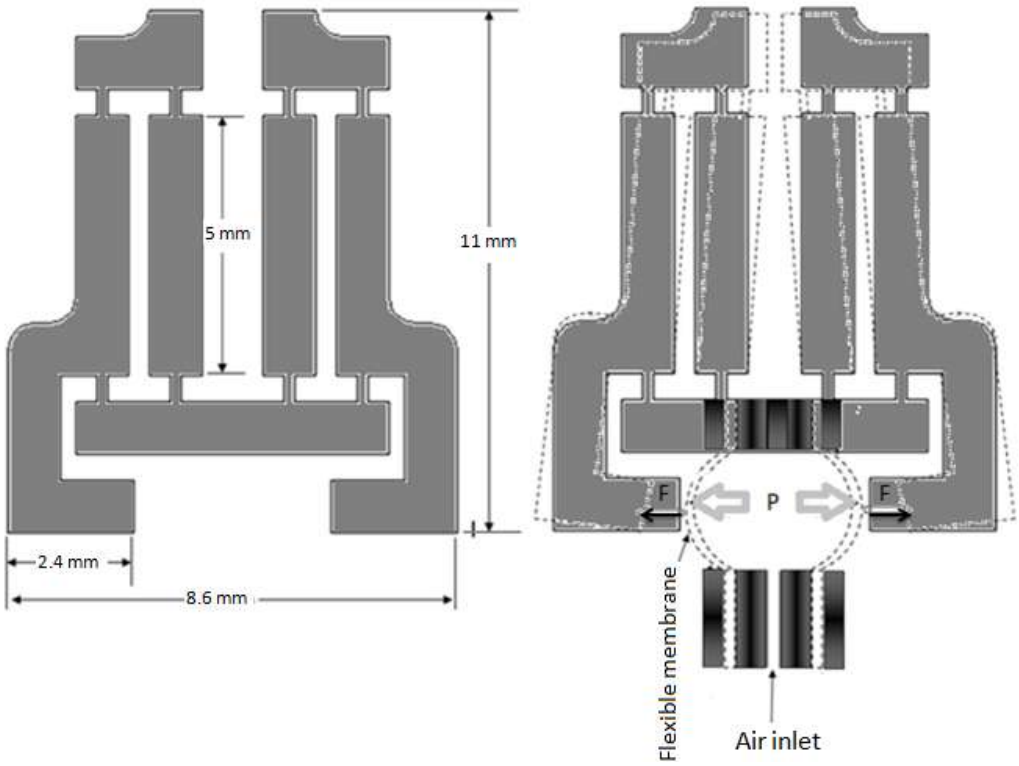

Figure 6.2: (Left) Dimensions of microgripper, (Right) Schematics of working principle of microgripper as the input force being applied to the gripper legs, a parallel closing of the jaws will occur.

6.2 Theory

The linkage mechanism of the grasping device is shown in Figure 6.3.

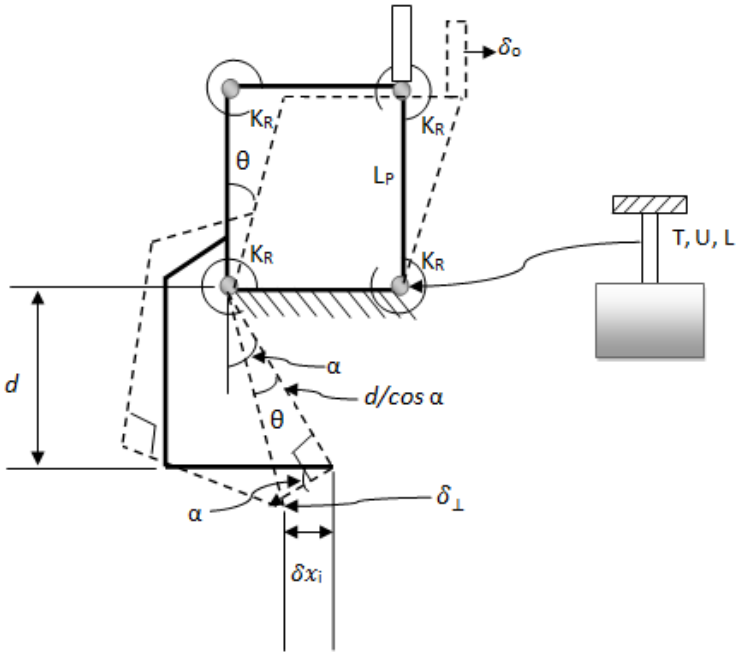

Figure 6.3: Linkage model of the gripper (Half)

According to the model in figure 6.3, the output displacement is related to the input force as follows:

$$\delta_o = L_p \times \theta \tag{6.1}$$

$$\delta_\perp = \frac{d}{\cos\alpha}\theta \tag{6.2}$$

$$\Longrightarrow \quad \frac{\delta_o}{\delta_\perp} = \frac{L_p}{d}\cos\alpha \tag{6.3}$$

$$\frac{\delta_o}{\delta_{xi}} = \frac{L_p\theta}{\delta_\perp \cos\alpha} = \frac{L_p}{d} \tag{6.4}$$

where,

$\delta_{\perp}$: is the resultant input displacement at the input point of the handle.

δ_o: the output displacement

δ_{xi}: the input displacement in the x-direction

Input Work = Potential Energy

$$\frac{1}{2}F_{in}\delta_{xi} = 4 \times \frac{1}{2}K_R\theta^2 \tag{6.5}$$

$$\frac{1}{2}F_{in}\delta_{xi} = 2 \times K_R\left(\frac{\delta_o}{L_p}\right)^2 \tag{6.6}$$

Substituting equation (4) into equation (6), gives:

$$\frac{1}{2}F_{in}\frac{\delta_o d}{L_p} = 2 \times K_R\frac{{\delta_o}^2}{{L_p}^2} \tag{6.7}$$

$$\Longrightarrow \quad F_{in} = 4K_R\frac{\delta_o}{L_p d} \tag{6.8}$$

$$F_{in} = 4 \times \frac{EI}{L}\frac{\delta_o}{L_p d} \tag{6.9}$$

where the rotational stiffness of each hinge is calculated using the Euler-beam assumption and the rotational centre is assumed to be located at the centre of the hinge.

$$F_{in} = 4 \times \frac{EUT^3}{12}\frac{\delta_o}{LL_p d} \tag{6.10}$$

$$F_{in} = \frac{EUT^3}{3}\frac{\delta_o}{LL_p d} \tag{6.11}$$

$$\Longrightarrow \quad \delta_o = \frac{3F_{in}L_p L d}{EUT^3} \tag{6.12}$$

where

L= 0.5 (length of hinge),	U= 1mm (out of plane thickness of the hinge)
L_p= 5.5mm,	T= 0.2mm (in-plane thickness of the hinge)
d= 3.25mm,	E= 1800 MPa

6.3 Fabrication and Assembly

The actuation mechanism is essentially flexible membranes that apply forces to the gripper legs when the air inlet is pressurized. The body of the actuator was assembled using 3 layers of laser cut PMMA 200µm thick; bottom, mid, and top layer providing a 1.02x1.02 mm leg groove on the top and bottom layers to enable the legs of the gripper to fit inside these grooves for actuation. The mid-layer was laser cut into a shape with 50 microns thick transfer adhesive layers attached to both sides. These layers of transfer adhesive themselves were laser cut to define micro-channels before attaching them to the mid-layer. Two silicone membranes, 65 micron thick each, were then applied to the adhesives. Fitting grooves were cut for all the previous mentioned layers to fit the actuation package to the base of the microgripper in order to provide more robustness to the device. An inlet hole should be present within all layers of the assembly apart from the bottom membrane and the bottom PMMA layer. This will allow air to enter the microchannel and inflate/expand the membrane layers. To ensure that the membranes do not slip and that there are no leaks in the set up, the microgripper assembly was laminated between two 75 micron thick layers of laminate sheet. The underside of the assembly was attached to a laminate, that is laser cut to allow the microgripper leg to flex, using the transfer adhesive already in place. The top layer of the laminate was laser cut to expose the inlet hole in the device and to allow the gripper leg to flex. This layer was then attached to the topside of the assembly again using the transfer adhesive that was already in place. The entire device was then laminated at 130 degrees on heavy gauge at a feed speed of

1mm/sec. The assembling steps and assembled prototype are illustrated in Figure 6.4.

The microgripper was laser cut from a PMMA sheets. A Trumpf-Tru Micro laser system, providing 125 µJ, 10.1 ps pulses at 1030 nm was selected. At this wavelength PMMA is transparent and as such machining is driven by non-linear absorption. This, combined with a low repetition rate of 10 kHz, effectively eliminates thermal accumulation allowing for a clean cut with no melting or heat affected zone but at the cost of a slow processing speed.

Laser beam steering is provided with an F-Theta (focal length of 163 mm) scan head translating the Ø 27.5 µm focal spot at 100 mm^{-2}. The PMMA sheet was suspended in free space mounted such that the free space focus of the scan head is in the centre of the sheet. Aerotech screw stages (resolution of ~6 µm) were used for fine control of the focal position. The pattern was scanned 250 times with a whole pattern repetition. Once completed, the microgripper was freed from the PMMA sheet with a pair of tweezers.

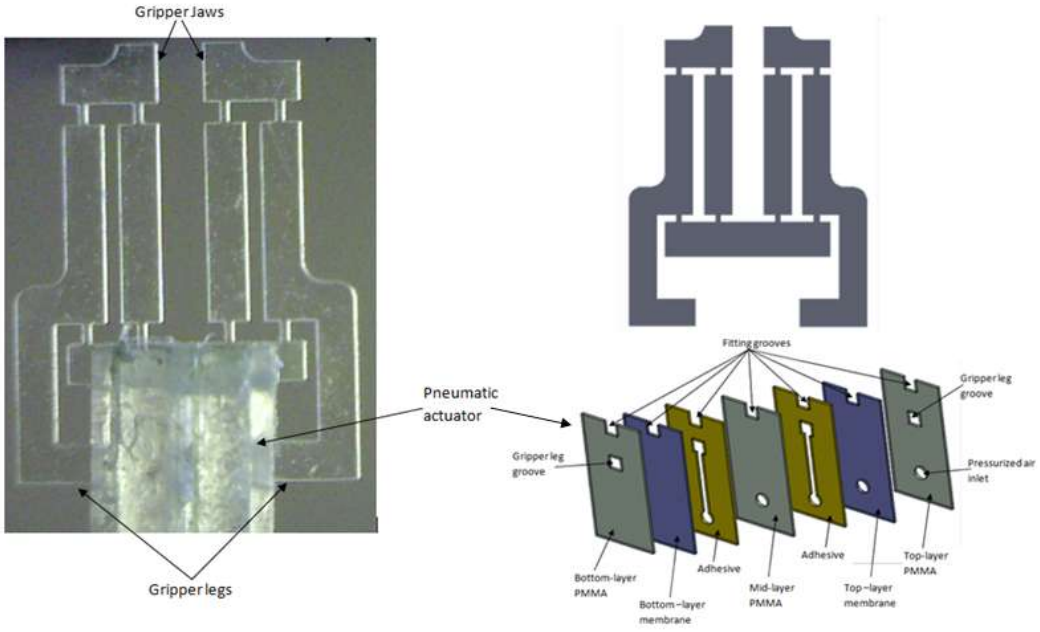

Figure 6.4: (Left) Assembled microgripper, (Right) Pneumatic actuator assembly

6.4 Finite Element Analysis Comparison

The performance of the device was also investigated using FEA and compared with analytical results. The FEA software package used for this investigation is ABAQUS 6.10. In the simulation, the gripper was analyzed as a 2D model with the material of PMMA, of which Young's modulus is 1.8 GPa, and Poisson's ratio is 0.35. Due to the symmetry of the two jaws, only one side of the microgripper needs to be analyzed. The mesh size was 0.01mm for the whole mechanism, but that for the critical regions it was decreased to 0.005mm as they govern the performance of the device as illustrated in the following figure, Figure 6.5. The total number of elements was 406685 and the number of nodes was found to be 403756.

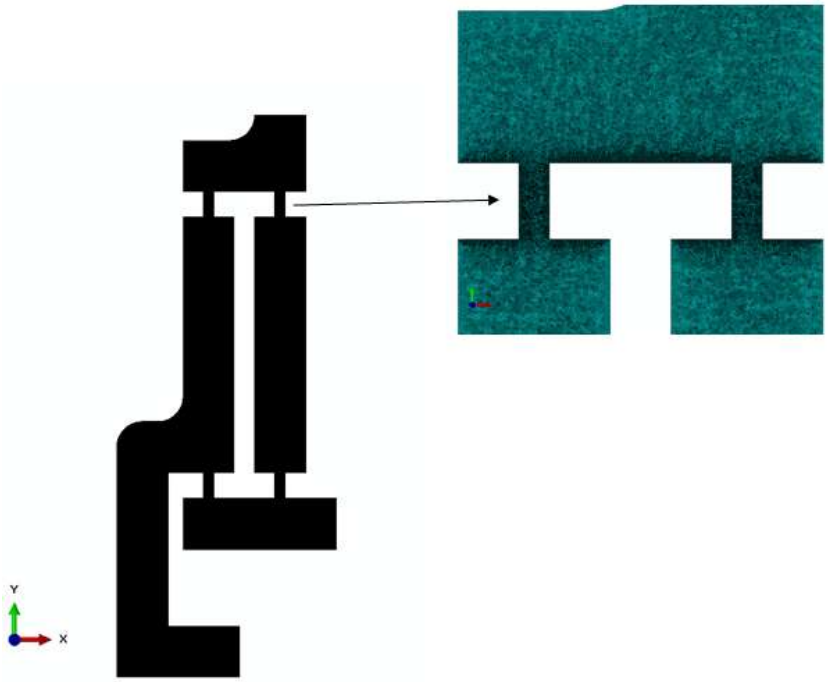

Figure 6.5: meshed part where the mesh density increased at the expected critical regions that influence the performance of the gripper (half of gripper)

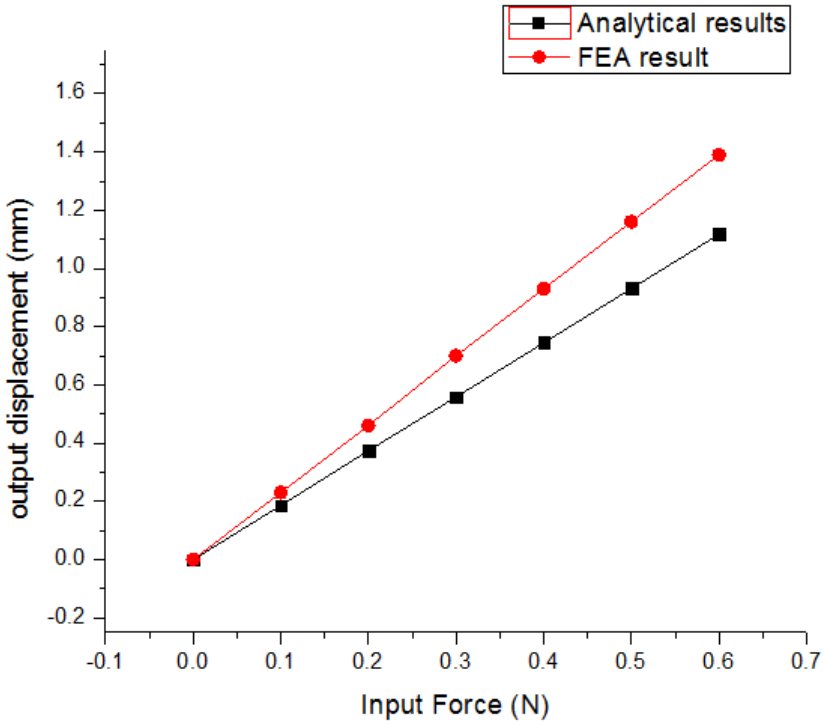

Figure 6.6: Analytical stiffness of the gripper compared with the simulated values

Also, FEA was implemented to obtain the relation between the input force and the output force and compare it with the analytical input force vs. output force as illustrated in Figure 6.7. Analytically, based on the principle of virtual work, the input and output forces are related as follows:

$$F_{in} \times \delta_{xi} = F_o \delta_o \qquad (6.13)$$

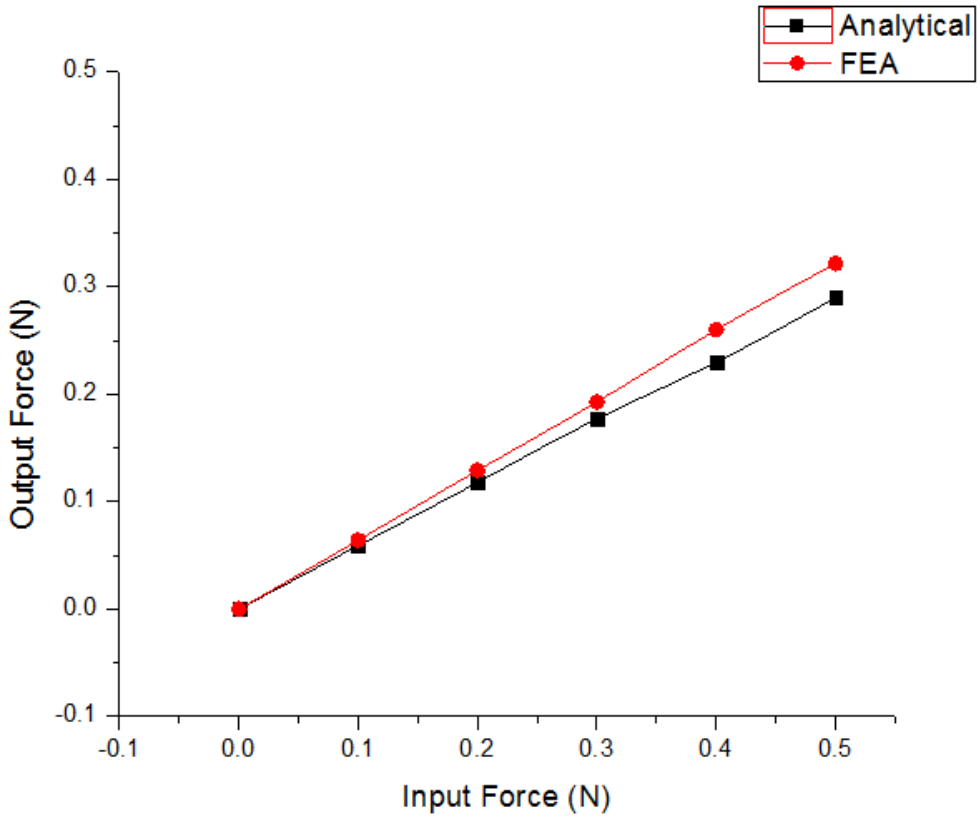

Figure 6.7: Analytical relation between the input force compared with the simulated values.

6.5 Results and Discussions

An analytical model has been established for the reported device as illustrated in Figure 6.3, where all the parameters affecting the performance of the gripper are mentioned. Equation (6.12) shows that the geometry of the hinge is a very important factor affecting the output parameters of the device.

In the following figure, the effect of the hinge geometry on the performance of the device is illustrated. The figure shows different resulting stiffnesses of the device while maintain the same stiffness of the hinge.

From Figure 6.6, it is shown that the FEA results are larger than the analytical results, which is sensible since FEA takes all bodies as the deformable one but the analytical model considers an idealized rigid-body treatment for the non-hinge

part as in Figure 6.8. As compared with the FEA approach, the proposed analytical linear model may enable rapid analysis and quick design synthesis.

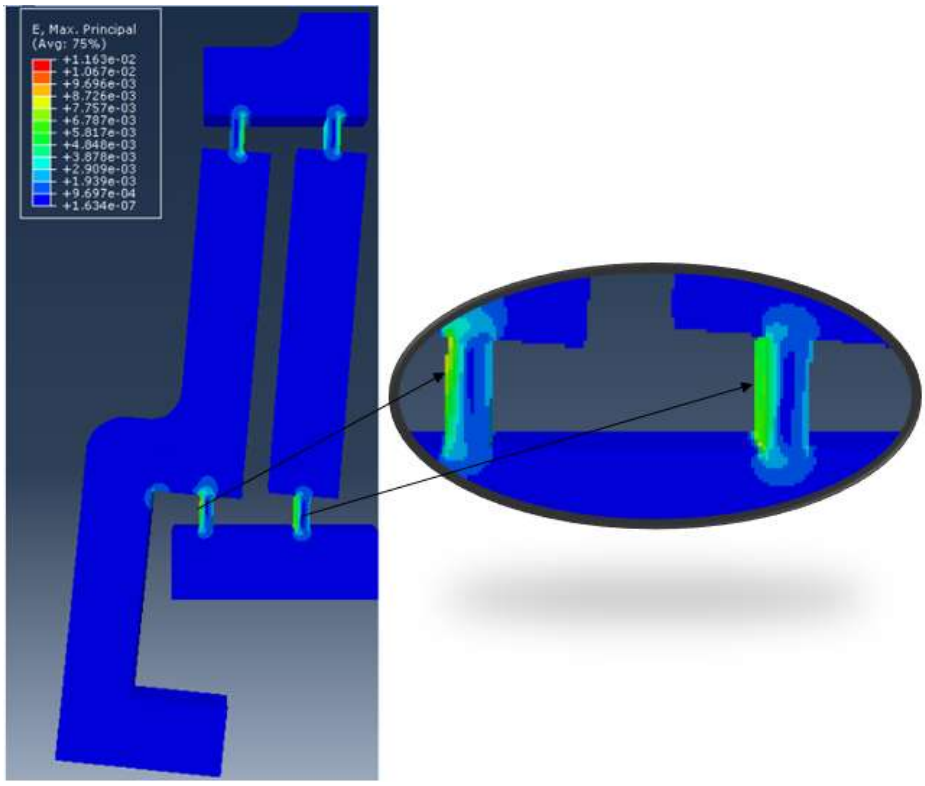

Figure 6.8: Strain distribution over the microgripper device, showing the deformation of hinges

In addition, the discrepancy between the FEA and analytical results can be attributed to the inaccuracy from the analytical modelling. On the one hand, the small deformation assumption is adopted in the modelling. On the second hand, the rotational stiffness estimation of each compliant hinge is based on the Euler-Beam assumption without considering the shear force effect, which means that the stiffness model become less accurate if the slenderness ratio (L/T) of the hinge becomes smaller which is clearly obvious in Figure 6.9. On the third hand, if the slenderness ratio of the hinge becomes larger, the rotation center drift will become dominant in the inaccuracy of the analytical model, which entails that the pre-assumed rotation center located at the center of the hinge is not feasible. In the proposed design, the slenderness ration was chosen to be L/T = 2.5. This value

will make the device reasonably flexible even though it leads to a discrepancy between analytical and FE results. This discrepancy will vanish if L/T increased, but on the other hand, increasing L/T implies increasing the in-plane thickness to maintain the same stiffness of the hinge where the problem of buckling will arise.

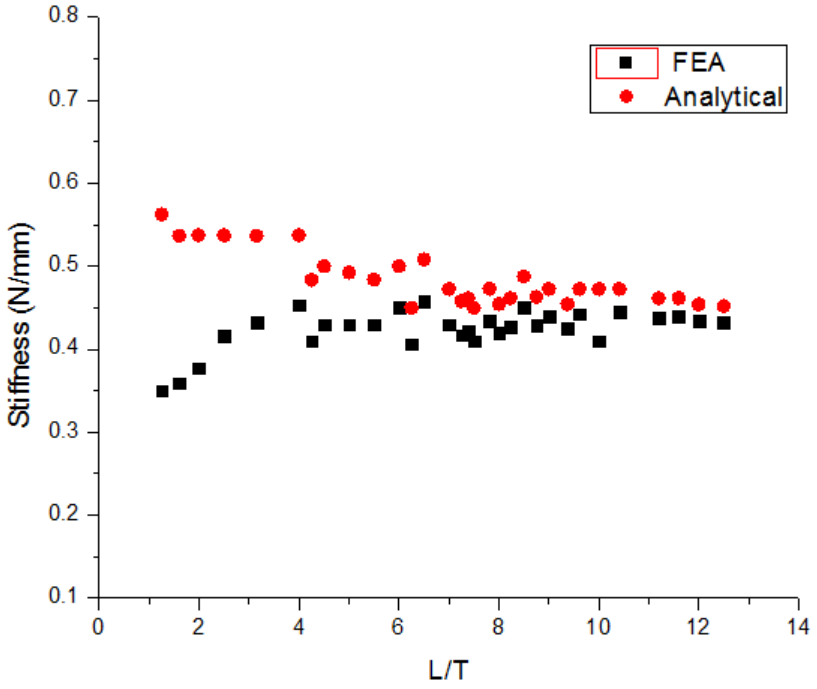

Figure 6.9: Analytical results for stiffness of the device with different L/T ratio compared with the simulated values.

6.6 Demonstration of Device

To verify the ability of the device to perform pick and place operations, a range of tests were conducted on objects of known size. The gripping actuation was controlled using pneumatic pressure. A positive pressure will close the gripper and the release of the pressure will open the gripper. Figure 6.10 shows the actuation mechanism can precisely manipulate a range of objects with the sizes down to 100 μm in thickness. It is expected this approach can be further scaled

down, by shrinking the dimension of the gripping arm, to manipulate single biological cells in liquid environment.

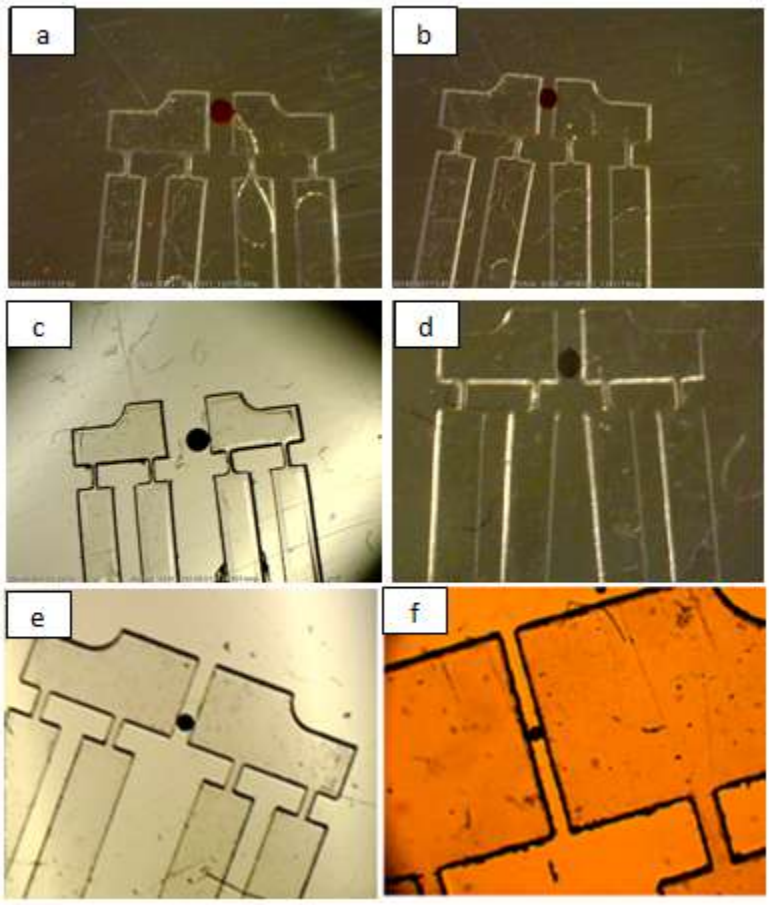

Figure 6.10: Demonstration of gripping (a-b) 500 , (c-d) 400, (e) 200, and (f) 100 µm microbeads

6.7 Conclusion

In this chapter, a low cost polymer based compliant microgripper following a parallel gripping scheme that can be actuated using pneumatic forces has been reported. An analytical model for the proposed device was established and validated using FEA. Also, it was clearly shown that the geometry of the hinges plays the most important role in the performance of the device. The shape of the hinge is also critical as it will change the maximum stress reached. Grasping micro-objects as small as 100 µm has been demonstrated using the proposed device.

6.8 References

ALOGLA, A., SCANLAN, P., SHU, W. & REUBEN, R. 2013. A scalable syringe-actuated microgripper for biological manipulation. *Sensors and Actuators A: Physical,* 202**,** 135-139.

BÜTEFISCH, S., SEIDEMANN, V. & BÜTTGENBACH, S. 2002. Novel micro-pneumatic actuator for MEMS. *Sensors and Actuators A: Physical,* 97**,** 638-645.

DEVOLDER M, R. D. 2010. Pneumatic and hydraulic microactuators: a review. *Micromechanics Microengineering,* 20**,** 18pp.

HOWELL, L. L. 2001. *Compliant mechanisms,* Wiley-Interscience.

JEONG, O. C., KUSUDA, S., SAKAKIBARA, T., KONISHI, S. & NOKATA, M. 2006. Pneumatic micro finger as endeffecter of robot. *In,* 2006. IEEE, 145-148.

KOTA, S., JOO, J., LI, Z., RODGERS, S. M. & SNIEGOWSKI, J. 2001. Design of compliant mechanisms: applications to MEMS. *Analog Integrated Circuits and Signal Processing,* 29**,** 7-15.

KYUNG, J. H., KO, B. G., HA, Y. H. & CHUNG, G. J. 2008. Design of a microgripper for micromanipulation of microcomponents using SMA wires and flexible hinges. *Sensors and Actuators A: Physical,* 141**,** 144-150.

LIN, C.-M., FAN, C.-H. & LAN, C.-C. 2009. A shape memory alloy actuated microgripper with wide handling ranges. *In:* Advanced Intelligent

Mechatronics, 2009. AIM 2009. IEEE/ASME International Conference on, 2009. IEEE, 12-17.

NIKOOBIN, A. & HASSANI NIAKI, M. 2012. Deriving and analyzing the effective parameters in microgrippers performance. *Scientia Iranica*, *19*(6), 1554-1563.

WANG, D., YANG, Q. & DONG, H. 2013. A monolithic compliant piezoelectric-driven microgripper: Design, modeling, and testing. *Mechatronics, IEEE/ASME Transactions on*, *18*(1), 138-147.

WENJIE, C. & WEI, L. Year. Design of a flexure-based gripper used in optical fiber handling. *In:* Robotics, Automation and Mechatronics, 2004 IEEE Conference on, 2004. IEEE, 83-88.

XU, Q. 2013. A new compliant microgripper with integrated position and force sensing. *In:* Advanced Intelligent Mechatronics (AIM), 2013 IEEE/ASME International Conference on, 2013. IEEE, 591-596.

YOSHIDA, K., PARK, J.-H., YANO, H., YOKOTA, S. & YUN, S. 2005. Study of valve-integrated microactuator using homogeneous electro-rheological fluid. *Sensors and Materials*, 17**,** 97-112.

ZUBIR, M. N. M., SHIRINZADEH, B. & TIAN, Y. 2009. A new design of piezoelectric driven compliant-based microgripper for micromanipulation. *Mechanism and Machine Theory,* 44**,** 2248-2264.

Chapter 7: Summary Conclusions and Outlook

7.1 Summary Conclusions

The main objective of the research reported in this thesis, was to develop a variety of low cost microgrippers that are; easy to fabricate, scalable in size, controllable in terms of output force and displacement, compatible with biological environments, and capable of operating in aqueous media. A review of the existing manipulation techniques was presented and it was noted that fluidic actuation *(hydraulic and pneumatic)* has been overlooked for micromanipulation despite its considerable advantages for such applications. Therefore, this thesis focused on the design and implementation of pneumatically actuators which can be incorporated to a controlled microgripper for the purpose of micromanipulation and assessing the gripped micro-object.

The first family of devices used low cost polymer materials and a high power laser cutter was used to rapidly fabricate the device at low cost, allowing rapid iterations between design, test and optimisation. The gripper was actuated through the inflation of an elastic membrane under a controlled pneumatic pressure, delivered either from an external pressure supply or a manually actuated syringe. The output force of the gripper was up to 8 mN both measured experimentally and validated theoretically. The gripper was effective in manipulating a number of objects ranging from 200 μm to 2 mm. The design is highly scalable in principle, with the gripper arms being limited only by the acuity of laser cutting and the minimum defect size in the machined material. The membrane actuator is similarly scalable provided that a planar configuration is used with a channel on the fluid side.

While the low cost pneumatically actuated gripper was easy to fabricate, the required 3D assembly of fabricated structures is challenging, particularly at smaller scales. To overcome this, another device, based two opposing micro-

cantilevers, was presented, with the dual functions of micromanipulation and force sensing. The design involves assembling the 2D membrane and gripping cantilevers layer by layer to form 3D structures, eliminating the need to assemble 3D structures whose planes of movement are perpendicular to each other. This type of device has the advantages of easy fabrication, easy assembly and greater scalability. The cantilever based actuator has a pressure-force relationship that can be simply measured and controlled in both static and dynamic modes. Besides controlling the input and output forces, the design of the gripper arms can be tuned in order to provide a deflection of the arms, whose measurement can be used to measure the gripping force in operation and can potentially be fed back to control the force or used to assess the gripped object. The devices have been tested for a range of micro-objects in the size range from 200 to 500 μm and were demonstrated in their ability to probe mechanical properties of hydrogel beads.

For a precise manipulation and control of the gripping system, an automated approach has been demonstrated. A programmable CNC setup has been used to control the pick-place position of the microgripper. This approach demonstrated a satisfactory performance for building different patterns precisely.

When testing the microcantilever based gripper, a challenge was identified in griping smaller spherical objects because of the intrinsic angle of the gripper. In particular, microbeads with diameters smaller than 200 μm were extremely difficult to handle. To overcome this problem, the approach of pneumatically actuators was extended to compliant microgripper structures employing a parallel motion scheme. In this way, a new pneumatically actuated compliant microgripper was designed and demonstrated. An analytical model for the proposed device was established and validated using FEA. Also, it was clearly shown that the geometry of gripper hinges played an essential role in the performance of the device and that the shape of the hinge was critical in affecting the maximum contact force. Grasping micro-objects as small as 100 μm microbeads was demonstrated using the proposed device.

7.2 Outlook

The current study is mainly focused on developing microgrippers controlled by a pneumatic actuation mechanism. The concept and technology are highly scalable and has been demonstrated in this thesis to be capable of gripping objects as small as 100 μm. However, the ultimate aim of a microgripper for cellular manipulation is to be able to manipulate single cells of size in the range of 5-10 μm. In order to achieve this, further investigation is needed to demonstrate scale down of the gripper devices and their associated actuators by a factor of about 10. From the point of view of design of the micro-actuator and gripper, this is highly feasible. Also, some of the work has demonstrated the use of a high precision picosecond laser system to fabricate the gripping devices, adding to the feasibility of fabricating such devices.

On the other hand, the manual assembly of some of the devices is a significant challenge. This challenge might be overcome using 3D micro-assembly techniques, but there remains an issue in micro-scale assembly as the leakage of driving fluid will have a significant effect on the manipulation procedure. For delicate pick-place operations, where particular care is needed to avoid damage on the handled objects, more quantitative force feedback may potentially be a solution.

Due to their low cost and ease of fabrication procedures, the prototype devices could be developed into a “microhand”, where an array of devices operate simultaneously and independently. This requires each device to have its separate microchannel for supplying the driving fluid posing further fabrication and assembly challenges. Such a device could provide tactile feedback, which could then be integrated into a haptic system whereby real hands can be interconnected with the microhand to manipulate micro-objects and even living cells.

Additionally, integrating strain gauges and force sensors into the tip of the device will be a powerful means of manipulating tissue at the histological scale and assessing its nanomechanical properties. This could be used in microsurgery procedures (e.g. in eye surgery) where a high degree of control and feedback are needed. The developed devices have another potential application in combination with surgery tools for *in-vivo* studies, where an endoscope could be used to guide the gripper for microsurgery procedures.